EFFECTS OF NON-UNIFORM AIR FLOW THROUGH FILTERS ON FILTRATION EFFICIENCY

By

RAJENDRA D. SABNIS

Bachelor of Engineering

Shivaji University

Kolhapur, India

1989

Submitted to the Faculty of the
Graduate College of the
Oklahoma State University
in partial fulfillment of
the requirements for
the Degree of
MASTER OF SCIENCE
July, 1993

OKLAHOMA STATE UNIVERSITY

EFFECTS OF NON-UNIFORM AIR FLOW THROUGH FILTERS ON FILTRATION EFFICIENCY

Thesis Approved :

Thesis Adviser

Dean of the Graduate College

ACKNOWLEDGMENTS

I would like to take this opportunity to thank the individuals who have assisted me in successfully completing this project and other requirements for my Masters Degree. In particular, I wish to express my sincere appreciation to my major advisor, Dr. F. W. Chambers, for his invaluable guidance, encouragement and help from time to time. I am also grateful to the other committee members, Dr. R. L. Dougherty and Dr. J. D. Spitler for their suggestions and help.

A thank-you is extended to my colleague, Qian Cai, whose cooperation throughout the project led to the successful completion of the project. I also wish to thank my two other colleagues, Manoj Haldhani and Faqiu Liang, who were also equally cooperative in this project.

The technical literature and information provided by Dr. T. Jaroszczyk of Nelson Industries, Inc. is sincerely appreciated. I also wish to thank Dr. P. B. Apfeld of Ahlstrom Filtration for his help in collecting the technical data.

The financial support provided by Purolator Products, Inc., and Oklahoma Center for the Advancement of Science and Technology (OCAST) is greatly appreciated. A special thanks is due to the personnel of Purolator Products, Inc. and in particular, to Dr. Gary Ferrell, for their suggestions and information regarding the filter project.

I would also like express my greatfulness to my late father and mother whose continuous support and encouragement has helped me to complete my studies.

TABLE OF CONTENTS

Chapter Page

Chapter Page

LIST OF TABLES

LIST OF FIGURES

Figure Page

NOMENCLATURE

a	radius of aerosol particle (m)
a_e	total area of media within an element (m^2)
b	radius of Happel and Kuwabara cell boundary circle (m)
c	packing density
C	particle number density at inlet to the air filter (m^{-3})
C_c	slip correction factor
d	fringe spacing (m)
E	single fiber efficiency
E_a	single fiber adhesion efficiency
E_c	single fiber collection efficiency
E_D	diffusion efficiency
E_I	inertial efficiency
E_R	interception efficiency
E_{RI}	single fiber efficiency due to inertial interception
E_{Sheet}	efficiency of a sheet of parallel fibers
$\overline{E}_{DR}$	single fiber efficiency in an intermediate range where both, diffusion and interception, are responsible for filtration.
E'	isolated fiber efficiency
h	filter thickness (m)
H_f	inclined height of a pleat (m)

i	number of identical layers of filtering material in a filter
J	complex integral
I	interception parameter (= a/R)
k	constant of proportionality
$\overline{K}^*$	volumetric aerosol deposition-rate coefficient (s^{-1})
Kn	Knudsen number (= λ/a)
Ku	Kuwabara hydrodynamic factor
l_f	characteristic length of filter (m)
L	length of all fibers in a unit volume of the media (m)
L'	length of diffuser (m)
m	mass of particle (Kg)
n	concentration of aerosol leaving the filter (m^{-3})
n_o	concentration of aerosol entering the filter (m^{-3})
N	total number of particles penetrating the filter per unit time (s^{-1})
N_e	number rate of particles penetrating an element (s^{-1})
N_p	number of particles passing a unit area per unit time ($m^{-2}s^{-1}$)
P	penetration
Pa	a particle parameter
Pe	Peclet number (= $2uR/\nabla$)
Po	porosity of the media
P_e	penetration through a small element in a filter
P_f	pitch of filter pleats (m)
Q_F	air flow rate through the filter (m^3/s)
R	fiber radius (m)

Re	Reynolds number (= $2Ru/\nu$)
s	number of fiber diameters between fibers in a sheet of parallel fibers
St	Stokes number (= $2a^2\rho_a u/9\mu R$)
St_c	Stokes number with slip correction factor(= $a^2\rho_a C_c u/9\mu R$)
t	depth of penetration of the aerosol (m)
u	mean air velocity inside the filter media (m/s)
u_g	rate of fall of particle due to gravity (m/s)
u_r, u_θ	radial and tangential velocity components (m/s)
$\overline{U}^*$	aerosol's Darcy-scale mean speed (a scalar quantity) (m/s)
V	velocity of fluid at entrance face of a filter (m/s)
V_e	velocity encountered by a small element of a filter (m/s)
V_{ip}	uniform normal velocity of the fluid entering a filter media (inside a pleat) (m/s)
V_{op}	local axial velocity of the fluid before the pleat of a filter (m/s)
w_1,w_2	width of diffuser at inlet and outlet respectively (m)
y	distance from stagnation point (m)
α	layer efficiency
δ	thickness of diffusion layer (m)
Δp	pressure drop across filter (Pa)
∇	diffusion coefficient of particles (m^2/s)
η	efficiency of a filter
η_c	collision efficiency
η_e	filtration efficiency of an element in a filter
η_F	overall filtration efficiency of a pleated air filter

η_R	particle retention efficiency
η_U	filtration efficiency of a pleated air filter with uniform velocity distribution
θ	polar coordinate angle (radians)
θ_1, θ_2	the two diffuser angles in two planes (degrees)
λ	mean free path of the fluid (m)
μ	dynamic viscosity of air/gas (Pa-s)
ν	kinematic viscosity of air/gas (m^2/s)
ρ_a	density of particle (Kg/m^3)
ρ_f	density of fibers (Kg/m^3)
ρ_F	density of filter or weight of fiber in unit volume of filter (Kg/m^3)

CHAPTER I

INTRODUCTION AND LITERATURE REVIEW

1.1 Introduction

A supply of clean combustion air, free of any particles, is necessary for internal combustion engines. The engine driving the automobile draws its combustion air from a variety of atmospheres, the dust concentrations of which could vary from very low to very high. The filter located in the air intake system of the engine performs the task of separation of the dust and any other particles from the combustion air. If any undesirable particles enter the combustion chamber, they act like an abrasive particle on the surface of the cylinder to result in accelerated wear of the engine. The filter and the housing that holds the filter must perform the above mentioned task while offering the least resistance to the air flow path. Since the pressure drop available across the air intake system is predetermined by the configuration of the air intake system, any excessive resistance in the filtration process would result in a reduced supply of air, which means the starved engine would produce lower power. The filter should consistently perform its function of providing clean air at an acceptable pressure drop over its entire period of life. Hence, even though the filter constitutes a small and inexpensive part in the engine, its importance should not be overlooked.

The efficiency of filtration and the pressure drop across the filter are both a strong function of the aerosol velocity through the filter media. The velocity distribution across the filter is determined by the configuration of the housing that holds the filter. One such housing is the Panel Filter Universal Test Housing standardized by the Society of Auto-

motive Engineers (SAE) standard J726 Air Cleaner Test Code, which is used to mount the filter for conducting the performance tests of filters. The test housing mainly consists of a section which is similar to a wide angled diffuser in two planes, with the exit of the diffuser being partially blocked by the mounting arrangement of the panel air filter. This construction strongly suggests the possible existence of non-uniform flow distribution across the filter. Filter performance tests conducted in this test housing were reported to be deviating from the design performance and were also inconsistent when conducted at different test locations. Hence a study of the flow fields inside the test housing was performed, the results of which have been presented in the present report.

A further study has been done to evaluate the effect of this non-uniform velocity distribution on the performance of the filter in terms of its efficiency. Various theories have been proposed which relate the filtration efficiency to parameters such as aerosol velocity through the filter media, aerosol particle size, filter media properties, etc. Experimental data acquired by different researchers to study such dependence is also available. All of the theories and experimental data is presented for filters that are subjected to uniform velocity. However most of the filters in reality operate under non-uniform velocity distribution. In the following work, the performance of a filter which is subjected to non-uniform velocity is calculated using available theories and experimental results.

1.2 Literature Review

The initial sections of the following literature review describe the single fiber model for filters. Then the *early theories of filtration,* as classified by Davies (1973), are explained followed by the most important sections which describe various modern theories. Then a few other models which are conceptually different from the single fiber model are discussed. A section is included which describes the models for predicting air

permeability of filter media. Finally pleated air filters which were used in this study and their performance test standards are discussed.

Various types of filtration media (Orr, 1977) are in use to cater to the diverse applications of filtration. The applications vary in the type of fluid being filtered, size and concentration of particles being filtered, expected life of filtration media, etc. Orr has classified the filtration media into eight main categories based on their construction and some of them are described here. Membrane filters which come under the category of porous media are capable of filtering extremely fine particles of the order of 0.005 μm. Woven fabrics are available in a vast variety of constructions and may have natural or synthetic fibers. Loose solids like beds of sand are widely used for water filtration. Metallic filters are also used in the form of perforated plates and woven wires. This study is mainly concentrated on the filtration by nonwoven sheets, especially paper.

The process of filtration occurs as an air-borne particle is effectively intercepted by the filtering media. Different mechanisms have been proposed for different media which are collectively responsible for the filtration.

Paper or cellulose, which is a nonwoven filtering media, consists of fibers of various diameters. The orientation of these fibers, which is not totally random, plays an important part in modeling of filters. If the media, which has a certain thickness, is assumed to be made up of a number of layers of sheets, then the fibers tend to lie in the planes of these sheets. Hence the preferred direction of orientation of the fibers is across the flow. This orientation of the fibers takes place due to the inherent characteristics of the manufacturing process. The fibers are however oriented randomly in these planes. Since the filter media is formed by a number of such overlapping layers, the pores so formed are of random size.

1.3 Mathematical Modeling of Filter Media

The above mentioned randomness in construction of filter media makes it difficult to mathematically model a filter. Models have been proposed with varying degrees of complexity and still none of them are generic models. While some models are suitable for one particular type of filtration application the others are suitable to some other types of filtration (ASHRAE Handbook, 1992; Cheikhrouhou and Sigli, 1988; Davies, 1973; Flagan, 1988; Grant et al., 1989; Harrop and Stenhouse, 69; Huang and Garcia-Maura, 1986; Ingham and Hildyard,1989; Jaroszczyk et al., 1993, 1991; Lee and Liu, 1982b; McLaughlin et al., 1986; Orr, 1977; Payatakes 1979; Ramarao and Tien, 1988; Rodman, 1979; Rodman and Lessman, 1988; Seo and Kim, 1992; Shapiro et al., 1991; Spielman 1977; Wake and Brown, 1991; Wilkinson and Davies, 1985; Zia et al., 1990). One model based on the fundamentals of fluid flow is the single fiber representation consisting of the study of flow fields around a single fiber and filtration by it. Another model consists of representing the filter by a series of parallel, capillary tubes representing the pores. Many more models exist but only a few of the models most suitable for fibrous filters were studied and are presented here in brief.

1.3.1 Single Fiber Representation of a Fibrous Filter

Let Po represent the porosity of the media and c the packing density, solidity or volume fraction of the fibers. Both, Po and c, are dimensionless quantities. If L is the length of all fibers in a unit volume of the media, then assuming the media to consist of fibers of uniform radius R, we can relate Po and c as (Davies, 1973)

$$c = \pi R^2 L = 1 - Po. \tag{1.1}$$

The collision efficiency of aerosol particles with single fibers, which is represented by E, is dependent upon both particle and fiber parameters. The single fiber representation takes into consideration the effects of the surrounding fibers and packing density of the

media by considering a cell surrounding the fiber, the diameter of which is related to the packing density of the filter, c. The single fiber representation must be distinguished from the isolated fiber representation. In isolated fiber theory the mutual effects of the surrounding fibers and the effect of packing density are not taken into consideration.

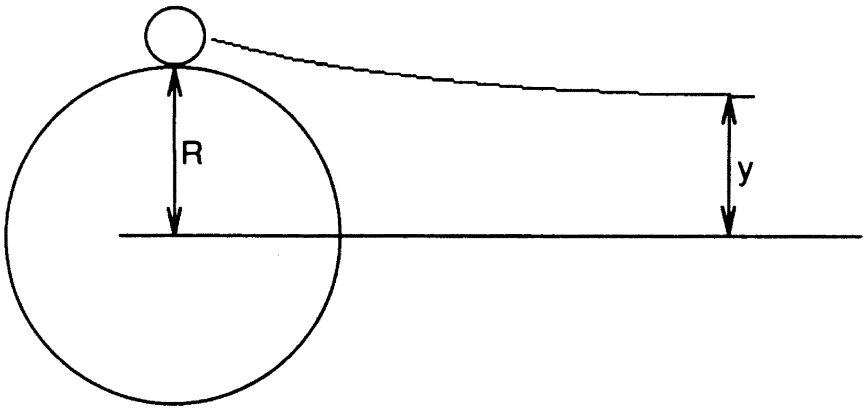

Figure 1.1 A Limiting Trajectory at a Distance y From the Axis of Fiber (Davies, 1973)

Consider a particle of radius a in a flow field across a fiber of radius R as shown in Figure 1.1. If the particle is assumed to have no mass, it will follow the streamlines perfectly. On the other hand, if a particle is considered to possess some mass, it will deviate from the streamline because of the inertial force acting on it. In either case, a particle of radius a is said to be intercepted by a fiber if the particle center approaches the fiber surface within a distance of $a/2$. Consider a streamline at a limiting distance y from the axis of the fiber such that a particle following this streamline is just intercepted by the fiber. It is clear that a particle following any streamline at a distance greater than y from the axis will escape without being captured by the fiber. This streamline is called the

limiting streamline and the trajectory followed by the particle is called the *limiting* or *critical trajectory*. Davies (1973) proposed that in spite of the tortuous path the fluid flow follows, the flow is still laminar. Turbulent wakes past an isolated fiber begin at a Reynolds number of about 50. In case of filters where the fibers are grouped, the transition to turbulent flow will take place at even higher Reynolds number. Hence E can be given by the ratio of the two limiting streamlines of the flow, $2y$, to the fiber diameter, $2R$. The underlying assumption being that all intercepted particles are necessarily captured or perfect adhesion occurs. In fact, the single fiber efficiency, E, is the product of the collection efficiency, E_c and adhesion efficiency, E_a, (Stenhouse, 1975),

$$E = E_c E_a. \tag{1.2}$$

A lot of research work has been done in the field of collection efficiency, but the knowledge regarding the adhesion efficiencies is still inadequate. The forthcoming discussion is mainly regarding the prediction of the collection efficiency or, to put it in other words, it is estimating E with the assumption that E_a is equal to unity which is nothing but perfect adhesion. However, it must be noted that this assumption holds good only for very low velocities. As the aerosol particle velocities increase, the kinetic energy of the particles also increase. When such particles collide with a fiber, the forces of adhesion are overcome by the forces of rebound and drag, and the probability of the particle intercepted by the fiber being captured reduces. Typical characteristics of E, E_a, and E_c presented by Stenhouse (1975) are shown in Figure 1.2.

For a filter of thickness, h, the concentration of aerosol entering, n_o, and the concentration leaving the filter, n, are related by (Davies, 1973)

$$\frac{n}{n_o} = \exp(-EL2Rh). \tag{1.3}$$

This equation assumes that E does not change as the air passes through the filter which means that the filter must be homogenous and the dust is monodisperse.

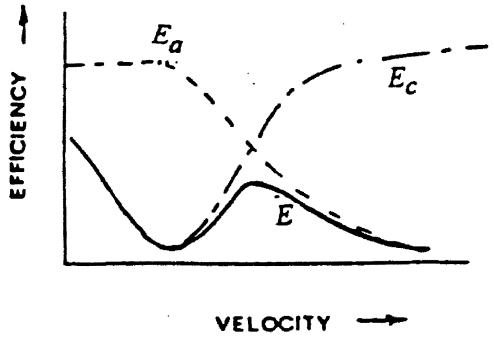

Figure 1.2 Typical Characteristics of E, E_a, and E_c (Stenhouse, 1975)

The penetration, P, of a filter is defined as

$$P = \frac{100n}{n_o}. \tag{1.4}$$

Equations (1.3) and (1.4) can be combined, so that

$$E = \frac{-\ln \frac{P}{100}}{2LRh}. \tag{1.5}$$

Assuming that the flow is uniformly distributed over the filter, which is not the case in reality as is shown by the measurements presented later, equation (1.5) would give E if penetration is known. Davies (1973) has pointed out that experimental values of single fiber efficiencies, E, found in such a way are always lower than those calculated from accurate theories of aerosol particle deposition on single fibers. This is because of the deviation of the actual filter structure from what is assumed. The deviations are mainly that the fibers in an actual filter always appear in clusters and are not always in a plane at right angles to the flow direction.

The value of the term LR in (1.5) can be obtained by using the formula

$$LR = \frac{\rho_F}{w}\sum_i L_i R_i \tag{1.6}$$

where L_iR_i is found by measuring the product of length and fiber radius of each fiber in a sample weighing w, and ρ_F is the weight of fiber in unit volume of filter. Note that L_i, which is the total length of a fiber of radius R_i, is different from L.

Another useful form of equation (1.3) has been presented by Flagan (1988)

$$\eta_e = 1 - \frac{n}{n_o} = 1 - \exp[-\frac{2cEh}{\pi(1-c)R}] \tag{1.7}$$

Where, η_e is the overall efficiency of a small element of a filter having thickness h.

1.4 Three Important Mechanisms of Filtration

Various mechanisms are responsible for filtration in any given medium. The properties of the fluid being filtered, characteristics of the aerosol particle and the filter medium determine which mechanism will be predominant in the filtration process. The three most commonly encountered filtration mechanisms are diffusive filtration, interception and inertia. Each of these mechanisms and a few others are very briefly introduced in this section.

The process of filtration in which the particles settle on the fibers mainly due to Brownian motion is known as *diffusive filtration*. Diffusive filtration is dominant in filtration of particles smaller than 0.2 μm. In filtration due to *interception*, a particle following the streamline of the fluid flow gets attached to the fiber and is separated from the flow. The mass of a particle is totally ignored when interception alone is considered. Davies (1973) defined interception as "It is a purely geometrical effect; if the center of the particle passes the surface of the fiber at a distance less then the particle radius, collision, or filtration, results". If a particle with inertia deviates from the streamline due to its inertia effects and gets intercepted by a fiber, then the mechanism is said to be *inertial*

impaction. When inertial impaction alone is considered, the mass of a particle is assumed to be concentrated at a point and the size of the particle is ignored. Hence, calculation of inertial impaction efficiencies constitutes the calculation of the path followed by the center of a particle, without any consideration of the size of the particle, and to see if the surface of the fiber intercepts this path. *Inertial interception* accounts for both; interception and inertial impaction, by considering the mass and size of the particle.

The various mechanisms of filtration discussed so far and a few other mechanisms involved in gas filtration are shown schematically in Figure 1.3. Gravitational settling occurs in large particles as result of low velocities. The electrostatic forces of repulsion or deposition occur when the particles and the fibers are charged relative to each other. These electrostatic forces play important roles in filtration by charged media.

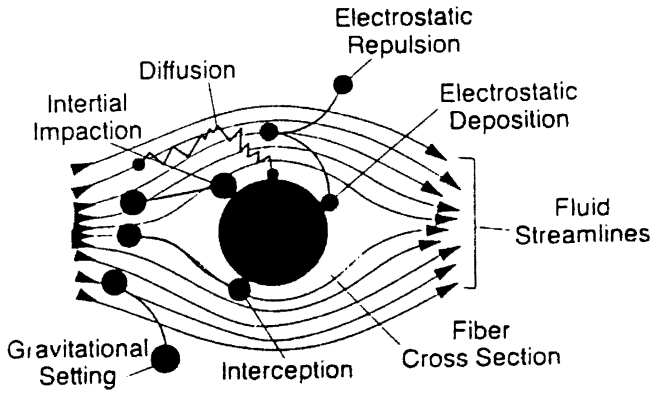

Figure 1.3 Particle Capture Mechanisms in Gas Filtration (Grant et al., 1988)

1.5 Early Theories of Filtration

The early theories of mechanical filtration have been summarized by Davies (1973). Some of the early theories were based on ideal and inviscid flow. The most important drawback of the early theories is that they failed to realize the existence of the inertial mechanism of filtration. The existence of the maximum penetrating diameter particle came to be known during World War I which lead to the theory of inertial impaction. The existence of the maximum penetrating diameter particle was appropriately interpreted to be an indication of the existence of two mechanisms of filtration, one of which enhanced filtration at higher velocities while the other mechanism enhanced penetration at higher velocities.

1.5.1 Concept of Stokes Number

Davies (1973) summarized the work of Albrecht in 1931, who solved the equations of flow of air past a transverse cylinder in two dimensions and the equations of the particles being filtered. The flow was considered to be inviscid and ideal. The dimensionless parameter, which is now known as *Stokes number*, was used in solving these equations. Stokes number is the ratio of the kinetic energy of a particle moving with a velocity, u, to the work done against viscous drag by moving the particle over a distance, R, in a fluid or air. The Stokes number as defined by Davies (1973) is given by

$$St = \frac{mu}{6\pi a\mu R} = \frac{2a^2\rho u}{9\mu R} \tag{1.8}$$

where ρ is the density of the particle and μ is the dynamic viscosity of the fluid. Flagan (1988) considers a slip correction factor also in the Stokes number, in which case the Stokes number, St_c, is defined as

$$St_c = \frac{a^2\rho C_c u}{9\mu R}. \tag{1.9}$$

where, C_c is the slip correction factor and is approximately given by Flagan as

$$C_c = 1 + 1.257Kn \qquad \text{For a}>>\lambda \quad (1.10)$$

where Kn is the Knudsen number ($=\lambda/a$) and λ is the mean free path of the fluid.

In the above equations the velocity of a fluid outside a filter media, V, is different than its velocity u inside the media and the two velocities are related through the packing density by

$$u = \frac{V}{(1-c)} \qquad (1.11)$$

Also, the Reynolds number in the case of filters is always defined with respect to the velocity inside the media, u, and the fiber diameter, $2R$. Hence,

$$\mathrm{Re} = \frac{2Ru}{\nu} \qquad (1.12)$$

1.5.2 Kaufmann's Theory

According to Davies (1973), Kaufmann in 1936 was the first person to come up with the idea of the particle deposition by the combined effects of Brownian motion and inertia. Kaufmann's mathematical formulation of the filter is based upon the limiting streamlines, as shown in Figure 1.1. It was already shown that the single fiber efficiency, E, is given by y/R. For parallel fibers in a plane, separated by a mean distance of $2sR$ between the centers, the efficiency of the sheet of fibers, E_{Sheet}, is given by

$$E_{Sheet} = \frac{y}{sR} = \frac{E}{s}. \qquad (1.13)$$

From experimental data the penetration of a real filter was related to the pressure drop across it, Δp, by the equation

$$P = C^{\sqrt{\Delta p}} \qquad (1.14)$$

where C is a dimensionless fraction. The penetration of a filter consisting of i number of layers, each of which obey equation (1.13), was given by

$$\frac{P}{100} = \left[\ 1 - \frac{E}{s}\ \right]^{\sqrt{i}}. \tag{1.15}$$

In the above equations, s is calculated by equating the mass of filter and mass of fibers, so that

$$\pi R^2 \rho_f = 4 s^2 R^2 \rho_F \tag{1.16}$$

or

$$s = \sqrt{\frac{\pi}{4}\frac{\rho_f}{\rho_F}}. \tag{1.17}$$

The value of E in equation (1.15) is dependent upon three filtration mechanisms *viz.* interception, inertial deposition, and diffusion. Kaufmann demonstrated for the first time the dependence of the these three mechanisms on the particle size and air flow. However, Davies has pointed out how his theory was incorrectly founded upon ideal fluid flow. The ideal flow assumes that the flow is dominated by the inertia of the fluid and viscous effects play a negligible part. In a filter with fibers of diameter 20 μm and air velocity of 15 cm/sec, the Reynolds number for flow around the fiber is on the order of 0.2. At these Reynolds numbers, the viscous effects are dominant near the solid boundaries and the flow is no longer ideal. This affects the upstream distance from the fiber at which the streamlines begin to diverge, which is shown in Figure 1.4. This departure from ideal flow diminishes the effect of interception, inertial impaction, and Brownian deposition, with the magnitude of inertial impaction being the one that is affected the most. This is because the gradual change in the direction of the streamlines in a viscous flow reduces the centrifugal force acting on the particle.

Davies (1973, pp. 19) first used viscous flow theory in 1940 and compared the results to practical measurements. He observed that penetration of carbon smoke particles, having diameters on the order of 0.16 μm, was related to flow velocity, V, by

$$\ln P = A - \frac{B}{V} \tag{1.18}$$

where A and B are constants. It is seen from the equation that an increase in velocity would result in an increased penetration for these small particles. This indicates the dominance of the diffusive filtration mechanism in filtration of small particles. This argument is strengthened by the fact that velocity has a favorable effect on inertial filtration and that interception filtration is independent of velocity.

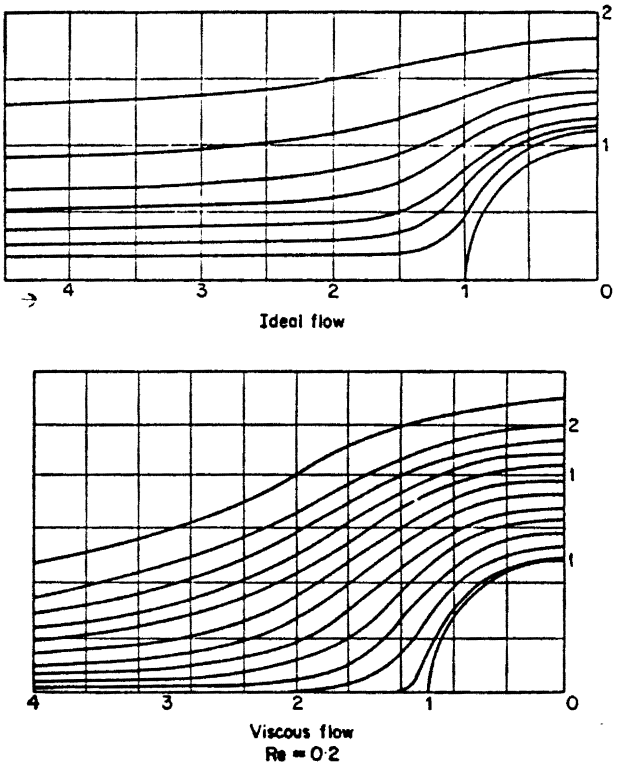

Figure 1.4 Stream Lines of Ideal and Viscous Flow Past a Cylinder (Davies, 1973)

1.5.3 Langmuir's Theory

Langmuir (Davies, 1973) proposed a theory of diffusion and interception mechanisms based on viscous fluid theory for isolated fibers. He rejected the possibility of filtration by inertia. Lamb's hydrodynamical equations were used to solve the flow field around an isolated fiber. The isolated fiber theory gave a non-linear dependence of flow resistance on the velocity. In practice the flow is influenced by the neighboring fibers and the flow resistance is linearly dependent on the velocity. Langmuire's equations were solved numerically to predict filter efficiencies for various particle sizes, fiber diameters, filter packing densities, areas, thicknesses, resistances and rates of flow. The existence of maximum penetrating particle diameter was clearly demonstrated. Filters could be entirely designed for a specific performance based on this theory and the particle size that would result in the maximum penetration could be predicted.

1.5.4 Development of the Concept of Particle Inertia

Davies (1973) pointed out that Langmuir rejected the theory of inertial deposition because he did not observe an increase in filtration with an increase in the face velocity. He also points out that it is very difficult to detect the existence of most penetrating particles in highly efficient filters. However, in 1949, Davies himself demonstrated experimentally that inertial deposition takes place under suitable conditions. His experiments demonstrated that the size of the largest particle which penetrated the filter decreased with increasing velocity, indicating that the particles of this size and over were deposited due to inertia.

Hence in 1952 Davies (1973) proposed a theory combining the effects of inertia, interception and diffusion. He used the single fiber efficiency formulation given in equations (1.1) to (1.6) with the addition of a term for taking into account the settling due to gravity. The equation he proposed is

$$E = \frac{y}{R} + \frac{u_g}{\pi V} \tag{1.19}$$

the second term on the right hand side of the equation representing the gravitational settling. u_g represents the rate of falling of the particle. The term y/R represents the combined efficiency due to the three mechanisms

$$\frac{y}{R} = [\ I + [\ 0.25 + 0.4I\ ]Pa - 0.0263IPa^2\ ][\ 0.16 + 1009c - 17c^2\ ] \tag{1.20}$$

where I (= a/R) is the interception parameter and the value of Pa is given by

$$Pa = \frac{2\rho a^2 u}{9\mu R} + \frac{\nabla}{a^2 u R} \tag{1.21}$$

where ∇ is the diffusion coefficient of aerosol particles.

The term in I of equation (1.20) was obtained for a flow with a Reynolds number of 0.2 past a cylinder.

Davies cautions about the exactness of predicting the value of E from the semi-empirical formula (1.20) because the fibers in the filter are not laid quite perfectly. However, he mentions that they show the correct trends of variation due to interception, a/R, packing density, c, and net action of diffusion and inertia, Pa.

Davies has obtained the following condition of maximum penetration when velocity is varied by differentiating equation (1.21) with respect to velocity and keeping a constant

$$u = \left[2.5118 \times 10^9 a^2\ \right]^{-1}. \tag{1.22}$$

Davies comments that the task of obtaining the maximal penetration where the particle size is varied and the velocity is kept constant is difficult. Davies says "In general the most penetrating particle size decreases rapidly when either the fiber radius or the air velocity is increased, thus confirming that diffusion is of little importance in filters of coarse fibers (>5 μm radius) and high-velocity loading (>5 cm/sec)".

1.6 Modern Concepts of Filtration

The first stage in the development of filtration theory was completed with the realization of the existence of inertial deposition. Davies (1973) argues that the efficient filters which have very fine fibers and which use high velocities made it difficult for inertial deposition to be noticed. This is better explained in the following section on isolated fiber theory. The sections to follow describe various models representing the three mechanisms viz. interception, inertial impaction and diffusion filtration.

1.6.1 Isolated Fiber Theory

As mentioned earlier, isolated fiber theory does not account for the effects of the neighboring fibers. Hence according to Davies (1973), this theory is accurate only for mechanisms like diffusive deposition and electrical deposition, which operate very near to the fiber surface. Also they are not accurate for higher values of Reynolds number. Finally Davies argues against this theory for filters because the isolated fiber efficiencies depend on the Reynolds number whereas the single fiber efficiency equations are independent of the velocity.

Davies (1973) used the diagrams (Figure 1.5) produced by Emi and Yoshioka's work on isolated fiber theory to explain the domains in which the various filtration mechanisms are dominant. Davies cautions that though these results do not predict accurately the results in a filter, the trends remain the same. It will be seen from Figure 1.5a that diffusion is dominant in the region of small particles, inertial deposition in the range of high velocity with large particles, and gravitational settling in the range of low velocities with large particles. Interception is seen to be occurring in nearly all the regions which would indicate independence of velocity. Figure 1.5b shows that for particles of radius smaller than 0.3 μm, the isolated fiber efficiency, E', decreases with increasing velocity, whereas for larger particles, the efficiency first decreases and then increases with

increasing velocity showing a maximum velocity of penetration. Also at a given velocity, the existence of a maximum penetrating particle radius is clearly seen in Figure 1.5b. For example, at a velocity of 4 cm/s the efficiency is minimum for particles with radius 0.45 μm, which is the maximum penetrating particle radius.

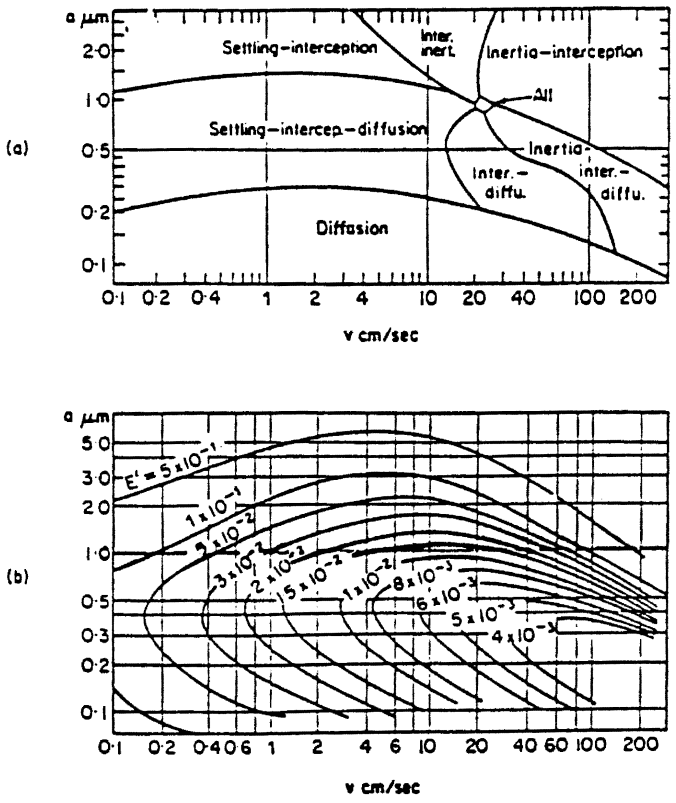

Figure 1.5 Filtration by an Isolated Fiber of Radius 5 μm Over a Range of Air Velocity (a) Domains in Which Various Mechanisms of Filtration are Predominant (b) Efficiency Contours (Davies, 1973)

1.6.2 The Kuwabara Model of Flow Cells

Kuwabara (Davies, 1973) came up with a model to represent the filter in the form of flow cells consisting of parallel fibers randomly distributed. Each fiber of radius R was assumed to be surrounded by an imaginary cell of radius b such that $c=R^2/b^2$. Navier-Stokes equations for flow transverse to the cylinders were used with the boundary condition of zero velocity at the surface of the fibers and zero vorticity on the surface of the cylinder, b. Kuwabara obtained the following solutions for the stream function, ψ, and radial and tangential velocity resolutes, u_r and u_θ respectively.

$$\psi = \frac{ur}{2Ku}\left\{2\ln\frac{r}{R} - 1 + c + \frac{R^2}{r^2}\left(1-\frac{c}{2}\right) - \frac{c}{2}\frac{r^2}{R^2}\right\}\sin\theta$$

$$\frac{1}{r}\frac{\partial\psi}{\partial\theta} = u_r = \frac{u}{2Ku}\left\{2\ln\frac{r}{R} - 1 + c + \frac{R^2}{r^2}\left(1-\frac{c}{2}\right) - \frac{c}{2}\frac{r^2}{R^2}\right\}\cos\theta \qquad (1.23)$$

$$-\frac{\partial\psi}{\partial r} = u_\theta = \frac{u}{2Ku}\left\{2\ln\frac{r}{R} + 1 + c - \frac{R^2}{r^2}\left(1-\frac{c}{2}\right) - \frac{3c}{2}\frac{r^2}{R^2}\right\}\sin\theta$$

where $$Ku = -\frac{1}{2}\ln c - \frac{3}{4} + c - \frac{c^2}{4}.$$

It was observed that these equations were independent of viscosity and Reynolds number. Kuwabara's model for the flow field is very important in the study of filtration models because most of the models are based on Kuwabara's flow field model.

1.6.3 Interception

Davies (1973) derived a formula for interception efficiency, E_R, based on Figure 1.1 and the solutions to the Kuwabara equations. Hence using

$$E_R = \frac{y}{R} \qquad (1.24)$$

and equations (1.23) the interception efficiency can be given by

$$E_R = \frac{1}{2Ku}\{2(1+I)\ln(1+I) - (1+I) + (1+I)^{-1} + c(2I^2 - \frac{I^4}{2} + \frac{I^5}{2} + ...)\} \qquad (1.25)$$

Lee and Liu (1982b) also derived an equation for interception efficiency from the Kuwabara flow equation, which is given by

$$E_R = \frac{1+I}{2Ku}[2\ln(1+I) - 1 + c + (1+R)^{-2}(1-\frac{c}{2}) - \frac{c}{2}(1+I)^2]. \qquad (1.26)$$

An approximate form of equation (1.26) is also presented which was obtained from the approximation for the stream function and is given by

$$E_R = \frac{1-c}{Ku}\frac{I^2}{1+I} \qquad (1.27)$$

Lee and Liu found that the filtration efficiencies given by equation (1.27) were in good agreement with Lee's (1977) and their own experimental data.

It is observed that equations (1.25), (1.26), and (1.27) are all independent of velocity. Davies explains the dependence of the interception efficiency on the ratio, *a/R*, with the help of hydrodynamic interference theory. For small values of *a/R*, the hydrodynamic interference between the fiber and the aerosol particle is very small. As the diameter increases, hydrodynamic repulsion increases and interception becomes less effective. In the limiting case, for very fine fibers and large particles, the particles are unaffected by the flow pattern around the fiber and there is no hydrodynamic influence. Hence the interception efficiency becomes independent of the flow pattern and

$$E_{R\lim} = 1 + \frac{a}{R} \quad \text{where } a >> R. \qquad (1.28)$$

The same thing is true for particles with high inertia and small values of *a/R*. The hydrodynamic forces would be less effective on these small particles and further, the high inertia particles would continue to travel in the same direction under the influence of inertia. In other words, these high inertia particles are less likely to follow the flow streamlines as compared to a low inertia particle. Hence the hydrodynamic effects would be suspected to be less effective on dust particles which have high inertia, when compared with other aerosol particles like fluid droplets which have low inertia. Consider a limiting

case in which a particle has a very high inertia, such particles would practically have a straight-line trajectory with no deviation. If such a particle is released from a distance of y from the center line of the fiber, such that, $y>R$ but $y<R+a$, the particle would still be collected by the fiber and the resulting single fiber efficiency ($=y/R$) would be greater than one. It may noted that the distance of particle release, y, is measured up to the center of the particle. Single fiber efficiencies of such very high inertia particles, given by equation (1.28), may reach any value greater than one depending on the ratio a/R.

As explained above, physically, equation (1.28) would mean that the single fiber collection efficiency can be greater than unity. This is possible either if $a>>R$ or if the particle inertia is very large. In terms of the particle trajectory, this would mean a particle is intercepted even when injected at a distance y in Figure 1.1, such that, $y>R$. It may further be noted that, although the single fiber efficiency exceeds a value of one, the efficiency of a media of a certain thickness, which is given by equation (1.7), would never exceed unity.

For large values of a/R, such that $a+R>b$, the center of the particle passes outside the Kuwabara zone of radius b. Hence the equation (1.25) is no longer reliable for such large particles.

1.6.4 Interception With Particle Inertia

Inertia of a particle enhances the filtration due to interception. As mentioned earlier, in the limit, for very heavy particles, irrespective of the particle size, the interception efficiency is given by equation (1.28). According to Davies (1973), there are two methods of finding the interception efficiency with particle inertia. The analytical method, involving simultaneous solution of equations of motion of the fluid and the particle, necessitates many simplifying assumptions making it applicable only in a narrow range of particle size. The second method consists of calculating stepwise, the trajectory of individual particles

which are released in the flow at different distances from the stagnation point at a certain distance upstream of the flow. If the critical trajectory is taken as the trajectory of a point mass which touches the fiber surface, then we obtain the efficiency due to inertia alone. Instead if the critical trajectory of a particle of finite mass and size is considered, then interception is automatically included within the analysis.

Stechkina et al. (1969) used the first method described in the previous paragraph to obtain an equation for inertial interception. The assumptions made make this method applicable only for particles near the maximum penetrating size. Mathematically the restriction on particle size is given by $St << 1$, which means the particle inertia must be very small. They proposed a formula for combined interception and inertia efficiency, E_{RI}, as

$$E_{RI} = E_R + \frac{J}{2Ku} St \qquad (1.29)$$
$$= E_R + E_I$$

where Ku is given in equation (1.23) and J is a complicated integral approximated by $J = (29.6 - 28c^{0.62})I - 27.5I^{2.8}$ for $0.01 \le I \le 0.4$ and $0.0035 \le c \le 0.111$.

When it comes to particles other than the most penetrating ones, the above mentioned equation (1.29) does not apply. The only method applicable to these high inertia particles is the second method mentioned in this section, which consists of calculating the trajectory of a particle step by step. Harrop and Stenhouse (1969) have presented some results using the Happel cellular model. The Happel cellular model is similar to the Kuwabara model described in section 1.6.2 except for the boundary condition of zero shear stress at the surface of the cell of radius b. Harrop simplified the Navier-Stokes equation using the assumption of creeping flow. Flagan (1988) has presented his results based on the Kuwabara model for a large number of cases in the form of the graph shown in Figure 1.6.

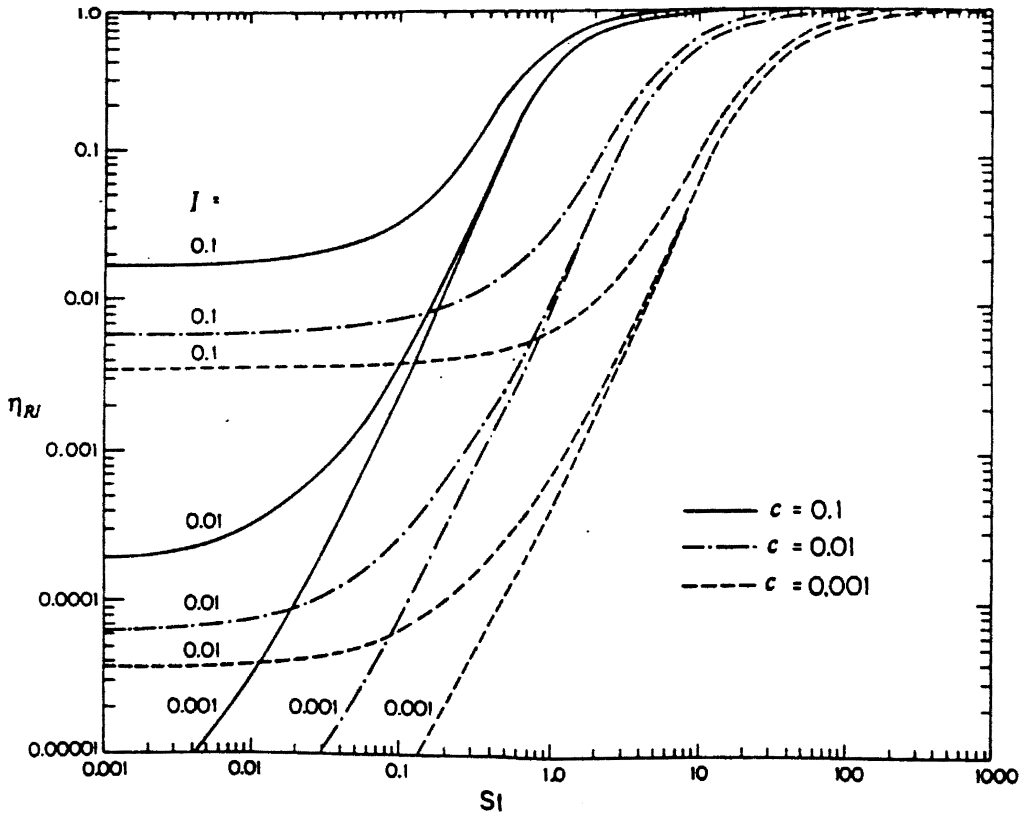

Figure 1.6 Single Fiber Efficiencies for Inertial Interception (Flagan, 1988)

Jaroszczyk and Wake (1991) have suggested an equation for inertial impaction based on the equation proposed by Landahl and Herrmann (1948). This equation can be combined with the equation (1.27) to obtain a combined equation for inertial interception. An aerosol particle may be captured either by interception or by inertial impaction. The probability that the particle will not be captured by either of the mechanisms is given by

$$(1-E_{RI})=(1-E_R)(1-E_I) \tag{1.30}$$

or

$$E_{RI}=1-(1-E_R)(1-E_I). \tag{1.31}$$

The equation suggested by Jaroszczyk and Wake (1991) for E_I is as follows

$$E_I = \frac{St_c^{\,3}}{St_c^{\,3} + 0.77St_c^{\,2} + 0.22}. \tag{1.32}$$

Hence, by substituting E_R and E_I from equations (1.27) and (1.32) into equation (1.31), the single fiber efficiency due to inertial interception can be given by

$$E_{RI} = 1 - \{1 - \frac{1-c}{Ku}\frac{I^2}{1+I}\}\{1 - \frac{St_c^{\,3}}{St_c^{\,3} + 0.77St_c^{\,2} + 0.22}\}. \tag{1.33}$$

Figure 1.7 and 1.8 are plots of E_{RI}, as a function of Stokes number, as given by equation (1.33) for various values of packing density, c, and interception parameter, I, respectively. These graphs compare very well with the results presented by Flagan (1988) which are reproduced in Figure 1.6. The curves for c = 0.1 are very similar in both the cases. For lower values of c, the two results do not agree for St above 0.5. However the trend is followed by the equation (1.33). The expression for E_I given by equation (1.32) is independent of c and I, while the expression for E_R given by equation (1.27) is independent of St. The inertial impaction is very insignificant compared to interception at very low values of St. Hence the E_{RI} curves for various values of c and I on a log-scale plot are wide apart at lower values of St. The independence of E_R on St makes E_{RI} curves horizontal at low values of St. The independence of E_I on c and I brings the E_{RI} curves close together at higher values of St. At very high values of St, all the particles released from the upstream projected area of the fiber are captured due to inertial impaction. Hence the single fiber efficiency due to inertial impaction reaches a value of nearly one, and the E_{RI} remains constant at value slightly larger than one. When inertia and interception are considered, particles released from upstream, even at a distance of a from the fiber projected area, are captured. This will result in E_{RI} values slightly larger than one.

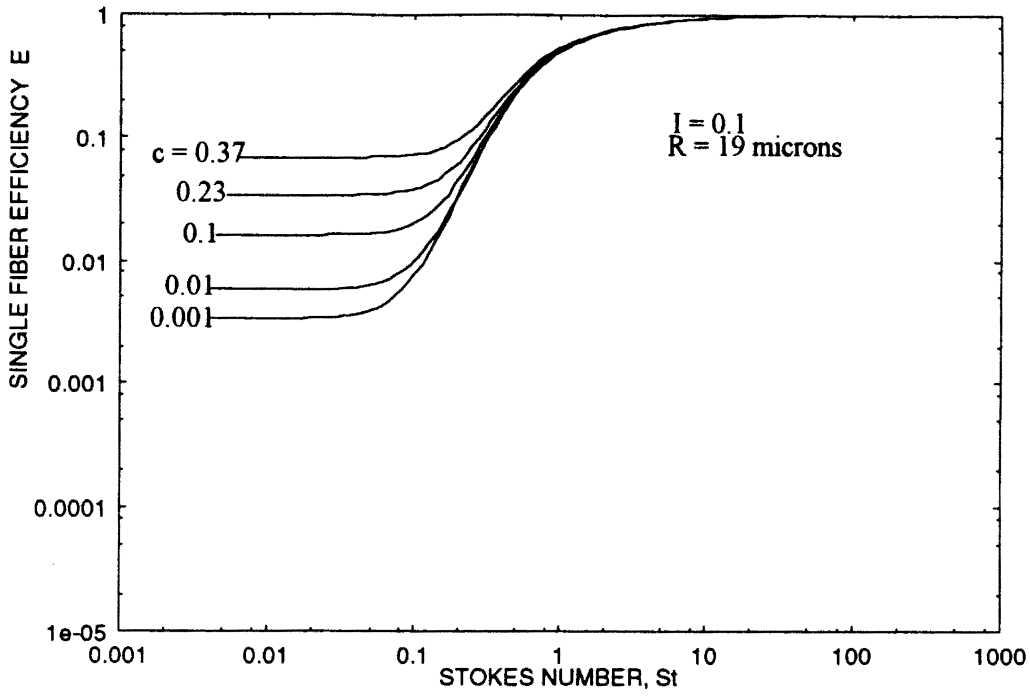

Figure 1.7 Single Fiber Efficiency Due to Inertial Interception Given by Equation (1.33) for Various Values of Filter Packing density, *c*

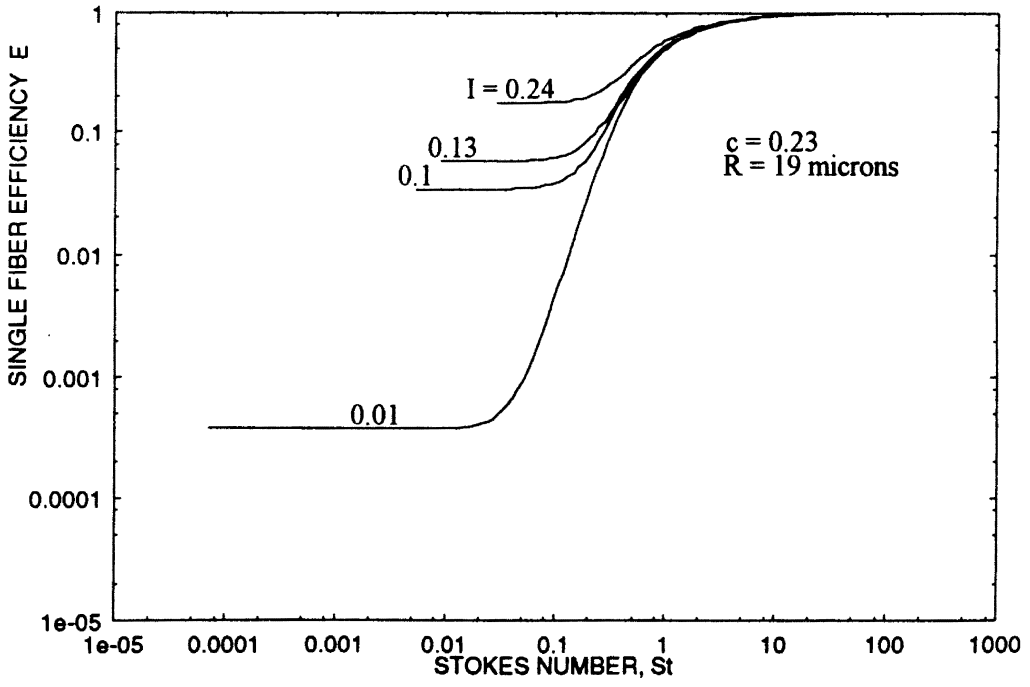

Figure 1.8 Single Fiber Efficiency Due to Inertial Interception Given by Equation (1.33) for Various Values of Interception Parameter, *I*

Ptak and Jaroszczyk (1982) have proposed an equation for inertial interception for an isolated fiber. Their analysis included the effects of particle adhesion and bouncing by including a few coefficients in the isolated fiber efficiency which were based on comparison with experimental data. The isolated fiber efficiency is given by

$$E_{RI} = [\frac{(St - 0.75\,\mathrm{Re}^{-0.2})^2}{(St + 0.4)^2} + I^2][\frac{90.6}{c^{0.3}(St\,\mathrm{Re}_p)^{0.68} + 190}]. \qquad (1.34)$$

The curves generated by equation (1.34) are shown in Figure (1.9). The curves overlapped for various values of c, although c appears in equation (1.34). Although the equation does not consider the diffusional filtration, the curve shows the portion with negative slope, which could correspond to diffusional filtration. However, as explained in the next section and as shown in Figure 1.10, the diffusional filtration efficiencies cannot be so large. Hence the equation (1.34) is not suitable for particles with Stokes number below about one.

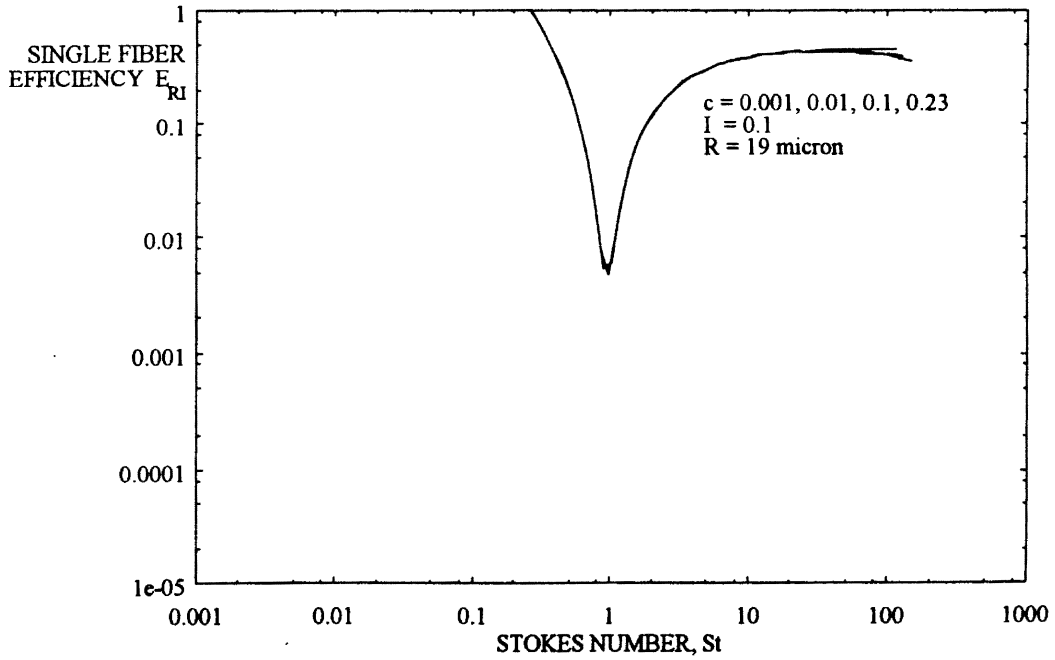

Figure 1.9 Single Fiber Filtration Efficiencies Given by Equation (1.34)

1.6.5 Brownian Motion and Diffusion

The Brownian motion of particles smaller than 0.2 μm causes diffusive deposition on fibers. This deposition increases with decrease in particle diameter. Concentration gradients are necessary for diffusion to occur. Concentration gradients are generated when the particles moving due to Brownian motion strike a fiber surface and remain adhered to it due to forces of attraction like van der Waals forces. This attachment, according to Davies (1973), depletes the concentration in the aerosol very close to the surface of the fiber to zero. This generates a concentration gradient and a flow of particles is established from the region of high concentration to the region of lower concentration.

The diffusion mechanism was studied by Davies (1973) with the help of the following differential equation of diffusion for moving air, in cylindrical coordinates, when there is no change in concentration with time or for a steady state system.

$$u_r \frac{\partial n}{\partial r} + \frac{u_\theta}{r} \frac{\partial n}{\partial \theta} = \nabla \left(\frac{\partial^2 n}{\partial r^2} + \frac{1}{r} \frac{\partial n}{\partial r} + \frac{1}{r^2} \frac{\partial^2 n}{\partial \theta^2} \right). \tag{1.35}$$

When this equation is non-dimensionalized, a dimensionless term called the *Peclet number*, *Pe*, is introduced. Peclet number is a measure of the ratio of the transport of the particles by fluid motion to the transport by particle diffusion.

$$Pe = \frac{2uR}{\nabla} \tag{1.36}$$

Very high concentration gradients are believed to exist near the fiber surfaces forming very thin concentration boundary layers in this region. Deposition due to diffusion takes place in this region only. The size of this diffusion layer, δ, can be calculated from equations (1.35) and (1.23). Usually δ is very small compared with R.

Stechkina and Fuchs (1966) presented their numerical solutions in the form of a curve fit which had three terms representing E_D, E_R, and a combined term $\overline{E}_{DR}$ which represents the efficiency in a transition range where both, diffusion and interception, are

responsible for particle capture. Hence the total efficiency due to interception and diffusion was given by

$$E_D + E_R + \overline{E}_{DR} = 2.9Ku^{-1/3}Pe^{-2/3} + 0.62Pe^{-1} + E_R + 1.24Ku^{-1/2}Pe^{-1/2}I^{2/3} \qquad (1.37)$$

where E_R, is given by equation (1.25) and I is the interception parameter given by the ratio a/R. The value of the interception parameter, I, in the above equation should not exceed 0.5 and value of Pe should be larger than 200.

Lee and Liu (1982b) have pointed out that in the above analysis by Stechkina, the effects of filter packing density were neglected and hence c does not appear in equation (1.36). The assumption of neglecting c is acceptable for filters with low packing density, but will not give acceptable results for densely packed filters. Lee and Liu have used the same analysis as Stechkina, but instead of neglecting c, they used an approximation for taking into account the effect of c. They proposed the following equation for diffusive filtration,

$$E_D = 2.6(1-c)^{1/3}Ku^{-1/3}Pe^{-2/3}. \qquad (1.38)$$

Lee and Liu combined equations (1.27) for E_R and (1.38) for E_D by simply adding the two equations without considering the combination term $\overline{E}_{DR}$ as considered in equation (1. 37), to come up with an equation for filtration efficiency due to diffusion and interception. Lee's equation for diffusion and interception efficiency is given by

$$E_D + E_R = 2.6(1-c)^{1/3}Ku^{-1/3}Pe^{-2/3} + \frac{1-c}{Ku}\frac{I^2}{1+I} \qquad (1.39)$$

In doing so he assumed that only either one of the two mechanisms will be active at any given time. His equations compared very well with his experimental results (Lee and Liu, 1982a). The curves represented by equation (1.39) are shown in Figure 1.10.

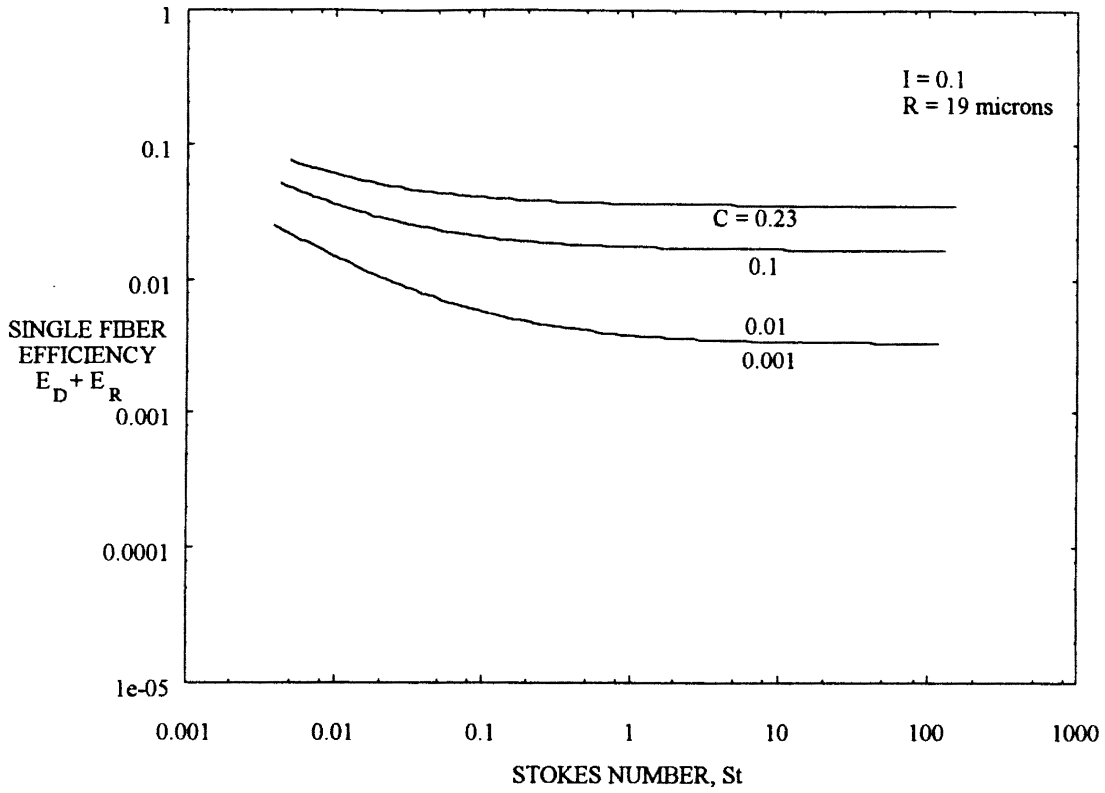

Figure 1.10 Curves for Single Fiber Efficiencies Due to Diffusion and Interception Given by Equation (1.39)

1.6.6 Overall Mechanical Efficiency of Filters

The overall efficiency of a filter due to the mechanical deposition of particles is due to the combined effect of the three mechanisms *viz.* inertia, interception, and diffusion. According to Davies (1973) there is no fundamental theory to combine different equations obtained for each of the mechanisms, each of which was based on different assumptions. However, since equation (1.37) represents efficiencies due to diffusion, interception and the combination of both, it is reasonable to add the inertial impaction efficiency, E_I, given in equation (1.29) to equation (1.37) to obtain the overall efficiency as a function of particle size. Hence the overall single fiber efficiency can be given by

$$E = E_D + \overline{E}_{DR} + E_R + E_I. \tag{1.40}$$

Filter efficiency can than be obtained by using equation (1.7). The following limitations on the above equations apply. The Reynolds number of flow past the fiber must be small.

$$\mathrm{Re} = \frac{2uR}{\nu} < 0.5. \tag{1.41}$$

Then the ratio a/R should be smaller than 0.5, and if a/R is smaller than 0.1 then St should exceed 0.3.

The analysis presented by Lee and Liu (1982b) shows that the diffusional mechanism is predominant only when the value of Pe is lower than 10^6. Also, according to Davies (1973), diffusion is predominant only when the particle size reduces below 0.2 μm. If diffusional filtration is not predominant in a particular system of filtration, then efficiency equation given by equation (1.33), which accounts just for inertial interception, can be used. One example is the automotive air filtration system, where most of the particles are sized above 0.5 μm and Pe values exceed 10^6.

1.6.7 Other Factors Affecting Filtration

It was pointed out earlier that gravitation also plays an important part in filtration, but only in a particular region of particle size and velocity. From Figure 1.5 it can be said that gravitational settling is predominant only if the particle size is larger than 1.5 μm and the aerosol velocities are lower than 4 cm/s. It will be seen in the forthcoming analysis that most of the filter operates at velocities higher than 0.12 m/s. Calculations indicate that for particles of size 20 μm have a settling velocity of about 0.035 m/s. Hence a few particles, sized larger than 20 μm and having velocities lower than about 0.12 m/s, fall in a range where separation can take place due to gravitational settling. In this study the effects of gravitational settling have been neglected as they are not very significant.

Effects due to changes in temperature are also expected to affect filtration by way of changing the viscosity and Brownian motion. Viscosity, and hence filtration, is affected by pressure changes also. However, for our experimentation the variations in temperature and pressure would not have any appreciable affect. Hence these variations are not of prime importance.

1.7 Particle Capture in Liquids

There are important similarities and dissimilarities involved in the capture of gas-borne particles and liquid-borne particles. But the difference in the conditions of liquid filtration and air filtration makes it impossible to apply most of the theories, which are developed around liquid filtration, to air filtration. Typical applications of air filtration require very high flow rates and least possible pressure drops. Whereas in liquid filtration, relatively higher pressure drops are acceptable. To withstand these higher pressures, liquid filtration media are much thicker in comparison to the air filtration media.

Spielman (1977) has studied the similarities and dissimilarities in liquid and gaseous filtration in an attempt to apply theories developed for air filtration to liquid filtration. It is pointed out that inertial impaction is not of as much importance in liquids as it is in gases. This is because the differences in densities of particle and fluid are lower in liquids and the higher viscosity of liquids oppose the particle deviation from streamlines. There exist basic differences in representation of the collectors in the models for liquids and solids. Fibers of air filters are very sparsely packed, typically 90% voids, making an array of cylinders a suitable form of representation in modeling. Liquid filters which consist of beds of granular media are more appropriately represented by spherical collectors.

Spielman (1977) has expressed his concern over the exactness of the applicability of different models for air filters. He has also mentioned that the data itself which is used

to compare the models has a lot of variations, which makes validation of models very difficult. Spielman has recommended Natanson's solution for the E_D

$$E_D = 3.64 A_F^{1/3} Pe^{-2/3} \tag{1.42}$$

and $$E_R = 2 A_F I^2 \tag{1.43}$$

where $$A_F = 1/\left[-\ln c - 3/2 + 2c - c^2/2\right] \tag{1.44}$$

and I is the interception number which is less than one. Spielman does not give any formula for inertial deposition and the combined effects of different mechanisms.

1.8 Other Work

McLaughlin et al. (1986) solved the Navier-Stokes equations and the equations of the particle by the finite element method and obtained the interception efficiency for particle collection on a row of cylinders. The comparison presented with the experimental data of Fan and Gentry, indicated that McLaughlin's model represented the real data better than other models in the comparison, which employed potential flow equations. This was especially true at low Stokes and Reynolds number where viscous effects are dominant.

Cai and Peterson (1989), in an attempt to simplify numerical calculations, proposed a model using honey-comb structure with hexagonal cells instead of the circular unit cell as was used by Kuwabara. The trajectories of the particles were calculated in the Kuwabara flow field. Linear regression was performed on the numerical calculation results for monodisperse particles in a flow field, described by Cai and Peterson as "constant flow field", to arrive at an empirical formula for cell efficiency.

Ingham et al. (1989) used the Boundary Element Method to find the trajectories of particles through a cascade of cylinders for both large (potential) and small (creeping) Reynolds number flows. Potential flows were taken into consideration because the air filters in internal combustion engines operate at Reynolds number larger than one. The entrance effects are taken into account using an asymptotic approach on the upstream side

to reduce the computations. Once the streamlines were obtained, the Stokes equations for the particle paths were integrated numerically using a finite difference method to obtain the collection efficiency. The results are compared graphically by Ingham with those of McLaughlin et al. (1986) and Choudhary. This method is claimed to be easily applicable to fibers of various cross sections, and as an example, results are obtained for an elliptical fiber with creeping flow.

Shapiro et al. (1991) calculated characteristic filtration lengths of fibrous filters collecting spherical sub-micron size particles using a finite element method for a range of particle sizes and filtration parameters. Leers' semi-empirical formulation for filter efficiency using the characteristic filtration length, l_f, was used.

$$\eta = 1 - \exp(-h/l_f) \tag{1.45}$$

The characteristic filtration length was found to be an intrinsic filter-thickness-independent physical quantity from Shapiro's earlier research papers. Diffusion and interception mechanisms are considered for the entrainment of the particle along with the consideration of re-entrainment of particles. The medium was represented by circular cylinders arranged in a spatially periodic square array. The dispersion/reaction model of aerosol filtration by porous filters proposed by Shapiro and Brenner was used to calculate the characteristic filtration length which is given by

$$l_f = \overline{U}^* / \overline{K}^* \tag{1.46}$$

where $\overline{U}^*$ is the aerosol's Darcy-scale mean speed (a scalar quantity), and $\overline{K}^*$ is the volumetric aerosol deposition-rate coefficient. A convection-diffusion equation for a conserved species with its boundary conditions is given and solved to obtain the necessary values of the two parameters $\overline{U}^*$ & $\overline{K}^*$. The effects of the changes in the direction of approach of the flow with respect to the array were also studied. Based on comparison with the theoretical model proposed by Stechkina *et al.* (1969), Shapiro claims that his model is a better representation of the experimental data given by Lee (1977).

Shapiro and Brenner (1989) have proposed another method to calculate the characteristic filtration length using equation (1.46) mentioned earlier. The values of the two parameters $\overline{U}^*$ and $\overline{K}^*$ were evaluated from the flow fields calculated in several simple arrays of circular cylinders. The flow fields in the arrays was calculated only for a representative unit cell by using a finite element method. It is claimed that this method eliminates the need for many *ad hoc* assumptions made in the classical theory.

Wake and Brown (1991) performed experimental measurements of filtration efficiency of porous foam filters using monodisperse aerosols and found that the measurements agree very closely with the gravitational settling theory at low velocities and with the inertial impaction theory at higher velocities. Layer efficiencies, α, are obtained from the measured penetration of the aerosol through a depth, t, by using the equation

$$P = \exp(-\alpha t). \tag{1.47}$$

Due to the problem associated with the generation of large sized monodisperse particles, polydisperse particles were used to measure the penetration of larger particles. The efficiencies in this regime were observed to be higher than those observed for the monodisperse regime. The values agree well when compared with a simple model of particle capture.

The following table summarizes the various available equations for single fiber efficiencies.

TABLE I

SINGLE FIBER EFFICIENCY EQUATIONS

Eq. No.	Equation	Reference	Comments
1.19	$E = [I + (0.25 + 0.4I)Pa - 0.0263IPa^2]$ $[0.16 + 1009c - 17c^2] + \frac{u_g}{\pi V}$ where $Pa = \frac{2\rho a^2 u}{9\mu R} + \frac{\nabla}{a^2 u R}$	Davies (1973)	Semi-empirical formula. Includes efficiency due to the three mechanisms - diffusion, interception & inertia. Last term represents gravitational settling.
1.25	$E_R = \frac{1}{2Ku}\{2(1+I)\ln(1+I) - (1+I) + (1+I)^{-1} + c(2I^2 - \frac{I^4}{2} + \frac{I^5}{2} + ...)\}$	Davies (1973)	Includes interception only.
1.26	$E_R = \frac{1+I}{2Ku}[2\ln(1+I) - 1 + c + (1+R)^{-2}(1 - \frac{c}{2}) - \frac{c}{2}(1+I)^2]$	Lee & Liu (1982b)	Includes interception only.
1.27	$E_R = \frac{1-c}{Ku}\frac{I^2}{1+I}$	Lee & Liu (1982b)	Approximate form of Eq. (1.26). Includes interception only.
1.29	$E_{RI} = E_R + E_I = E_R + \frac{J}{2Ku}St$ where E_R is given by eq. (1.25) and J is a complex integral approximated by $J = (29.6 - 28c^{0.62})I - 27.5I^{2.8}$ for $0.01 \le I \le 0.4$ and $0.0035 \le c \le 0.111$	Stechkina et al. (1969)	Considers inertial interception. Applicable near the maximum penetrating size or mathematically the restriction is $St << 1$.
1.32	$E_I = \frac{St_c^{\,3}}{St_c^{\,3} + 0.77St_c^{\,2} + 0.22}$	Jaroszczyk & Wake (1991)	Empirical formula for an isolated fiber inertial efficiency.
1.31	$E_{RI} = 1 - (1 - E_R)(1 - E_I)$ where E_R is given by eq. (1.27) and E_I is given by eq. (1.32)		This combined equation give results comparable to those presented by Flagan (1988).

TABLE I (Continued)

1.34	$E_{RI} = [\frac{(St - 0.75\mathrm{Re}^{-0.2})^2}{(St + 0.4)^2} + I^2]$ $[\frac{90.6}{c^{0.3}(St\,\mathrm{Re}_p)^{0.68} + 190}]$	Ptak & Jaroszczyk (1982)	Considers inertial interception by isolated fibers. Includes effects of particle adhesion and bouncing by including empirical coefficients.
1.36	$E_D + E_R + E_{DR} = 2.9Ku^{-1/3}Pe^{-2/3} + 0.62Pe^{-1} + E_R + 1.24Ku^{-1/2}Pe^{-1/2}I^{2/3}$ where E_R is given by eq. (1.25)	Stechkina & Fuchs (1966)	Considers diffusion and interception and a term for the combination of diffusion and interception. Limitations are $I < 0.5$ and $Pe > 200$. Effects of c are neglected.
1.39	$E_D + E_R = 2.6(1-c)^{1/3}Ku^{-1/3}Pe^{-2/3} + E_R$ where E_R is given by eq. (1.27)	Lee & Liu (1982b)	Considers diffusion and interception but no combined term. Effects of c not neglected.

1.9 Air Permeability of Filters

Air permeability is a convenient way of measuring and comparing the air flow resistance offered by different filter media. Mathematically, the quantity $Q_F h/A\,\Delta p$ represents the permeability of a filter and results from the dimensional analysis of the equations involved in the resistance of filters (Davies 1973). A common measure of air permeability is the *Frazier Air Permeability*, which is defined as (Apfeld, 1993) the number of ft³/minute of air passing through one ft² of media of given thickness at a Δp of 0.5 inches of water column.

Dimensional analysis for filters (Davies, 1973) shows that

$$f\{\frac{\Delta p A R^2}{\mu Q h}, \frac{QR\rho}{A\mu}, c, \frac{\lambda}{R}\} = 0. \qquad (1.48)$$

The first dimensionless group in the above equation represents Darcy's law if the other three groups are kept constant. The second group represents the Reynolds number of flow past the fibers and the last group represents the Knudsen number. For filters that obey Darcy's law, the first group which represents the resistance, is independent of the Reynolds number and the Knudsen number. Hence,

$$\frac{\Delta pAR^2}{\mu Qh} = f(c). \tag{1.49}$$

Various forms of the function in equation (1.49) have been proposed by different theories. Davies (1973) has compared the theories proposed by Happel and Kuwabara with empirical results of Davies. Both, Happel's and Kuwabara's theories give results close to the experimental results, and it would be difficult to decide which one of the two is a better model. Since the Kuwabara flow field is used for Lee's efficiency equations, which are used in the forthcoming calculations of pleated filter efficiency, this theory is used to relate the air resistance and c. According to Kuwabara theory,

$$\frac{\Delta pAR^2}{\mu Qh} = \frac{8c}{-\ln c + 2c - c^2/2 - 3/2}. \tag{1.50}$$

1.10 Pleated Air Filters

Although most of the available theories and experimental data apply to a plane sheet of filtering media, most of the filters found in practice are pleated to increase the effective surface area of filtration. There are two types of configurations in pleated filters; one is a panel filter and the other is the circular filter. The work presented here is carried out with regard to the panel filter.

Obviously, the pleating of the filter media introduces many complexities in the design and analysis of the filters. One approach widely used in the industry in designing of the filter is to base the calculations on the surface area of the media without any

consideration of the effects of pleating. It is known for sure that the velocity distribution within the pleats is non-uniform but the extent of the non-uniformity has not yet been studied adequately. One of the first attempts to study this has been done by Cai (1993) using computational fluid dynamics to calculate the flow velocities within a single pleat of the filter. The study suggests that the flow does not enter the media at right angles, and also provides the direction and the magnitude of the velocity changes within the pleat. For the conditions calculated, the velocity variations over the pleat are from 85% to 125%, where 100% is the velocity corresponding to uniform distribution over the pleat. It was felt that for the present work, the consideration of these small scale non-uniformities of velocity within the pleats would be too complex. Hence it is assumed that the velocity is uniform within the pleats which would still give sufficiently accurate effects of the large scale non-uniformity of the flow distribution over the filter.

1.11 Filter Testing Standards

For a given application, the filter may be manufactured by a different manufacturer, or the same manufacturer may use different raw materials, or for some other reason filters manufactured under the same specification could vary from one to another. This necessitates the formulation of a uniform filter testing code which should enable the measurement and comparison of various performance characteristics of the filters. In the case of automotive air filters, the Society of Automotive Engineers (SAE) specifies a standard air filter test code under SAE J726 "Air Cleaner Test Code".

1.11.1 Air Cleaner Test Code (SAE J726)

Testing equipment and procedures for measurement of air flow restriction or pressure drop, dust collection efficiency, and dust holding capacity for dry and oil bath air filters are specified in this test code. A schematic of the test set-up is shown in Figure

1.11. It consists of a dust metering and feeding mechanism, a test housing, a device to measure the pressure differential across the filter housing, an absolute filter housing, flow rate measuring system, flow control system and a blower.

The two grades of standard dust used are called *fine* and *coarse*. Particle size distributions of these dusts are given in Appendix B. A drawing of the panel filter universal test housing is given in Figure 1.12. Typically the test consists of injecting dust onto the filter until the pressure across the filter reaches a specified amount, called the *terminal restriction* or *pressure drop*. The amount of dust accumulated during this period gives the dust holding capacity. The dust that escapes the test filter is captured by the absolute filter. Filtration efficiency can be arrived at by weighing the amount of dust captured by the filter and that escape into the absolute filter.

1.12 Summary

Out of the various models available for representing a filter, the single fiber model is applicable to a wide range of filter and aerosol systems. The Kuwabara model for the flow field is widely used to represent the flow around the fiber. Air flow resistance in the form of air permeability for filters can be obtained from these flow field models by simple equations. Once the flow field is established, the single fiber efficiencies of two of the three significant filtration mechanisms, *viz.* diffusion filtration and interception filtration, can be represented by simple equations like those given by Lee and Liu (1982b). The third mechanism, inertial impaction, cannot be represented by simple equation, but the efficiencies must be calculated for each individual case by computing the critical trajectory of the particle. It was shown in the earlier sections that a fairly good approximation of the inertial impaction efficiencies can be obtained by the empirical formula given by equation (1.32). The filter efficiency and single fiber efficiency are correlated by a fairly simple and straight forward equation (1.7). All other approaches of finding the filter efficiency tackle

problems of very low packing density filters and low Stokes number aerosol particles. These results are difficult to extend to filters of higher packing density and particles with high Stokes number. Hence the single fiber model is the most appropriate model to present the filter efficiencies as a function of filter and aerosol particle characteristics.

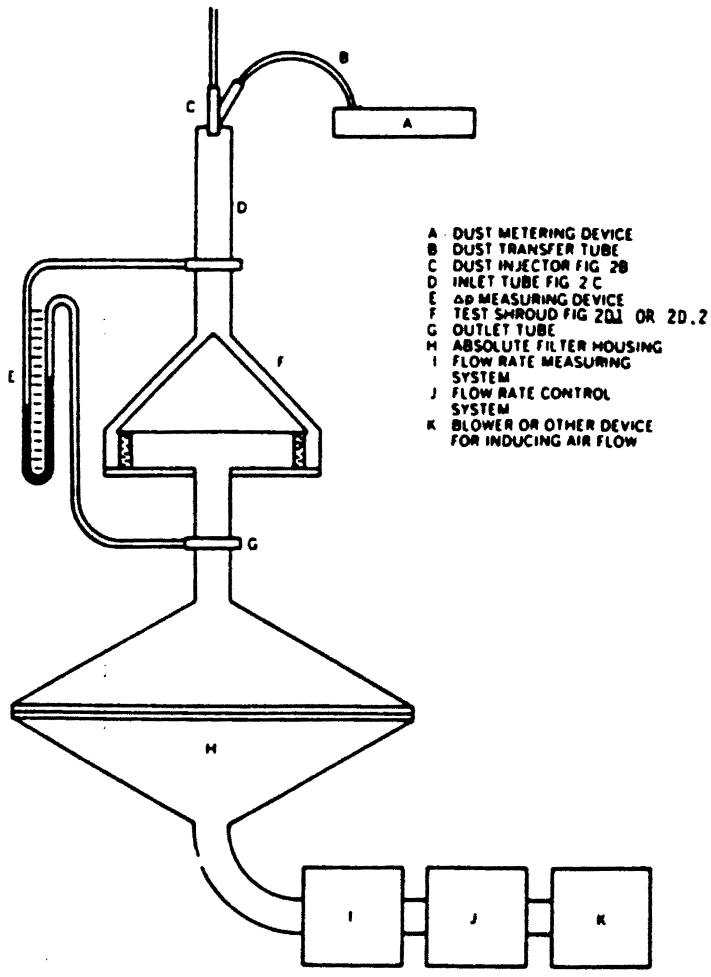

Figure 1.11 Efficiency/Capacity Air Filter Element Test Set-up as per SAE J726 Standards

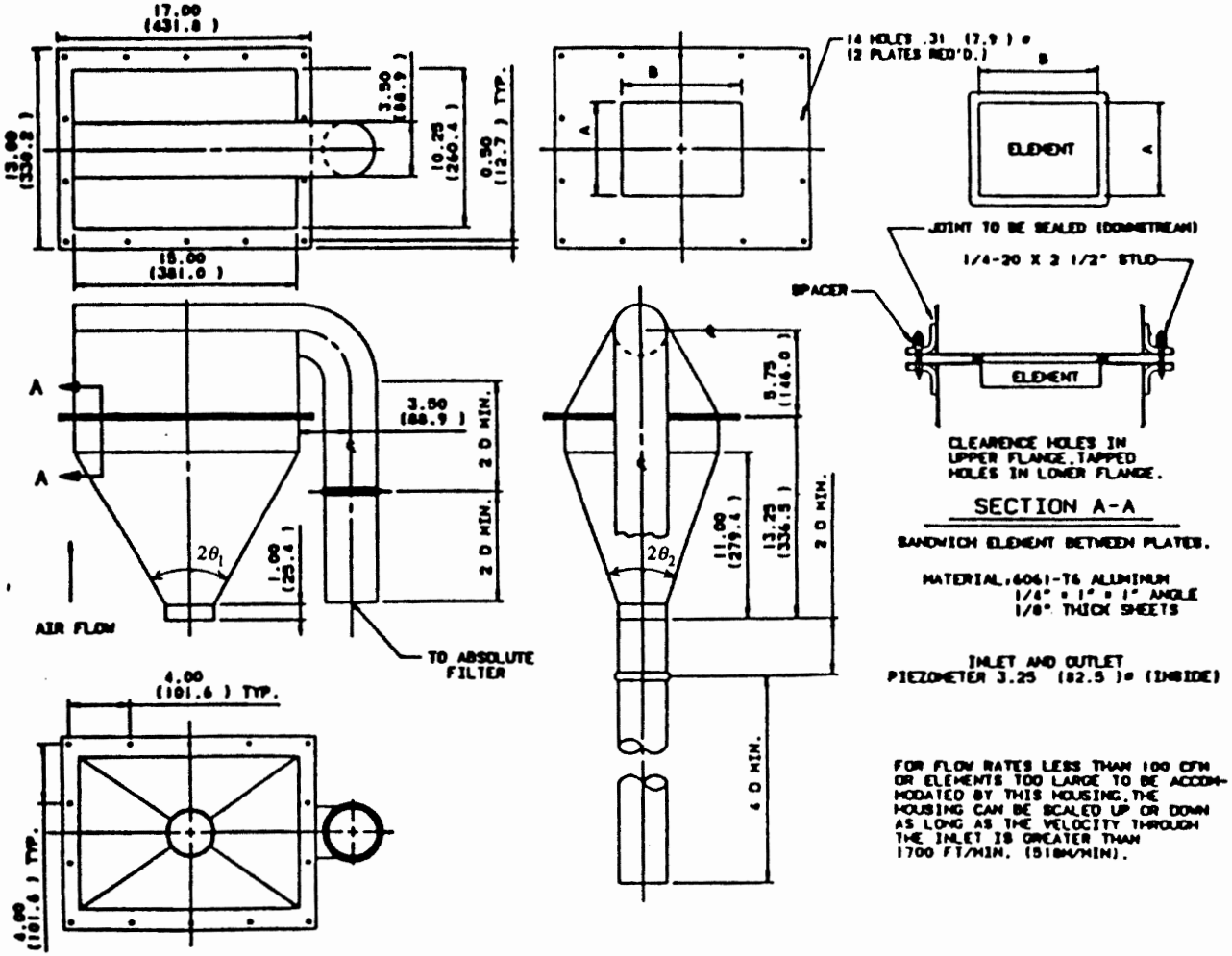

Figure 1.12 Panel Filter Test Housing as per SAE J726 Standards

1.13 Objective of Present Study

The velocity distribution over two different sized pleated air filters mounted in a universal panel filter test housing was obtained by performing experimental measurements. The velocities were found to be non-uniform over the filter. The filtration efficiencies of these filters deviate from the design conditions in part due to the non-uniformities in flow distribution. The extent of deviation from the ideal design condition has been predicted by using a filter model discussed in the preceding sections.

CHAPTER II

EXPERIMENTAL SETUP FOR FLOW VISUALIZATION AND VELOCITY MEASUREMENTS

The panel filter universal test housing, shown in Figure 1.12, makes use of a flat-walled diffuser to distribute the flow and the injected dust onto the filter surface area. The two included angles between the diffuser planes for the test housing are $2\theta_1 = 59.8^\circ$ and $2\theta_2 = 37.4^\circ$ (Figure 2.1a) and the ratio $L'/w_1 = 2.86$. Based on the diffuser angle and the ratio L'/w_1 the diffuser could operate in any of the regions indicated in Figure 2.1b. Although this figure is applicable for open ended diffusers with two of the faces parallel to each other and the other two making an included angle 2θ, it is possible to get an idea of the possible regimes of operation of the diffuser in the housing. For the case of $2\theta_1 = 59.8^\circ$ and $L'/w_1 = 2.86$, the flow could be in the region of jet flow, whereas for the case of $2\theta_2 = 37.4^\circ$ and $L'/w_1 = 2.86$, the flow could be in the region of transitory stall. A more appropriate way would be to consider a flat-walled diffuser with an equivalent area change, in which case we have $2\theta=127^\circ$ and $L'/w_1 = 2.86$ which corresponds to a jet flow in Figure 2.1b. Unless the blockage of the exit of the diffuser by the filter holding plate forces the operating regime into the no stall region, separation of the flow near the housing walls can be almost certainly expected to occur. Besides, if the flow rate changes or if the size of the filter changes, the regime of operation of the flow can be expected to change which would eventually alter the large scale flow distribution over the filter. It would be totally unreasonable to compare filters at different flow rates or filters of different size without proper knowledge of the flow distribution. Hence it is necessary to

study the flow distribution inside the test housing. Two different filters at two different flow rates were analyzed using the techniques of flow visualization and detailed velocity measurements. The dimensions of the two filters analyzed are given in Appendix A.

(a)

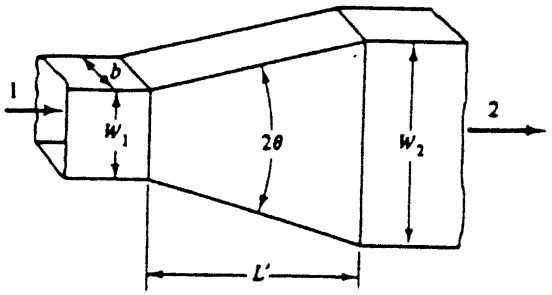

(b)

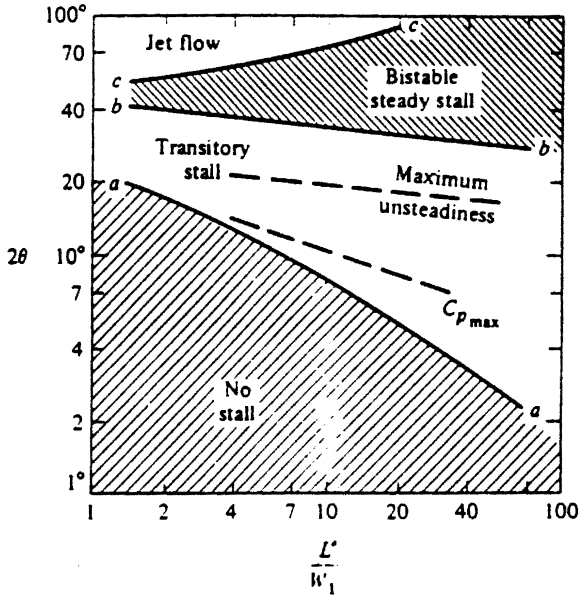

Figure 2.1 Diffuser Geometry and Typical Flow Regimes:
(a) Geometry of a Flat-Walled Diffuser
(b) Flat-Diffuser Stability Map (White, 1991)

2.1 Flow Visualization

Flow visualization techniques provide a very good means of acquiring an insight into the qualitative aspect of the flow field. These techniques provide an overall perspective of the flow field with a setup that requires less time and money. The amount of work put into the setup was even further reduced as the Plexiglas housing was already built with intention of using it for LDV measurements. It was felt that the insight gained into the flow fields from these techniques would complement the conclusions that would be drawn from the detailed measurements performed using LDV. With the above reasons in mind, flow visualization experiments were performed as soon as the Plexiglas housing was constructed, i.e. even before performing measurements with LDV.

A number of complementary techniques were used which were recorded on still photography and video camera. Some of the conventional techniques did not work for this separated and highly turbulent flow. A brief description of each of these techniques follows.

2.1.1 Surface Flow

For a separated flow the shear stress at the separation point is zero. Surface flow visualization makes use of this property in determining whether the flow is separated, and if separated, it can give the location of separation. Since the flow in the diffuser section of the housing was suspected to be separated, we applied this technique on one of the walls of the diffuser which is a part of the housing. The surface on which the flow visualization was to be carried out was leveled horizontally and covered with Tempera paint powder mixed with motor oil or kerosene. The flow was started only after the surface was covered with the pigments. In the portion of the flow where the flow was attached to the wall, the paint was carried in the direction of the flow by the wall shear stress. Since the paint could not be carried further from the point of separation, all the paint accumulated at

the point of separation. Simultaneously the flow evaporated the kerosene leaving behind streaks indicating flow direction and a line indicating the separation. This technique worked very well for high flow rates of the order of 200 SCFM because of high shear stress in the initial portion of the attached flow region. But for a flow rate of 150 SCFM or lower, the wall shear stress was very weak and was not sufficient to mobilize the paint. Kerosene is less viscous than motor oil but still the shear force was not sufficient.

2.1.2 Tufts

Small pieces of tufts when attached to the wall reveal the flow pattern near the wall. The spatial flow pattern can be observed by tufts mounted on a grid. The tuft material must be light weight and flexible enough to bend due the weak shear stress exerted on them. The tuft material used was thin unraveled yarn. It was observed that if thicker tufts were used, the tufts moved only at higher flow rates of about 200 SCFM. Two of the four diffuser surfaces were divided into a grid as shown in Figure 2.2, and tufts were attached at each of the corners using pieces of cellophane tape. The length of the tufts was so chosen that the ends of adjacent tufts would not easily interfere or stick to each other. Another spatial grid was formed by attaching fishing lines on a rectangular steel frame. This spatial grid was placed at a distance of one inch in upstream direction from the edge of filter pleats. The spatial grid indicated the flow directions very close to the filter. Since the flow in most of the region near the wall was separated and unsteady, the tufts kept moving and did not indicate the direction of flow continuously. Still photographs also captured the direction of the tufts which were not a true representation of the average flow direction. So the video clips of each tuft were observed several times in slow motion. The direction of the flow was mapped for all the tufts.

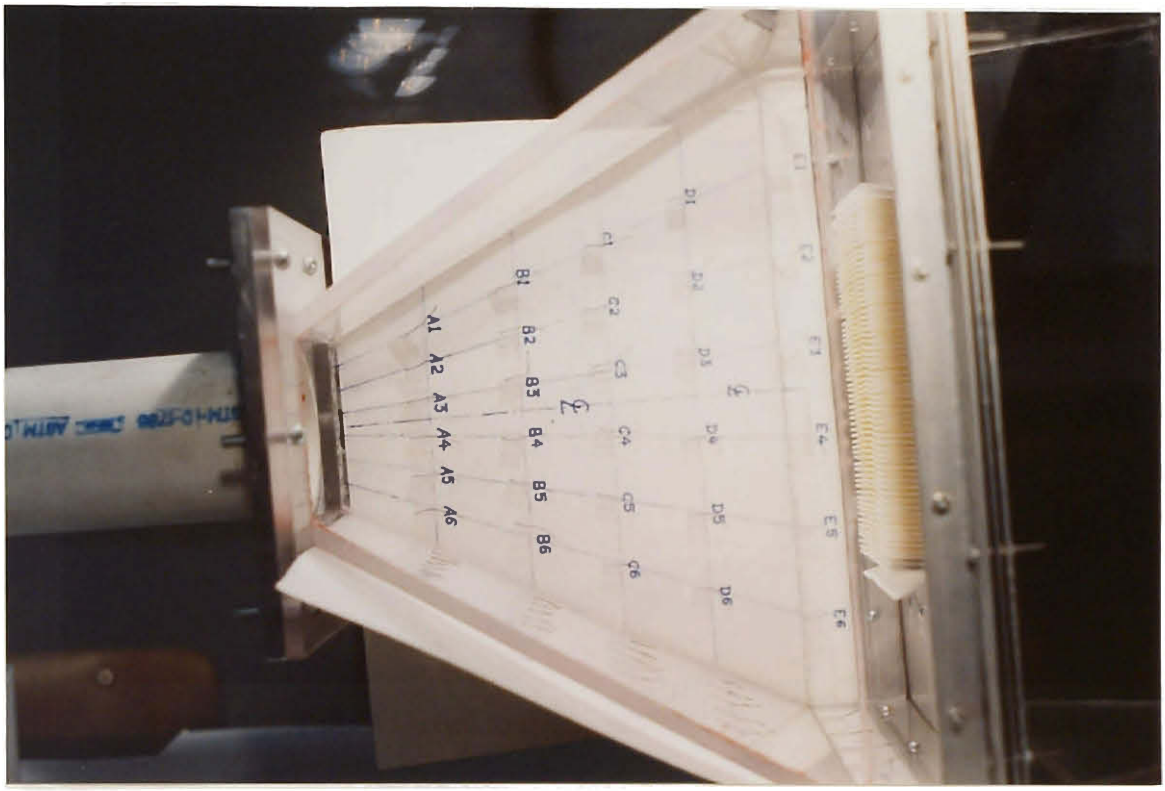

Figure 2.2 Tufts Attached to the Surfaces of the Housing Marked With a Grid

2.1.3 Smoke

Unlike the two techniques mentioned earlier, which can visualize the flow at surfaces and a few other locations only, smoke techniques can visualize the whole body of the flow. The traditional way of smoke visualization consists of injecting kerosene mist smoke into the flow and observing the path the smoke takes. However, due to the turbulent nature of the flow and the recirculation in the housing, this traditional method did not give much useful information. The problem appears to be that the smoke gets mixed very fast into the flow and spreads throughout the housing because of the turbulent and recirculating nature of the flow. Although some flow patterns could be seen by the

eye, nothing could be recorded on a photograph or on video tape. Two other techniques were successfully tried with smoke.

One of the techniques was to intermittently inject smoke into the flow with the smoke flow being almost instantly turned on and after a period 2-3 seconds smoke flow being turned off almost instantly. The other technique used consisted of seeping the flow with the use of small tubes right into the housing and into the separated and recirculating zone near the wall. Since the mixing here is not very vigorous, the housing did not get filled up with smoke, and the flow near the walls of the housing could be visualized.

2.1.4 Intermittent Smoke With Laser Sheet Lighting

A sheet of laser light was used to illuminate a very thin plane inside the housing. When light scattering particles like smoke or water droplets were introduced into the flow, the bright laser sheet showed up the flow pattern in that plane. This laser sheet can be projected vertically or horizontally and at any location in the housing revealing the flow patterns. Laser sheet was produced by passing a laser beam of intensity of nearly 5 watt power through a cylindrical lens. This produced a fan shaped sheet with a thickness nearly equal to the original beam diameter which is a fraction of a millimeter. Continuous smoke injection does not work for the same reasons mentioned in previous section. When the smoke was introduced intermittently, the flow pattern was seen as the portion where the smoke spread, illuminated brightly due to the scattered light. Figure 2.3 shows a photograph of flow visualization with intermittent smoke and horizontal or transverse laser sheet. The flow enters from the top side of the photograph and passes through the filter, seen mounted in the lower portion of the photograph. The transverse laser sheet can be seen intersecting the housing walls and the smoke is seen as bright part in the housing. It is a means to provide instantaneous cross-sectional views of the flow.

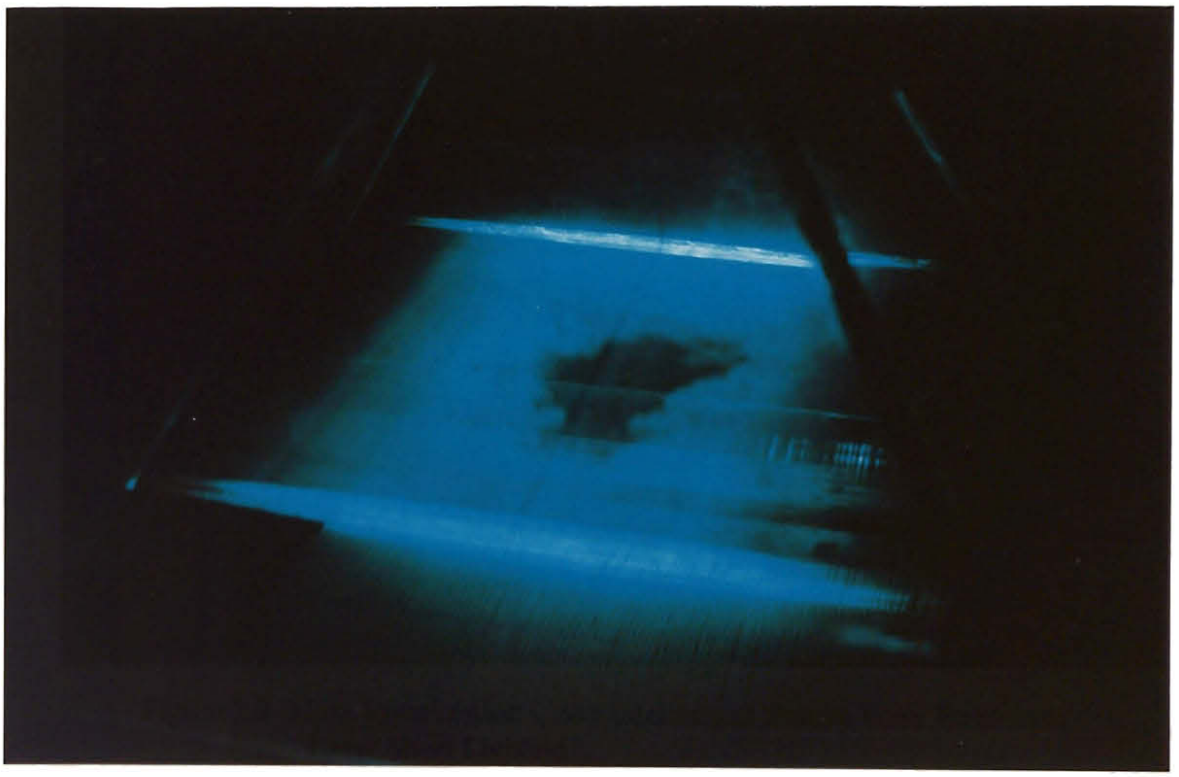

Figure 2.3 Flow Visualization Using Intermittent Smoke With Transverse Laser Sheet Lighting

2.1.5 Water Droplets With Laser Sheet Lighting

When water droplets are introduced into the housing, which is placed in a laser sheet produced as mentioned in the previous paragraph, the path of the water droplets is visible indicating the flow patterns in that plane. An appropriate shutter speed on a still photography camera shows the path followed by a water particle in the form of streaks in the photograph indicating flow patterns. One such photograph is shown in Figure 2.4. Maximum light is scattered in the forward direction of the beam and side scatter is minimum. Hence the droplets are brightest when viewed looking towards the beam

(although directly looking into the beam must be avoided as it will cause a permanent damage to the eye), but flow structure will not be revealed in these edge views. A side view of the flow is most desired, but the light scatter may not be sufficiently strong to reveal the necessary details. Best results can be obtained when viewed or pictured from about 30-45 degrees from the plane of the beam.

Figure 2.4 Flow Visualization Using Water Droplets With Vertical Laser Sheet Lighting

2.2 Velocity Measurements

For a detailed analysis of the flow fields, velocity measurements were performed all across the test housing using a Laser Doppler Velocimeter (LDV). The principle of operation of a LDV and then its application in the velocity measurements inside the test housing is described in the forthcoming sections of this chapter.

2.2.1 Principle of Operation of Two Component Laser Doppler Velocimeter

A Laser Doppler Velocimeter (LDV) is a sophisticated instrument for making velocity measurements. As the name implies, it makes use of a pair of laser beams to measure each component of velocity. Each pair of beams intersects at the focal length of the lens as shown in Figure 2.5, forming interference fringes. The volume in which the interference pattern is established is called the *probe volume*. Velocity measurements are made in this probe volume. A cross-section of the probe volume is shown in the same figure. It consists of fringes evenly spaced at a distance, d. Consider a particle introduced into the flow, sized such that the velocity of the particle is the same as that of the fluid. When this particle passes the probe volume, it scatters light in all directions. This scattered light signal, called the *Doppler signal*, consists of maximas and minimas of intensities which correspond to the bright and dark bands in the fringe pattern. The light signal that is scattered in the backwards direction is collected by the same lens focusing the laser beams, this arrangement is called the *back-scatter arrangement*. The collected Doppler signal is analyzed by the LDV and the frequency, f, of the Doppler signal is obtained. With the fringe spacing, d, known from the laser system's optical properties, the velocity of the particle can be obtained by the relation

$$V_{op} = fd. \tag{2.1}$$

The frequencies of the two beams are shifted by a certain amount so that the fringe pattern is not stationary but is moving through the probe volume at a certain velocity.

This enables the LDV to detect stationary particles and distinguish between positive and negative velocities, a feature that is not provided by hot wire anemometry. A second pair of beams, of different color, is employed in a plane perpendicular to the plane of the first beam pair to obtain the second (perpendicular) component of the velocity. From the earlier discussions, it is clear that if the LDV is to be used, the flow must be seeded with particles that would scatter light. From both optical and fluid mechanics points of view, the seeding particles must be small, on the order of micron size. Analysis shows that such particles follow the fluid flow very closely.

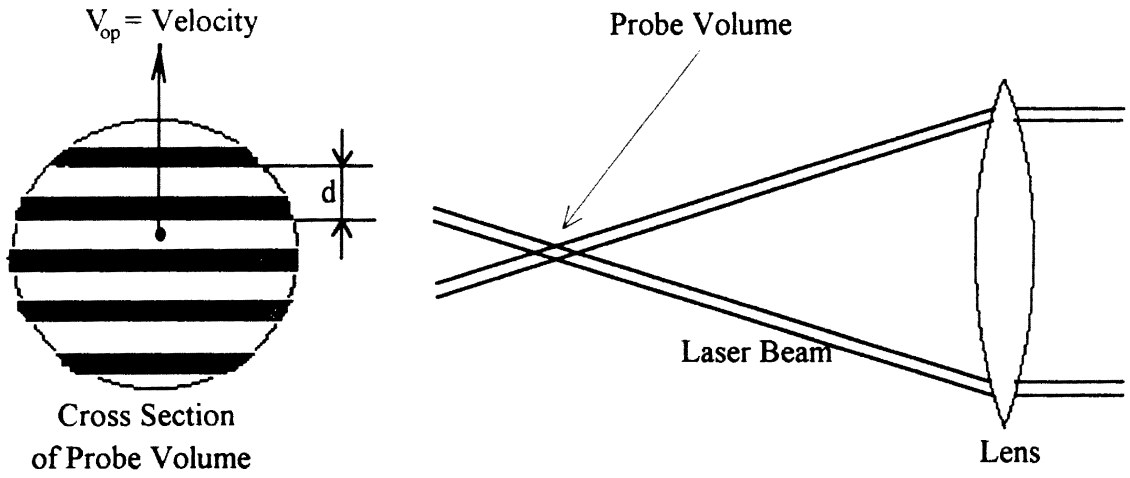

Figure 2.5 A Particle Passing Through the Fringe Pattern

The advantages of using an LDV are that the flow need not be disturbed while making measurements. This does not disturb the flow and the housing in which the measurements are taken need not be drilled or tampered with. Another advantage is that the complex velocity fields inside the housing can be measured without the prior knowledge of the flow directions. Also the back-scatter arrangement, which uses the

same lens for focusing beams and collecting Doppler signal, is very convenient for measurements. The disadvantages of using an LDV are that the flow must be seeded so as to enable velocity measurements. The apparatus in which the velocity measurements are to be done must be constructed of transparent material to pass the laser beam and to receive the signal. Also the optical properties of the construction material must be uniform throughout so that the laser beams are not distorted. The setting of the parameters for Doppler signal processing could be cumbersome sometimes.

2.2.2 Equipment Used

Following is a list of the equipment employed in measurement of flow field inside the test housing.

1) Plexiglas SAE Universal Air Filter Test Housing: A fully transparent housing was constructed from 0.375 inch thick Plexiglas to enable measurements using the laser Doppler velocimeter. The dimensional details of the housing are given in Figure 1.12 which is according to the SAE J726 Air Cleaner Test Code and reproduced from the same. A picture of the final constructed housing is shown in Figure 2.6. The flange is made of aluminum and is bolted to the housing. All other joints were glued and the housing was finally tested for any leaks using soapy water. The inlet pipe has a diameter of 3.5 inches and is 35.0 inches long. Initially for flow visualization techniques, straws and wire mesh was used at the inlet of the tubes to straighten and reduce the turbulence of the entering flow. But during measurements with the laser, the water droplets from the flow seeding settled on these flow straighteners and reduced the seeding. Hence the straws and wire mesh were removed, in which case the inlet flow tube configuration is more close to what is recommended in the SAE standards. The whole test housing was mounted upside-down on a specially manufactured stand which made the measurements and handling a lot

easier. The regular configuration is used only to ensure that dust does not settle on the filter solely as a result of gravity.

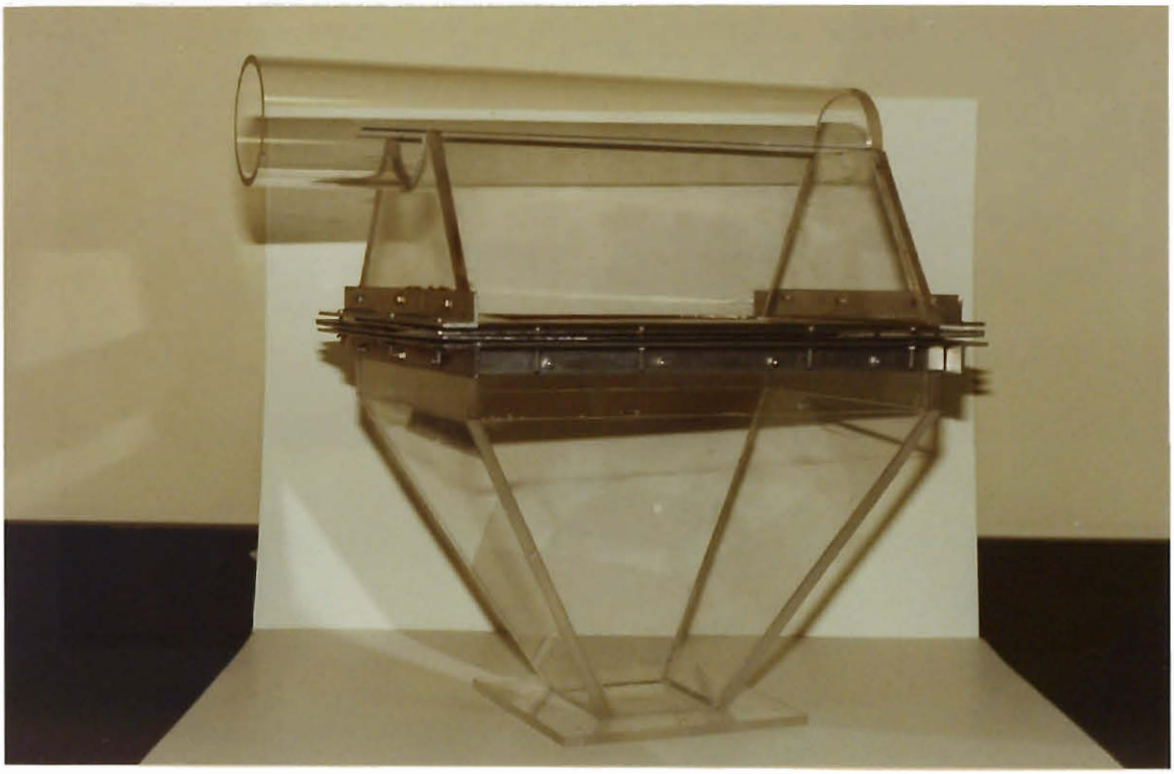

Figure 2.6 Plexiglas SAE Universal Air Filter Test Housing

2) Two-Component Laser Doppler Velocimeter: This mainly consists of the following equipment.

a) Laser: This consists of a Coherent power supply model Innova 70-A and Argon ion plasma tube to provide a laser of 4 Watt power. The intensity of the beam can be controlled and monitored by a remote control.

b) Fiber Drive: The laser from the plasma tube is directed into the Aerometrics fiber drive, model FBD.1240, through a pair of beam steering mirrors. A combination of beam splitting prisms and the Bragg cell located inside the fiber drive split the incoming beam into a pair of blue and a pair of green beams. The frequency of one of the two beams in each pair is shifted with respect to the other by the Bragg cell. The four beams are each directed into separate fiber optic cables which take the beams into the transceiver.

c) Bragg Cell Driver: An IntraAction Bragg cell driver model ME-40H drives the Bragg cell located inside the fiber drive.

d) Transceiver: The Aerometrics Transceiver model XRV.1212 receives a pair of blue and a pair of green beams from the fiber drive through the fiber optic cables. These beams are projected in two mutually perpendicular planes with one pair of beams in each plane. The beams are focused to form a probe volume at the focal point by a lens of focal length 500 mm. The probe volume is shaped like an ellipsoid with a probe length of 737 μm and a diameter of 66 μm. The interference of the beams produce 22 fringes across the minor diameter. When a seeded particle passes through the probe volume, it scatters light which contains the information necessary to obtain the velocity of the fluid. This scattered light is collected by the same lens mentioned above and transmitted to the photodetector unit through a fiber optic cable. The back scatter arrangement of the transceiver is very convenient as just one piece of equipment performs the job of both transmitting and receiving.

e) Photodetector Unit: The Aerometrics photodetector unit model ROM.2200.L receives the optical signal from the transceiver. The two channels for measuring the two components are provided with individual photomultipliers which each amplify and convert

the signal into an analog electrical signal and pass it to the Doppler signal analyzer for further analysis.

f) Doppler Signal Analyzer: The Doppler signal is processed in the Aerometrics Doppler signal analyzer model DSA.3220. The Doppler burst signal consists of a sine wave superimposed on a Gaussian envelope or pedestal. The signal is first high pass filtered to remove the pedestal. A low pass filter is used to remove the noise from the signal. A combination of peak detector and burst detector is employed to locate the maximum amplitude of the signal, and further processing of the signal is done in this central part of the signal which has the maximum amplitude and signal to noise ratio (SNR). A one bit analog to digital converter converts the signal to a square wave with the same frequency as the original signal. The discrete Fourier transform is then applied to determine the frequency of the signal. The Doppler signal analyzer (DSA) is programmed through the attached computer to accept only those signals that have a signal voltage above a selectable level called *threshold* and a SNR above a selectable level. Due to these two limitations on the acceptability of the signal, not all burst signals result in a valid velocity measurement. The rate of validation varies from 30% to 90%. No bias corrections are applied to the resulting velocity measurements in this study.

g) Personal Computer: A 486/33 MHz personal computer controls the entire equipment required for the LDV through software developed by Aerometrics called DSA. Various parameters in this software must be suitably changed whenever the velocity being measured crosses certain ranges. The velocity measurements at a particular location are in the form of the velocities of the individual particles passing that location over a pre-specified period of time. There is also a provision which allows the velocity measurements to terminate once a predetermined number of valid particle velocity measurements has been obtained. In both the cases, the velocities of the particles are represented in the form of a histogram, the mean velocities of each of the two components of the velocity, rms

velocities of each component, angle of the flow and the mean total velocity. Other information like turbulence intensity is also available.

3) Centrifugal Blower: A low power blower was used for the velocity field measurements as only clean filters, which have a relatively low pressure drop were used. The blower was driven by a Dayton electric motor, 1.5 hp, giving a maximum flow rate of 225 SCFM through the test housing and flow meter assembly.

4) Mass Flow Sensor: A TSI model 2021 mass flow sensor with a measuring range of 0 to 500 SCFM was used to continuously monitor the flow rate through the filter.

5) Ultrasonic Humidifier: One or two Pollenex model SH55R ultrasonic humidifiers were used to provide the flow seeding necessary for enabling measurements using the laser Doppler velocimeter. Water droplets of the size on the order of micron are produced which are drawn into the flow by the sucking action of the blower through the test housing. The humidifier is so positioned so that the mist is drawn into the inlet tube of the test housing.

6) Automated Table Traverse: The table which mounts the transceiver can be traversed in a horizontal plane with the help of two lead screws providing motion in two perpendicular directions. The lead screws were powered by a computer-controlled stepper motor system. During velocity measurements, the height of the test housing was adjusted using the stand holding the housing. Readings in a particular horizontal plane were taken by precisely moving the traverse table to the desired location.

2.2.3 Experimental Setup and Procedure

Flow Control and Flow Seeding: A schematic diagram showing how the various pieces of equipment are configured to regulate the flow and provide the seeding is shown in Figure 2.7. The blower sucks air through the housing. One or two humidifiers, as the seeding requirements may be, were placed at a distance of about 14-16 inches from the inlet of the

housing. The water droplets are sucked into the housing along with the air. A valve at the outlet of the blower was used to control the flow rate. The flow indicator had a 20 foot section of 6 inch diameter straight pipe preceding the flow sensor instrument.

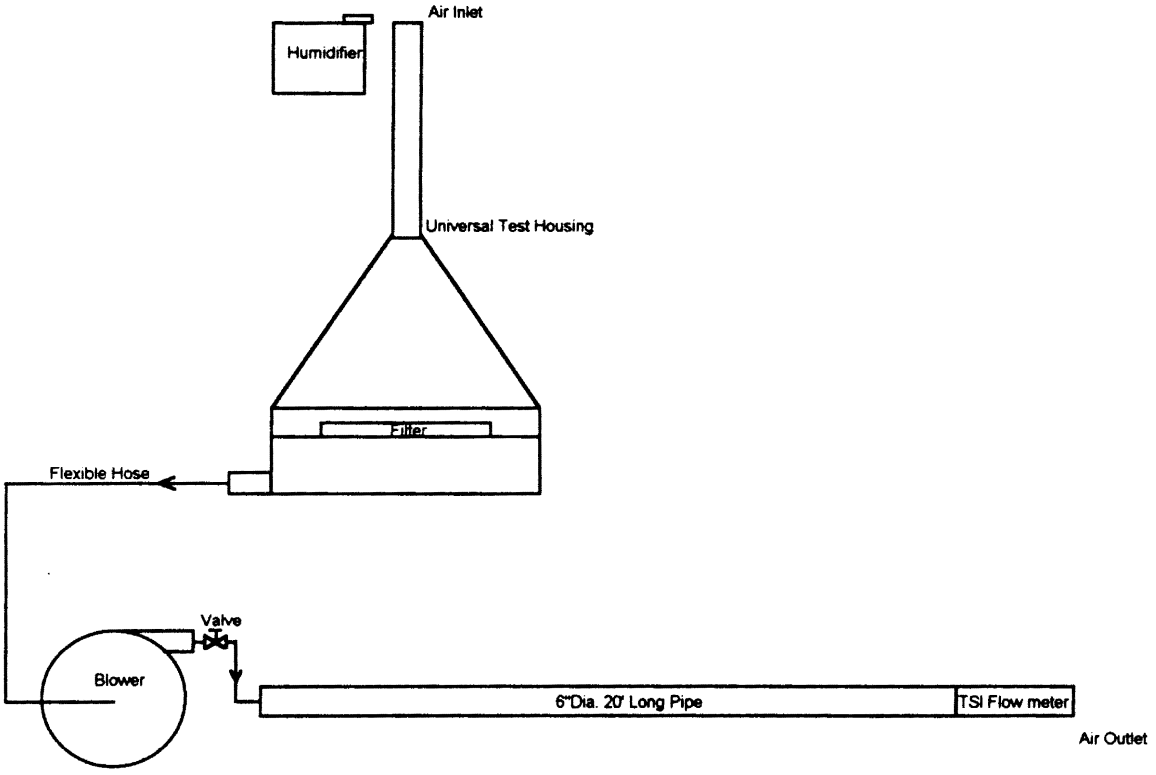

Figure 2.7 Test Setup of SAE Universal Test Housing

Locations of Measurements: Although the prime interest in measurements lies in a region very near to the filter, a few measurements were performed through the rest of the housing. Measurements were performed at the four horizontal planes 1, 2, 3, and 4 as shown in Figure 2.8. The distance of each plane from the top of the aluminum flange is indicated in the figure. Each plane was subdivided into a fine rectangular grid and

readings were taken at each of these points. The size of the grid in the plane 4, which is nearest to the filter, was very fine so that no details of the changes in the gradient of the velocity profile were missed. It is reasonable to expect the velocity profiles to be fairly symmetrical about the vertical center line shown in Figure 2.8. Hence the measurements were performed only in the left half of each plane. However, readings were taken over the entire plane 1 so that the assumption of symmetry for the rest of the planes could be verified.

Test Housing Alignment: Figure 2.9 shows a top view of the relative positions of the test housing and the transceiver. It is very important that the test housing and the transceiver be properly positioned relative to each other. This was achieved by drawing lines, with removable ink, indicating the planes of measurement and the vertical center line. The horizontal and vertical pair of laser beams were used for final alignment, positioning the test housing so that the beams intercepted the lines.

Conventions for Measurements: The convention followed for indicating the location of measurement is shown in the top view of the housing in Figure 2.10. The vertical center line of the housing can be considered to be the Z axis so that at every horizontal plane of measurements the (0,0) position corresponding to X and Y axis is the center of the housing. The positive directions for the X and Y axis are indicated in the top view of Figure 2.10.

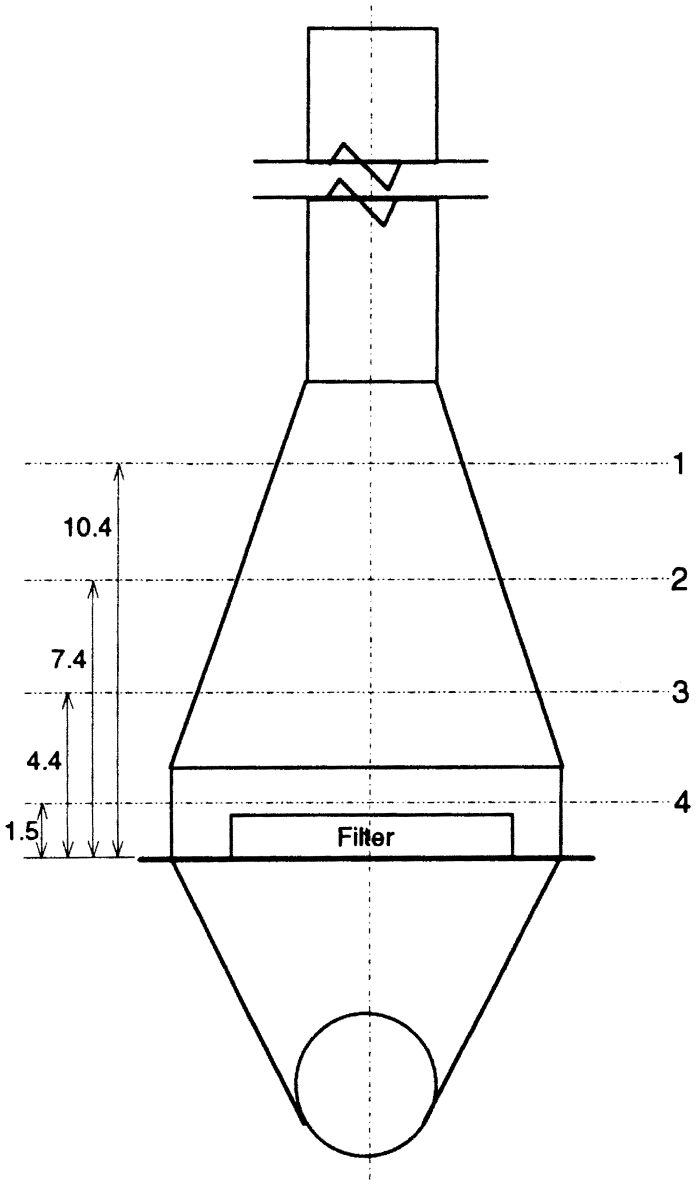

Figure 2.8 Planes of Measurements. Dimensions in Inches. Scale 1:5

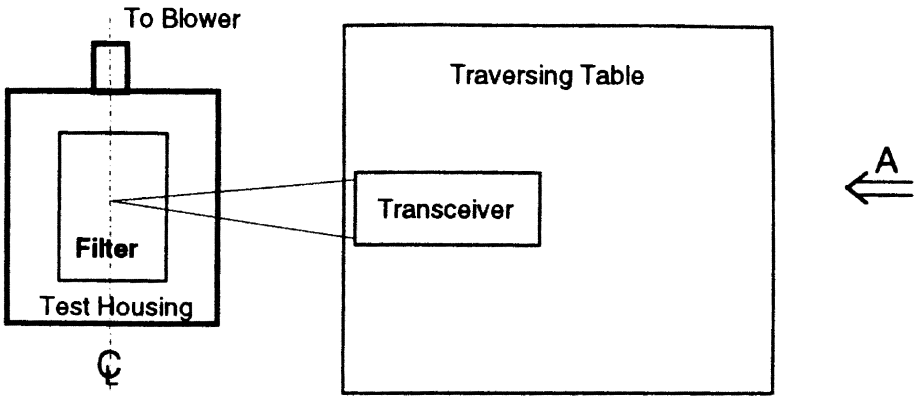

Figure 2.9 Top View of Relative Positions of the SAE Universal Test Housing and Transceiver

The two components measured by the LDV are the vertical or axial and the horizontal or transverse velocities. The positive direction of axial velocity is the velocity into the filter as shown in the front view of Figure 2.10. The positive direction of the transverse velocity is also shown in the front view of Figure 2.10. It should be noted here that the convention for locations of measurements, which is shown in top view of Figure 2.10 and convention for directions of velocities, which is shown in the front view of Figure 2.10 are not the same. Hence when a location on the filter is referenced by the coordinates, say (p,q), where p and q are positive real numbers, then the point (p,q) would lie in the lower left quadrant of the filter in Figure 2.10. Whereas, a positive transverse velocity would mean flow in the direction as indicated by the arrow in the front view.

Setting Parameters in DSA Software: Before any velocity measurements can be done by the LDV, it is necessary to set a few parameters through the DSA software. These parameters vary when the velocity is outside certain velocity bands. It is too complicated and outside the scope of this thesis to explain in detail the various parameters involved. However it may be mentioned here that a lot of practice and care is involved in setting these parameters.

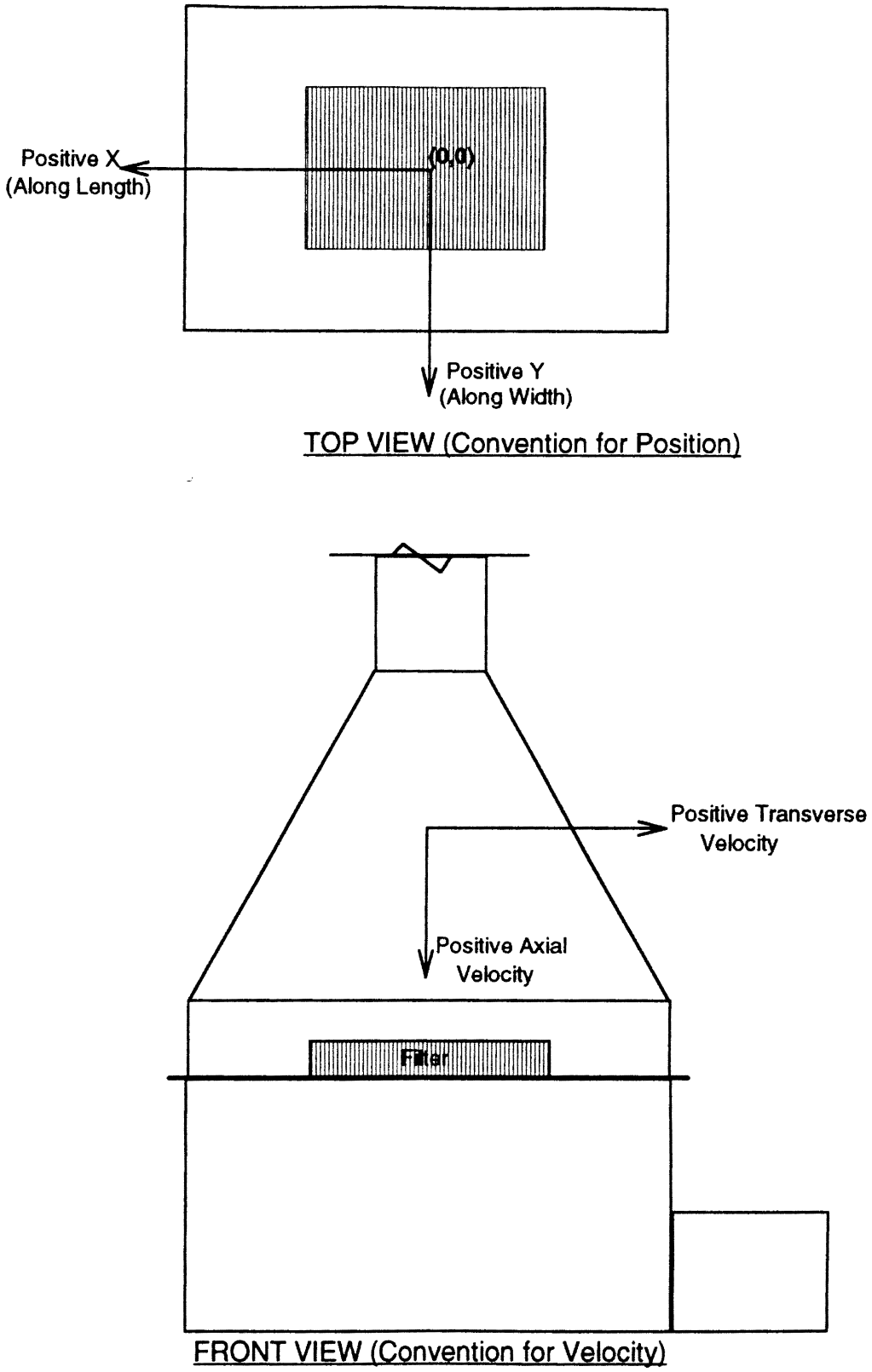

Figure 2.10 Conventions for Position and Velocity Measurements. Scale 1:5

2.2.4 Difficulties Encountered

The water particles can tend to settle on the Plexiglas forming big droplets which sometimes obstruct the laser beam. This causes a sudden termination of data acquisition. The humidifier must be switched off inbetween the measurements whenever possible so that the filter does not get excessively wet. Both of the above mentioned problems can be reduced by lowering the mist intensity by adjusting the intensity control on the humidifier. Lower mist intensity will also cause a reduction in the rate of data acquisition, hence the mist intensity must be lowered cautiously. The problem of distortion of the laser beam can also occur if any glue marks on the Plexiglas obstruct the beam. There is no way to eliminate this problem but to take appropriate precautions during the construction of the housing.

The concentration of the water droplets is high in the central region of the flow. But in the region near the walls where there is recirculation, the concentration of the particles is very low. This causes a delay in the acquisition of data towards the edges of the housing. To overcome this difficulty, two humidifiers were used at their maximum intensity whenever the readings were being taken at the edges. This increased the concentration of seeding particles, increasing the data acquisition rate. In any case, to have uniformity throughout the measurements, the DSA software was set so that all the velocity measurements contained at least 300 valid seeding particle velocities. So the overall elapsed time required for measurements in the main stream of the flow was very much less than that at the edges of the flow.

CHAPTER III

RESULTS AND DISCUSSION OF FLOW VISUALIZATION AND VELOCITY MEASUREMENTS

Since visualization techniques give the overall perspective of the flow, although only qualitative, it is felt appropriate to discuss the results of flow visualization first. The results of detailed LDV measurements would provide information in terms of numerical values of velocities, recirculating velocities, and turbulence intensities.

Before getting into any discussions of the results, it is brought to the notice of the reader that at the end of all the experiments the TSI mass flow sensor was found to be off the calibration by about 25%, showing lower than actual flow rates. The TSI mass flow sensor was checked against a laminar flow element before these experiments were started, and both the instruments were in good agreement with each other. It was known only a long time after the experiments were performed that the TSI mass flow sensor was out of calibration with respect to the laminar flow element. The flow through the filters was later computed from numerical integration of the velocity measurements over the entire filter and is indicated in 8th row in Table III given in Appendix A. The flow rates indicated by the TSI mass flow sensor are given in 5th row of Table III. It can be seen that the filter AF3192, which was analyzed first when the TSI mass flow sensor was within calibration, has nearly equal values of mass flow sensor readings and the actual flow rate. Whereas, the filter AF3592, which was analyzed later, showed mass flow sensor reading about 25% lower than the actual flow rate. However, this will not drastically affect the results

presented. Although high numerical accuracy cannot be claimed in the experimental measurements and the resulting calculations, all the results will show the correct trend with respect to all the parameters involved.

3.1 Flow Visualization

3.1.1 Surface Flow

When the flow rates are 200 SCFM, the shear stress at the wall was sufficient to move the paint and clearly indicated a line of separation. Hence at lower flow rates of 150 SCFM, although the paint was not moved and no final line of separation was indicated, it could not for sure be said that there was no separation. In fact the only reason for the flow not being able to move the paint was that the shear force near the wall was very low. This same reasoning is further strengthened by some of the observations in other visualization techniques.

3.1.2 Tufts

From the highly fluctuating movement of the tufts, it is clearly seen that the flow is very turbulent. The tufts do not remain close to the wall but form an angle varying from about 0 to 100° with the wall which indicates the separation of the flow from the walls. Had the flow been laminar and unseparated, the tufts would have remained in a relatively very still position and attached close to the wall indicating the direction of flow. Figures 3.1 and 3.2 show the estimated direction of the tufts on the two surfaces of the housing. Figure 3.1 shows the tuft positions for the larger of the two surfaces. Along the larger surface, the flow initially enters almost in the axial direction and as it approaches the filter it spreads. The tufts near the filter can be seen pointing outwards indicating the spreading flow. The angle made by the tuft with the housing wall is indicated below the tuft

wherever the video pictures could reveal such an angle. This angles are of the order of 10-30° at the inlet and increase to 90-100° towards the filter. This is clearly an indication of a separated flow although the exact location of separation can not be pointed out. Figure 3.2, for the smaller of the two surfaces and which has a smaller diffusion angle of the two planes, shows that the flow is almost axial throughout the housing. Towards the filter the flow is slightly converging. Also the fact that thicker tufts did not move due to the flow is again an indication of weak shear stress at the walls.

3.1.3 Intermittent Smoke

During the part of the cycle when the smoke is being turned on, the smoke is seen to be entering into the housing from the central part of the housing only. The smoke can be seen coming from the long straight pipe and impinging upon the filter without any spread into the housing. Then after a very short while, the smoke fills up the housing. The smoke is turned off at this time, and then it can be observed that the central mass of the air and smoke in the housing is drawn into the filter first, and then the rest of the housing is cleared of the smoke. This indicates that most of the mass flow occurs in the central part of the filter which would also mean that high velocities would occur in this part of the filter. It can be said for certain that recirculation occurs from the fact that the smoke in the central part of the housing was cleared first, and it took some time for the smoke in the sides of the housing to be removed.

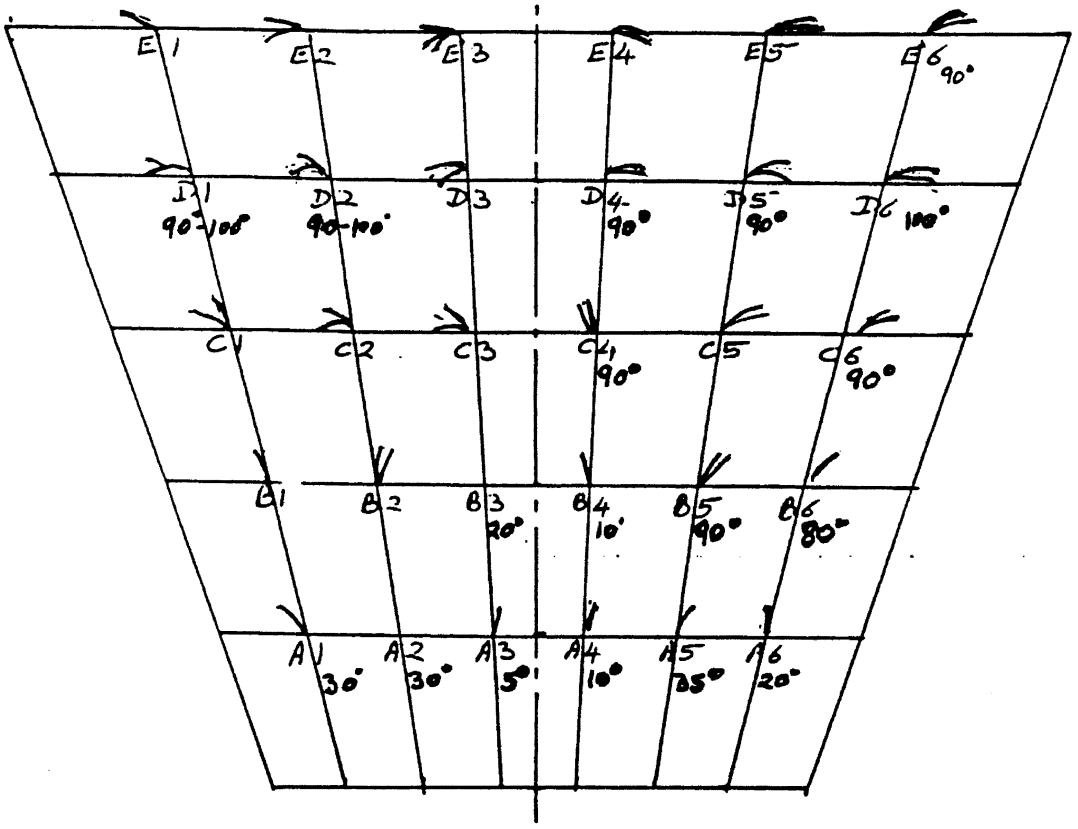

Figure 3.1 Estimated Direction of Tufts on the Larger Surface of the Test Housing

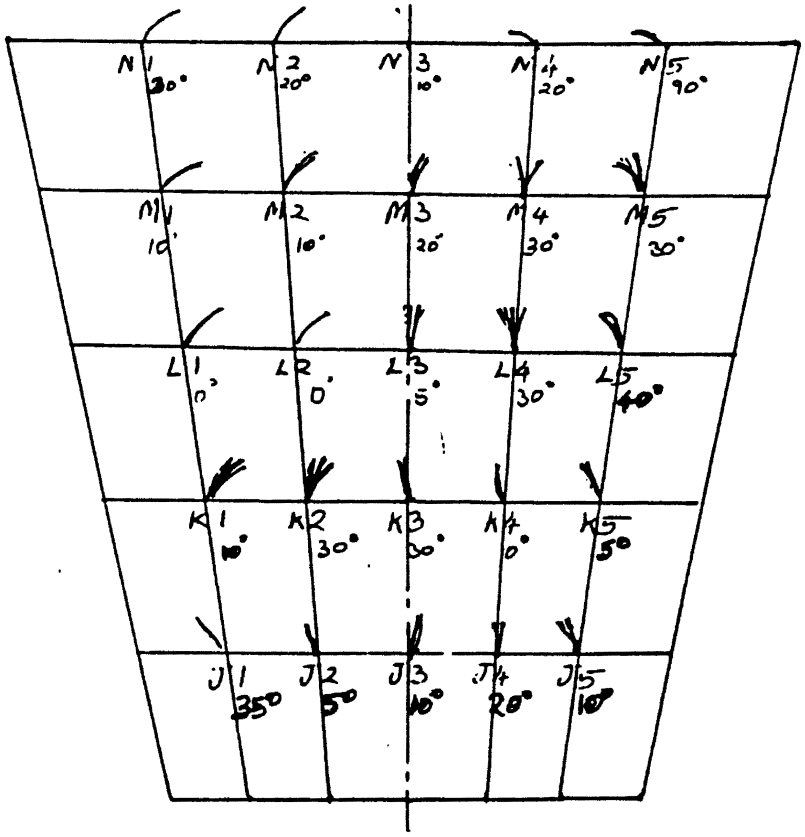

Figure 3.2 Estimated Direction of Tufts on the Smaller Surface of the Test Housing

When the smoke was seeped into the housing with the help of a long tube up to the walls of the housing, the unsteady and separated nature of the flow was clearly visible. The smoke was seen to be attached to the wall for a short distance from the inlet and then clearly separated from the wall. This point of separation kept moving unsteadily back and forth. The smoke did not accumulate in the recirculating zone, indicating that although the flow is recirculating, there is a substantial amount of mixing between the main region of the flow and the separated region of the flow.

3.1.4 Intermittent Smoke With Laser Sheet Lighting

The same details as mentioned earlier in the section discussing the smoke flow visualization were observed in this visualization but very distinctively, from corner to corner, and individually at every plane of observation. One of the interesting revelations was in the transverse plane very close to the filter. Even after the flow had the distance from the inlet to the filter for spreading, the jet-like flow did not spread to cover the entire filter. This could be seen in the laser sheet very close to the filter. When the smoke enters, it tends to remain in the central part, and while leaving, it first clears from the central part. In Figure 2.3, which is photographed of transverse laser sheet after the smoke is shut down, most area of the laser sheet is filled with smoke except for the central most part. This central most part above the filter, where smoke was first sucked into the flow, was exposed to higher flow rates compared to the surrounding areas. Thus the non-uniformities of the flow distribution are seen in this photograph.

3.1.5 Water Droplets With Laser Sheet Lighting

Visual inspection revealed all the separated and recirculating nature of the flow. The photographs also show the streaks indicating the recirculating regions and the central region of high concentration of particles with jet like flow. A vertical laser sheet with water droplets is shown in Figure 2.4. The central part of the housing is densely filled with water droplets indicating more particles in the central part of the housing. The central part of the sheet shows the straight streaks, whereas, towards the corners of the sheet, curved streaks are seen which indicates recirculation at the corner areas.

3.2 Velocity Profiles

3.2.1 Two-Dimensional Representation of Velocity Measurements

The measured velocities can be collectively represented either in a 2-dimensional plot or a 3-dimensional plot. A few 2-dimensional plots have been presented to give a better understanding of the 3-dimensional plots. Figure 3.3 is a plot of velocity measurements taken in plane 4 (see Figure 2.8) at locations on a line at X=0.0 (conventions in Figure 2.10). Therefore in Figure 3.3, as the value of ordinate increases above zero, we move away from the center of the filter. It can be seen that the axial velocity is positive for most of the locations. It gradually decreases as the filter edge is approached and finally becomes negative. As per the convention of velocity explained in Figure 2.10, the positive axial velocity would mean that the flow is into the filter. Negative axial velocity towards the edge of the housing means a flow away from the filter, which is also the recirculation. The transverse velocity is nearly zero and its significance will be explained later.

Figure 3.4 and Figure 3.5 are also 2-dimensional plots for measurements done in plane 4 and at X=+0.8 inch and X=-0.8 inch respectively. The axial velocities show the same trend as in Figure 3.3 except that the velocities have reduced in magnitude. In Figure 3.4 some portion over the filter has negative transverse velocities, which when interpreted by looking at Figure 2.10 would mean that the air is flowing away from the center line. In the same manner it can be said for Figure 3.5 also that the air is flowing away from the filter. A better explanation of the transverse velocity profiles is given in the following section.

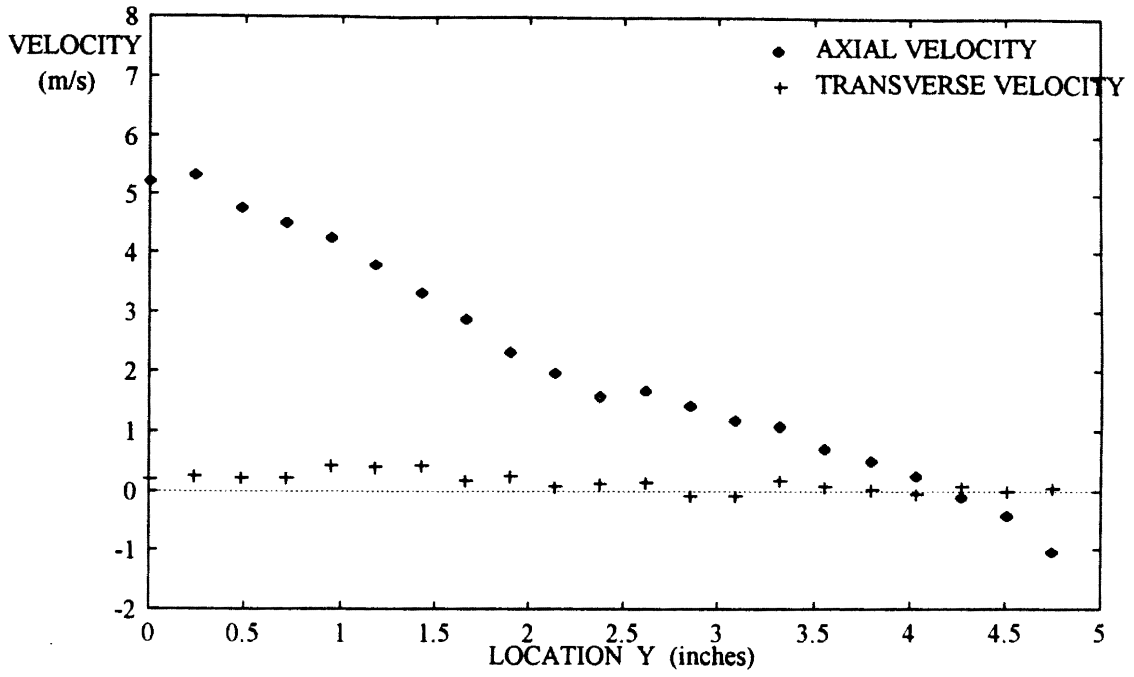

Figure 3.3 Axial and Transverse Velocity in Plane 4 at X=0.0 Inches for Filter AF3192

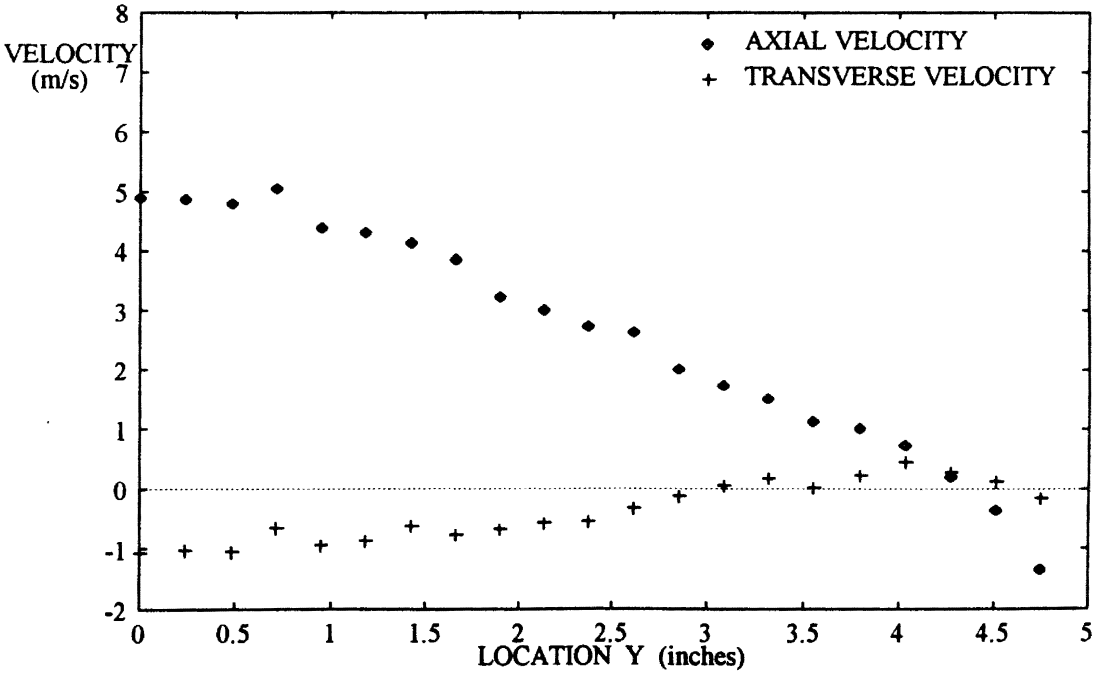

Figure 3.4 Axial and Transverse Velocity in Plane 4 at X=0.8 Inches for Filter AF3192

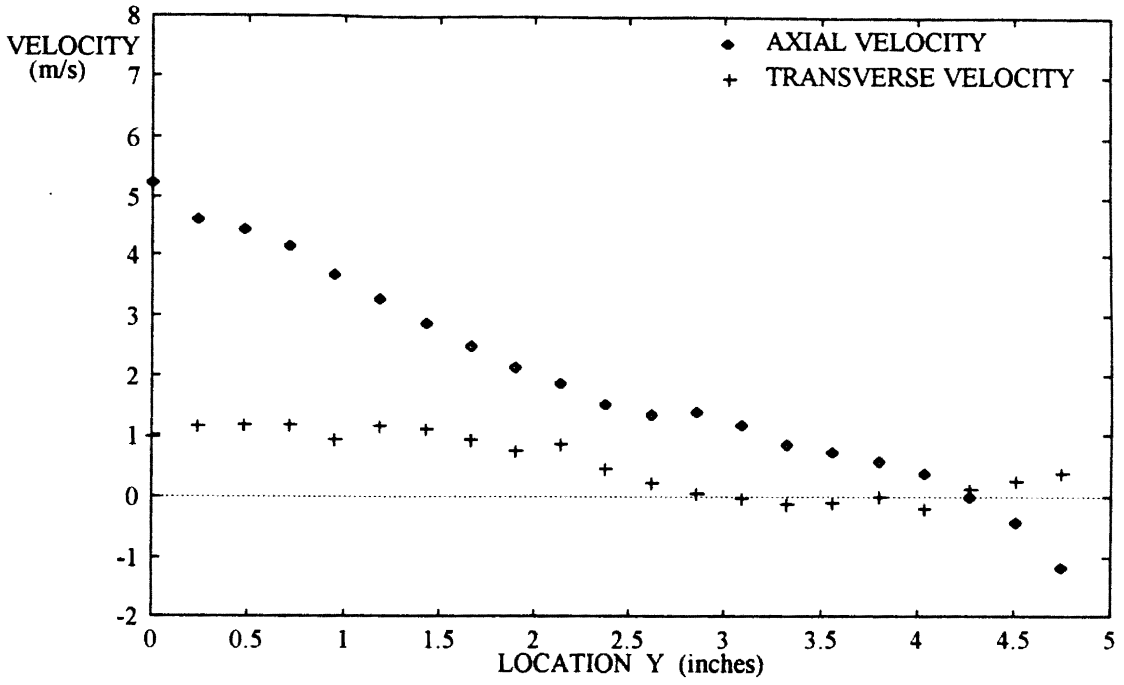

Figure 3.5 Axial and Transverse Velocity in Plane 4 at X= -0.8 Inches for Filter AF3192

3.2.2 Three-Dimensional Representation of Velocity Measurements

The data collected at various locations can be better represented by combining the 2-dimensional graphs at different X locations into one 3-dimensional graph. The axial and transverse velocities for each plane have been plotted in two separate 3-dimensional plots. Figure 3.6 is a such a 3-dimensional plot of axial velocities in the plane 1 for filter AF3192. The X and Y axes represent the location on the filter with the position (0,0) representing the center of the filter. The surface representing the axial velocities is shaped like a dome indicating velocities of the order of 6 m/s in the central region and gradually reducing to nearly zero towards the edge of the housing. The velocity surface is also marked with constant velocity contours which are projected on the XY plane. The values of the contours is indicated on the XY plane. Since this is the plane immediately after the long flow straightening pipe, most of the central region of the plane has a flat velocity

profile with velocities above 6.4 m/s. The velocity gradually reduces as we move towards the edges of the plane which is indicated by the concentric velocity contours of diminishing values. The contours are fairly symmetric about the center line along the X axis. The same thing can be said about the symmetry about the center line along the Y axis, except for some amount of distortion in the central-most contour.

With this symmetry in mind, it was assumed to be appropriate to map the velocities in just one half of the filter with the other half having velocities almost the same as the half that is mapped. Hence the measurements in the other three planes *viz.* 2, 3, & 4 are performed in the half that is symmetric to the center line parallel to the x axis.

Figure 3.7 is the plot of axial velocities in plane 2. Again the symmetry about the center line parallel to Y axis is evident. The peak velocity still appears in the central portion of the filter but the magnitude of the peak has reduced from 7.8 m/s in plane 1 to 7.1 m/s in this plane. The evenly spread contours indicate that the flow is spreading slowly as it passes through the housing. The velocity profiles of the flow as the flow proceeds into plane 3 are shown in Figure 3.8. The flow has spread further with the peak velocity also showing a drop. The contour towards the edge has negative values indicating the existence of the recirculating, separated flow.

Velocity contours in plane 4 are indicated in Figures 3.9 and 3.10. This plane which is closest to the filter is studied in greater detail since it would reveal the flow properties as the flow is entering into the filter. The grid size for measurements was reduced to a very small size so that the smallest flow variations were captured. It is seen from Figure 3.9 that the axial velocity profile has retained the same shape. The peak velocity observed in this plane is 5.308 m/s and the minimum velocity is -1.342 m/s. In the figure the thick lined frame indicates the borders of the filter. It is evident that the filter is exposed to nonuniform velocity with very high velocities in the central part of the filter and lower velocities towards the edge. From the design point of view, what this means is that half part of the filter is operating at conditions more severe than the filter is designed

for and other half parts are subjected to milder conditions. These velocity variations are expected to affect the performance of the filter in terms of efficiency (as discussed in Chapter II) and pressure drop which in turn would affect the dust holding capacity. The continuation of the separated flow is indicated by the negative axial velocities towards the edge of the housing.

The transverse velocities in plane 4 are indicated in Figure 3.10. The positive velocity direction is indicated in the figure by the arrow. The convention for representing coordinates of the velocity measurement locations is shown in Figure 2.10. A point to be noted here is that the right half of the XY plane in Figure 3.10 actually represents the left half of a filter. In Figure 3.10, the left half of the XY plane (which actually represents the quarter of the filter on right hand side) has positive transverse velocities indicating that the flow is away from the center of the filter. In right side half of the XY plane, the velocities have negative values which again means that the flow is away from the central region of the filter. The shapes of the contours in the left and right side halves have similar shapes with the signs interchanged. The contours have slightly higher absolute values in the left half as compared to the right half. Hence it can be said that the transverse velocity profiles are also symmetric about center line parallel to Y axis. Overall the flow can be said to be spreading very close to the filter, just like a an impinging jet.

3.2.3 Turbulence Intensities Near the Filter

The axial turbulence intensities in plane 4 for filter AF3192 are plotted in Figure 3.11. The axial turbulence intensity is obtained by dividing the local rms value of the axial component of velocity fluctuations about the local mean axial velocity by the mean axial velocity at the center of the filter. This plot is an indication of the distribution of the turbulence in the flow. From the velocity distribution in plane 4, it is clear that the flow is very much similar to that of a round jet. Typically a jet profile has a zero velocity gradient

at the center, where the turbulence production is zero, a maximum velocity gradient radially surrounding the zero gradient portion, where the turbulence production is at its maximum, and in the outermost region, the velocity gradients are again very low, and in this region too there is little turbulence production. The above mentioned velocity gradient variations in a round jet flow are visible in the axial velocity profile for the filter in plane 4 as shown in Figure 3.9. The central region has turbulence intensities of about 0.17 and is surrounded by a region of relatively higher turbulence intensities. The region of maximum turbulence production, which occurs in a region surrounding the central dip in turbulence intensities, is clearly seen in Figure 3.11. The maximum turbulence intensity contour also occurs in this region of maximum turbulence production. The turbulence intensities are very low, about 0.07, at the edges of the housing where the turbulence is dissipated. Symmetry about the center is not very prominent but is sufficient to show the similarity with the jet flow.

A similar study of the flow fields was performed for another filter, AF3592, which is of different size and operated at a different flow rate. The dimensions and flow rate for filter AF3592 are given in Appendix A. The plots, similar to the ones presented for filter AF3192, are presented for filter AF3592 in the Figures 3.12 to 3.17. All the characteristics of the flow seen in AF3192 are also seen in AF3592.

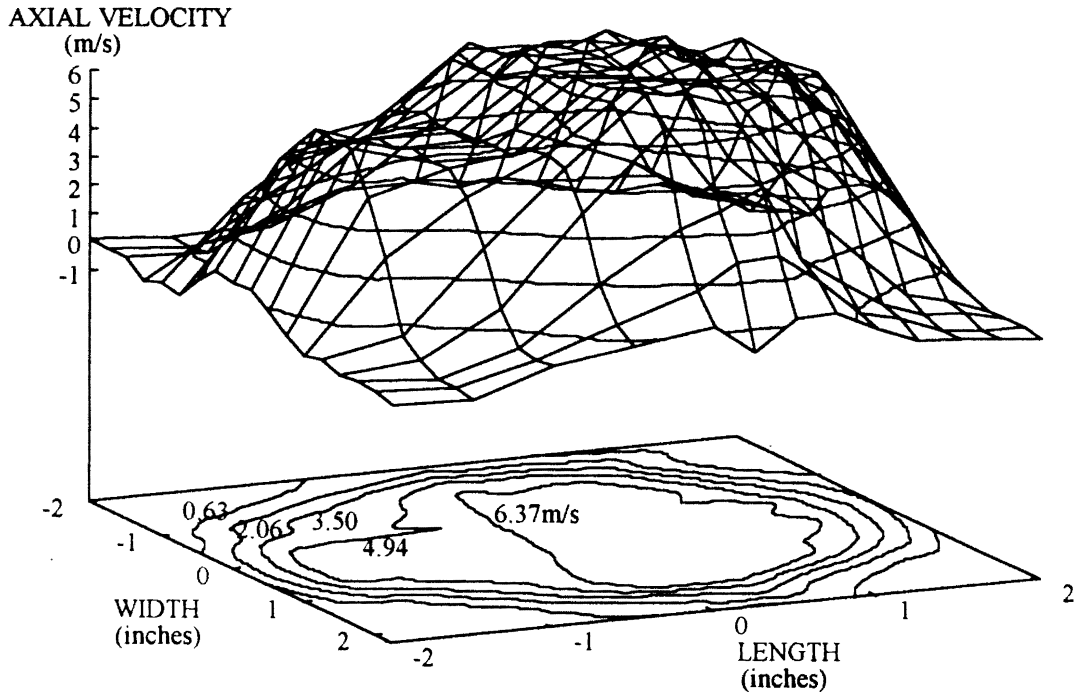

Figure 3.6 Axial Velocity Distribution in Plane 1 for Filter AF3192

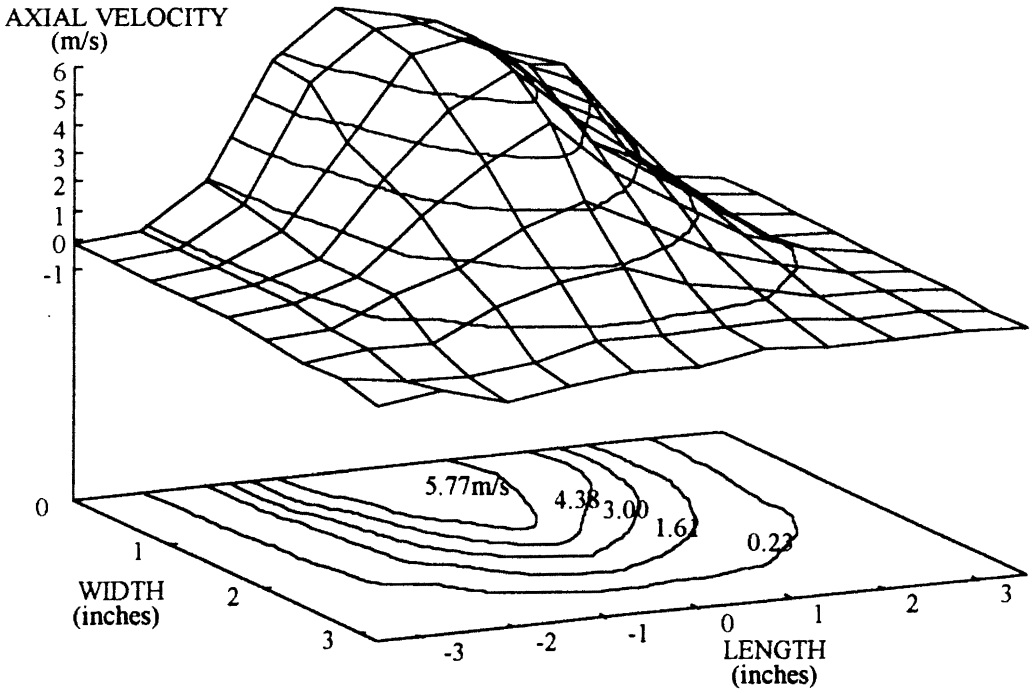

Figure 3.7 Axial Velocity Distribution in Plane 2 for Filter AF3192

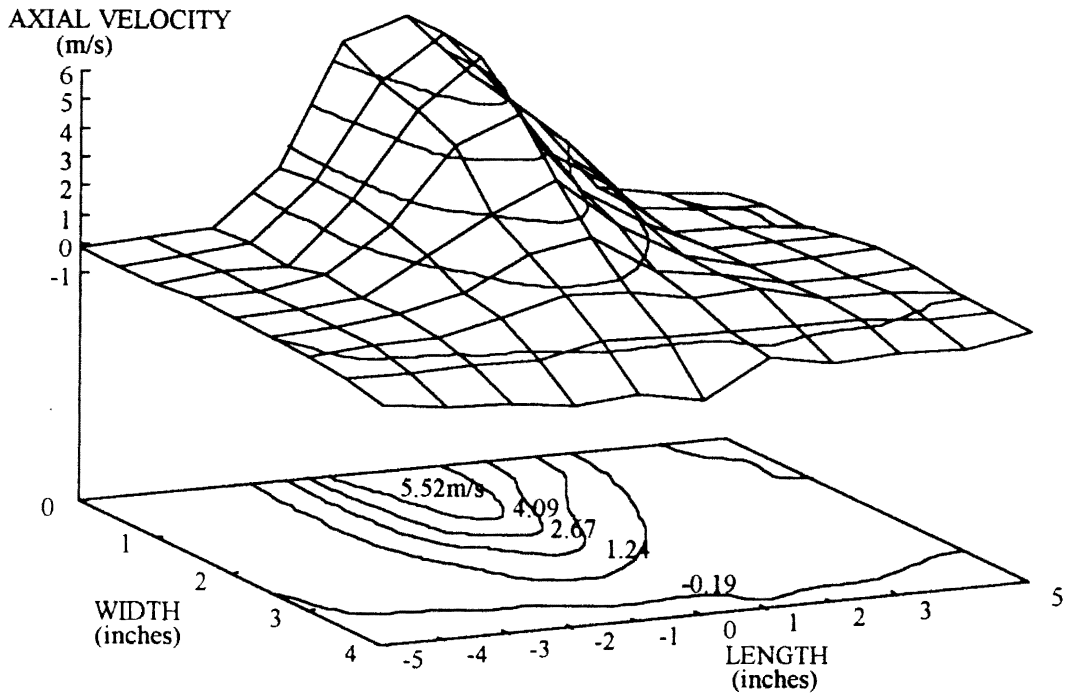

Figure 3.8 Axial Velocity Distribution in Plane 3 for Filter AF3192

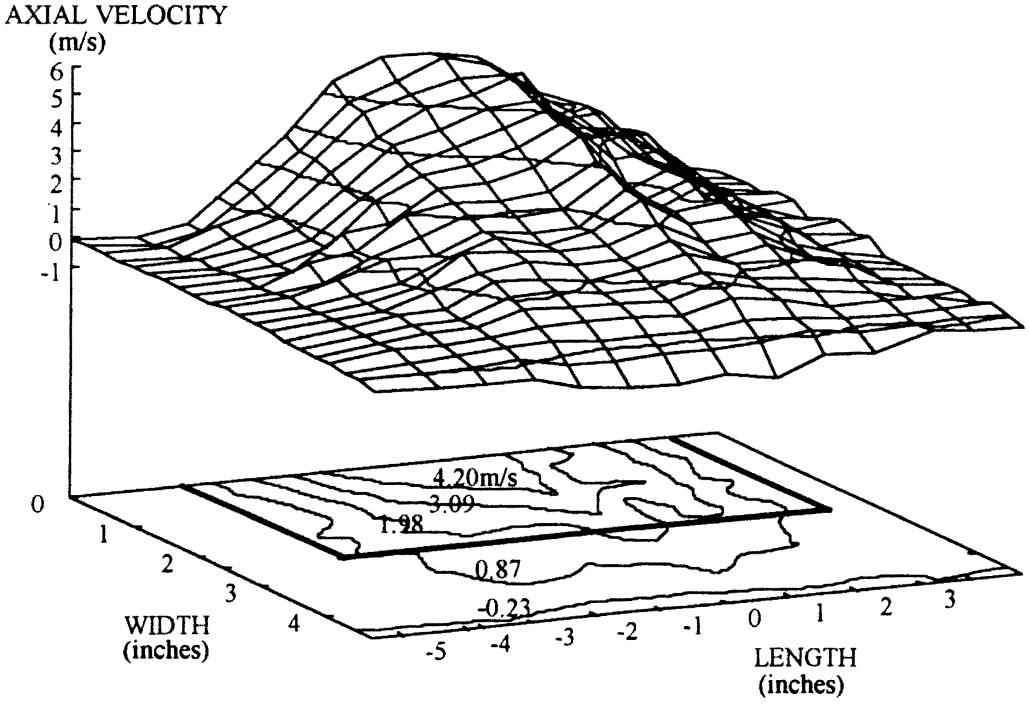

Figure 3.9 Axial Velocity Distribution in Plane 4 for Filter AF3192

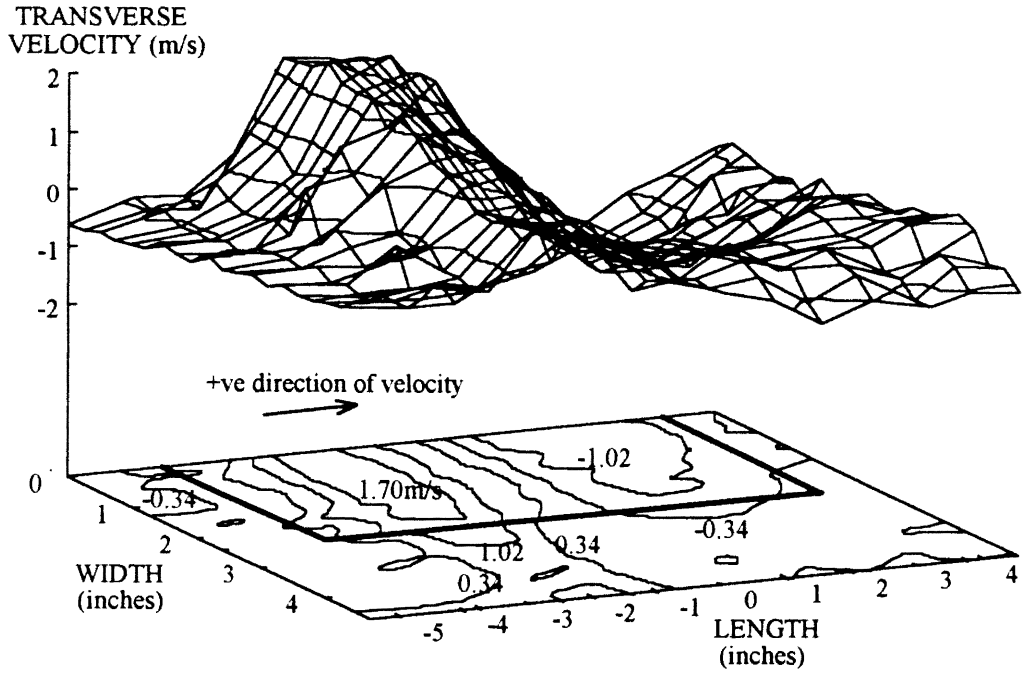

Figure 3.10 Transverse Velocity Distribution in Plane 4 for Filter AF3192

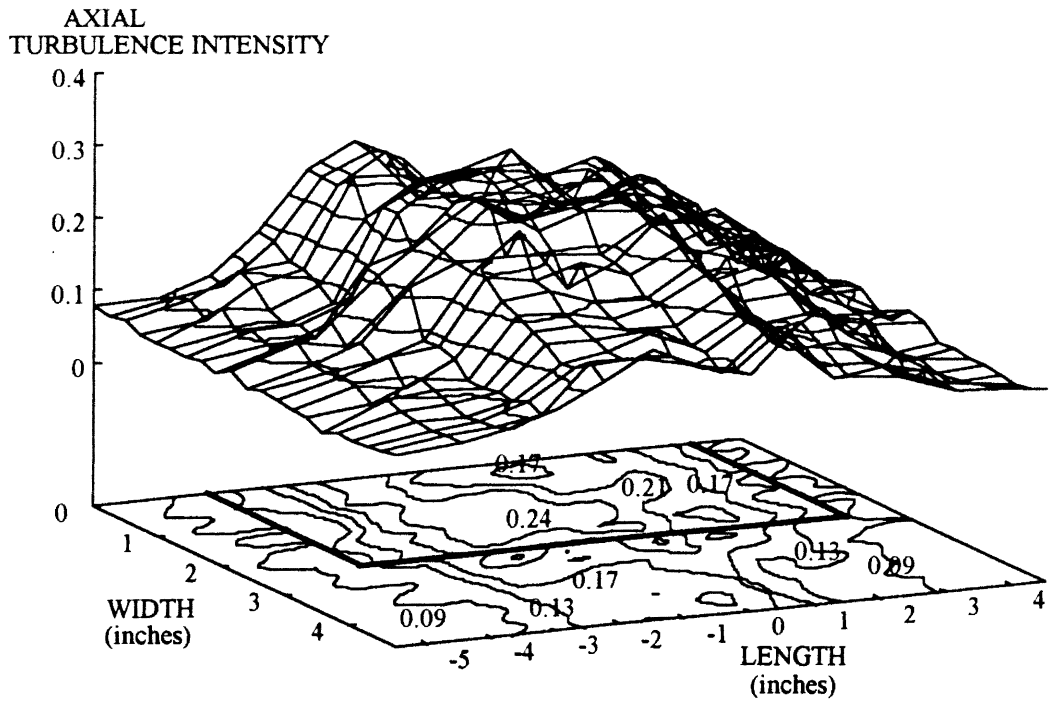

Figure 3.11 Axial Turbulence Intensity in Plane 4 for Filter AF3192

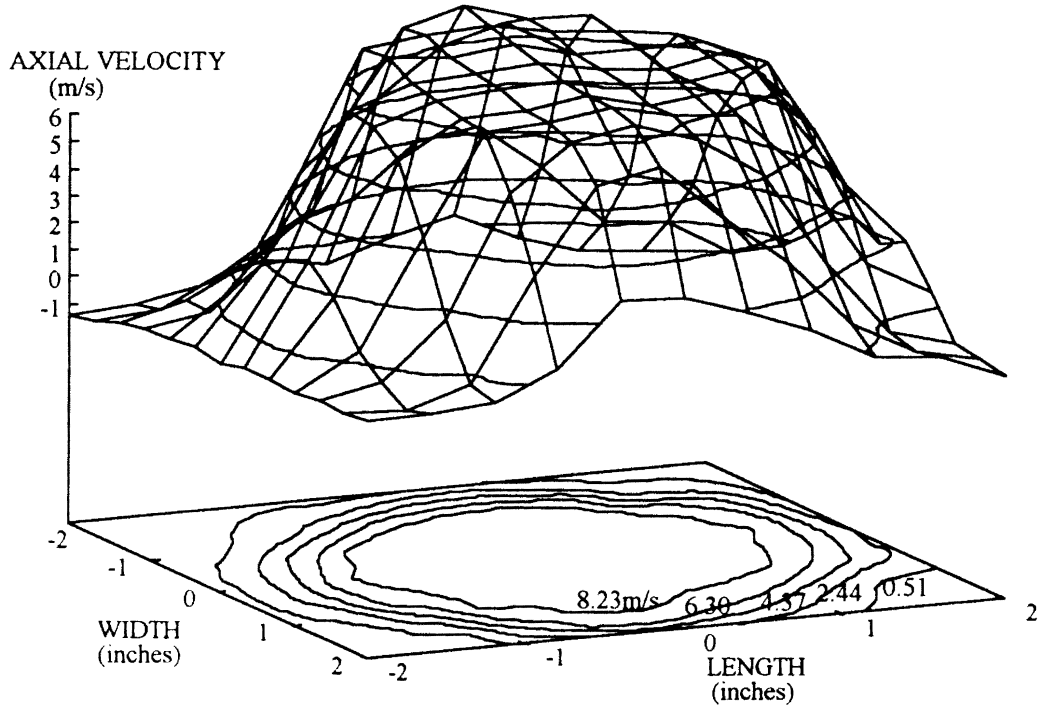

Figure 3.12 Axial Velocity Distribution in Plane 1 for Filter AF3592

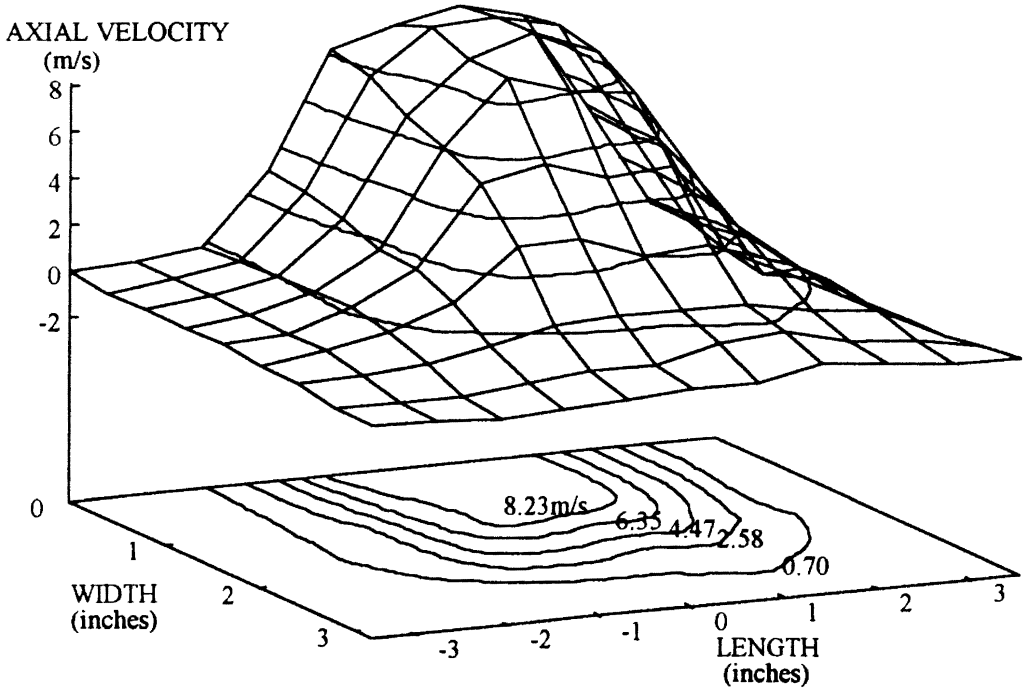

Figure 3.13 Axial Velocity Distribution in Plane 2 for Filter AF3592

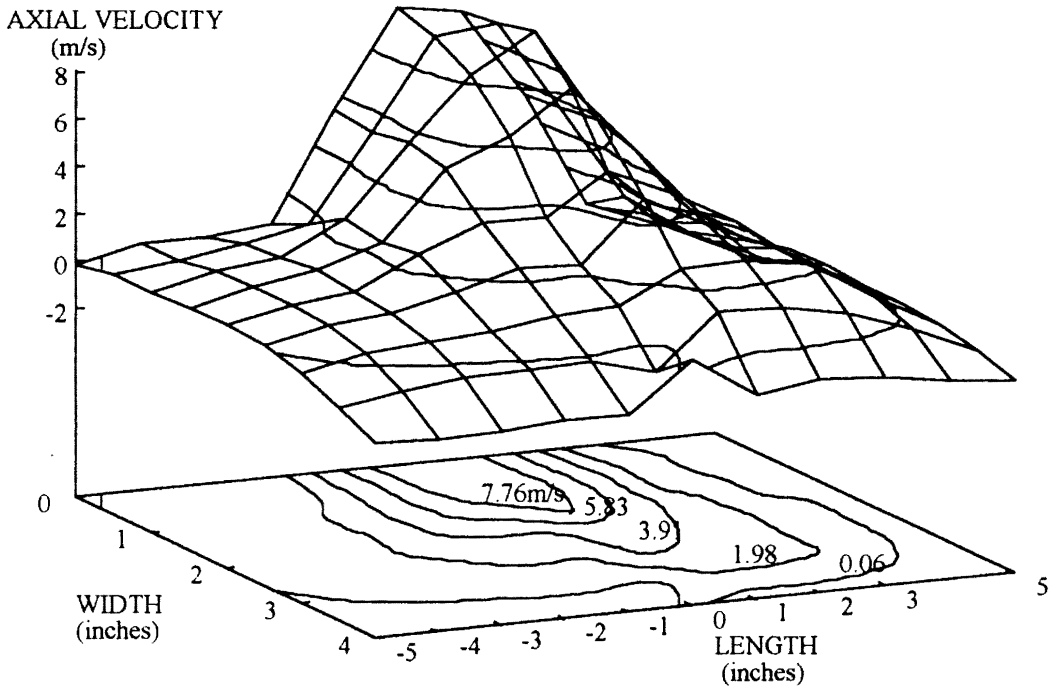

Figure 3.14 Axial Velocity Distribution in Plane 3 for Filter AF3592

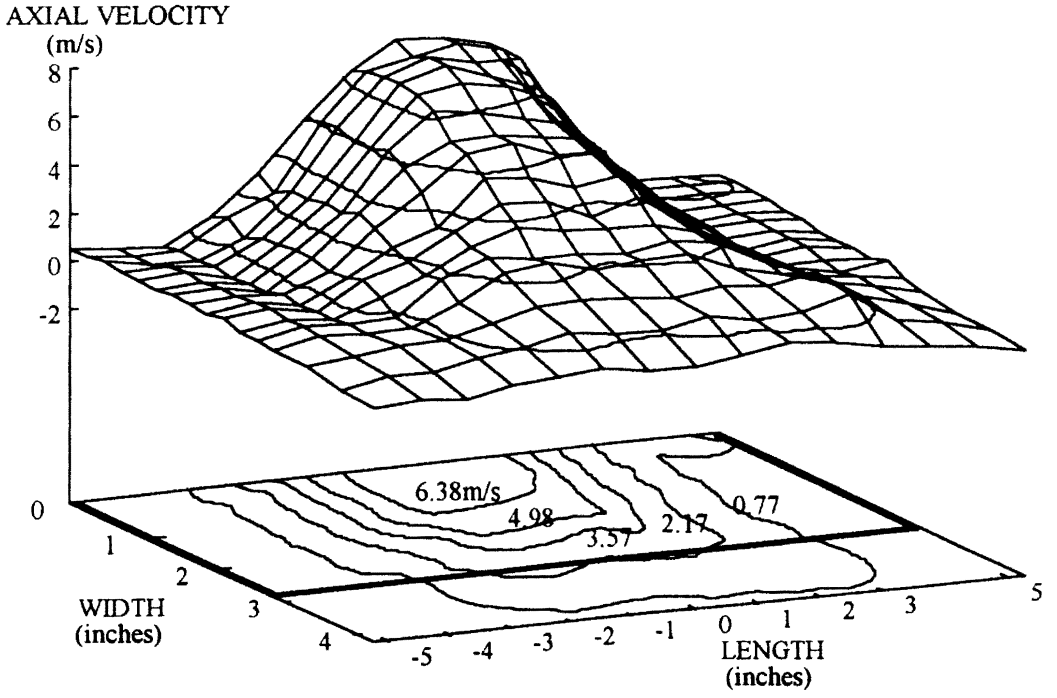

Figure 3.15 Axial Velocity Distribution in Plane 4 for Filter AF3592

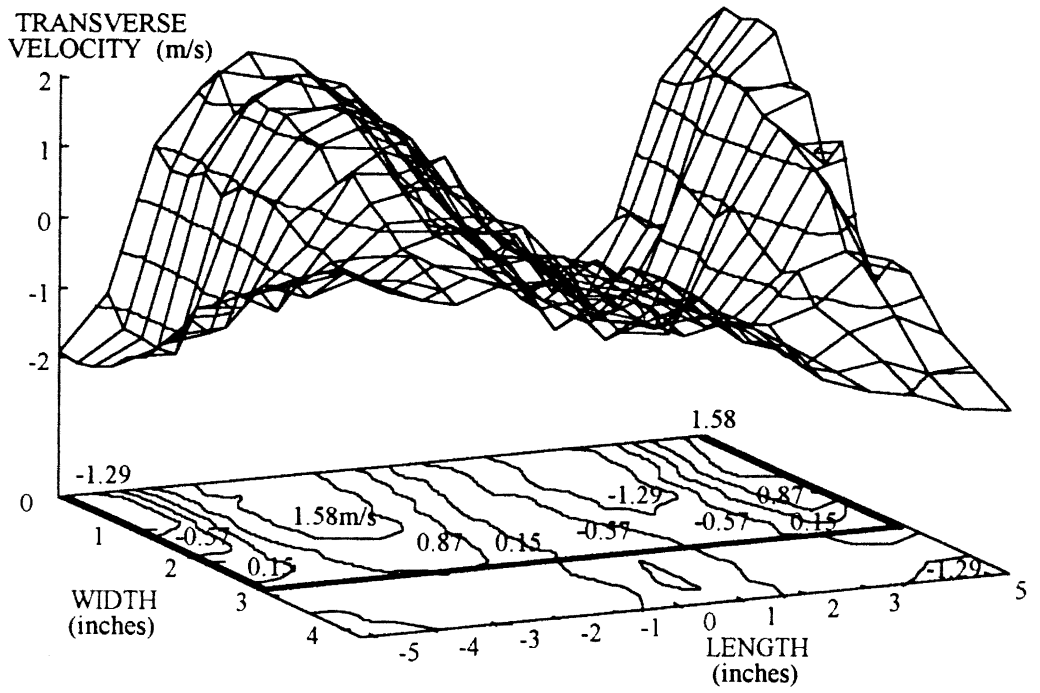

Figure 3.16. Transverse Velocity Distribution in Plane 4 for Filter AF3592

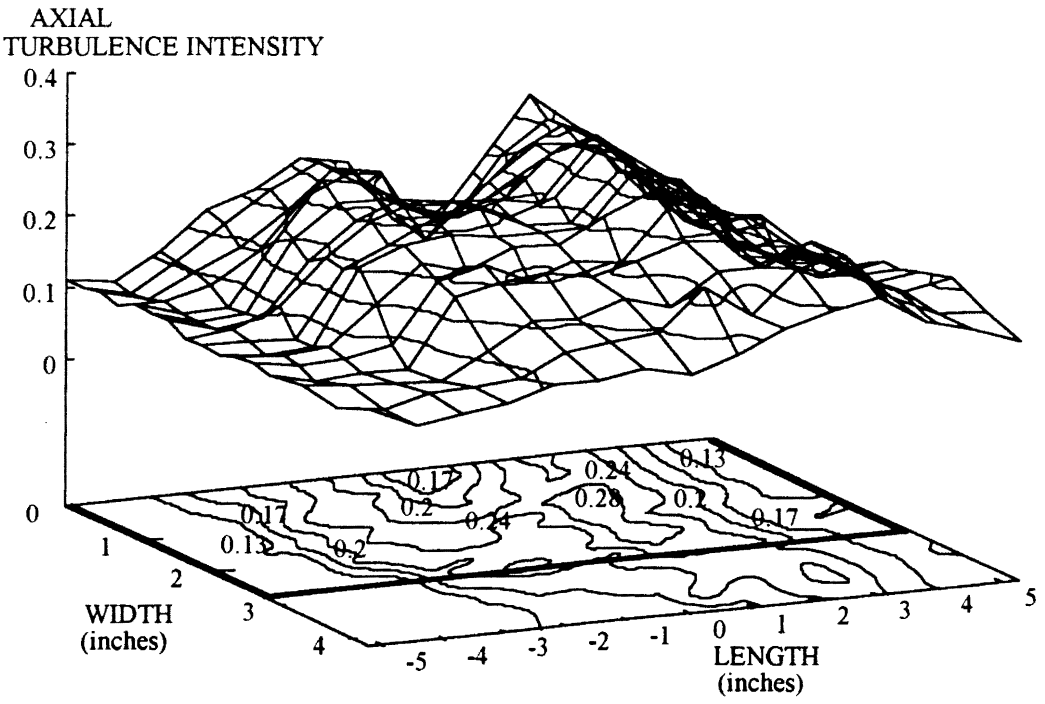

Figure 3.17 Axial Turbulence Intensity in Plane 4 for Filter AF3592

3.3 Summary of Results

The flow visualizations performed in the universal panel filter test housing indicate very clearly the existence of a separated and recirculating flow inside the test housing. It was also observed that the flow is turbulent and approaches the filter just like a jet flow. All of the above observations were confirmed from the results of the velocity measurements which were performed using the LDV. The velocity distribution over the filter is bell shaped with the central part of the filter being subjected to higher velocities as compared to the edges. The flow is more like a impinging jet than a free jet. The turbulence intensities near the filter also closely resemble jet flow. These non-uniformities in the flow distribution are roughly similar for the two different sized filters analyzed at two different flow rates. Further work is necessary to see if the results can be scaled for different sized filters and flow rates.

CHAPTER IV

FILTRATION EFFICIENCIES IN PLEATED AIR FILTERS

Aerosol velocity in the filtering media is one of the most important factors in determining the filtration efficiencies. The existence of large scale variations in the velocities encountered by a pleated air filter would mean that the filtration efficiencies also vary over the filter. Therefore the filter performance is expected to deviate from the specifications in the design which are based on uniform velocity distribution. As mentioned in the previous chapter, an attempt has to be made to scale the non-uniformities for larger filters. This makes it difficult to directly compare performances of different size filters. The important question then arises as to whether these variations in velocities are conducive to filtration or not and to what extent. The answer to this question also holds the key to the ways in which the filtration performance can be enhanced.

4.1 Filter Media Efficiencies

After a thorough study of the various models available for representing filters, a review of which was presented in Chapter I, the best models that could represent a filter were thought to be those by Flagan (1988), represented by Figure 1.6, and those of Lee and Liu (1982b) and Jaroszczyk and Wake (1991) given by equation (1.33). However, the results presented in Chapter I are for single fiber analysis and do not indicate how a particular filter media will perform. In this section, efficiency curves for the plain paper filter, the properties of which are described in Appendix C, are presented. In the forthcoming calculations in this chapter, most of the results, unless specifically mentioned,

are presented for a specific case of fiber radius, R=19μm, filter thickness, h=700μm, and packing density, c=0.23μm, the reasons for these choices is explained in Appendix C.

The efficiency calculations are based on the equations (1.7) and (1.33). Families of curves for various values of packing density, c, and interception parameter, I, are presented in Figures 4.1 and 4.2 respectively. Figure 4.1 shows how the filter efficiencies are altogether different from the single fiber efficiencies indicated in Figure 1.7 which is drawn for the same parameters. Although the single fiber efficiency reaches a value of one in Figure 1.7, it does not mean that the filter of a finite thickness will have 100% efficiency as can be seen in Figure 4.1. This is because filters with low packing density do not have sufficient collecting surface for collecting all the aerosol particles. Figure 4.2 shows efficiency curves for various values of interception parameter for the specific filter paper to be used in the forthcoming calculations.

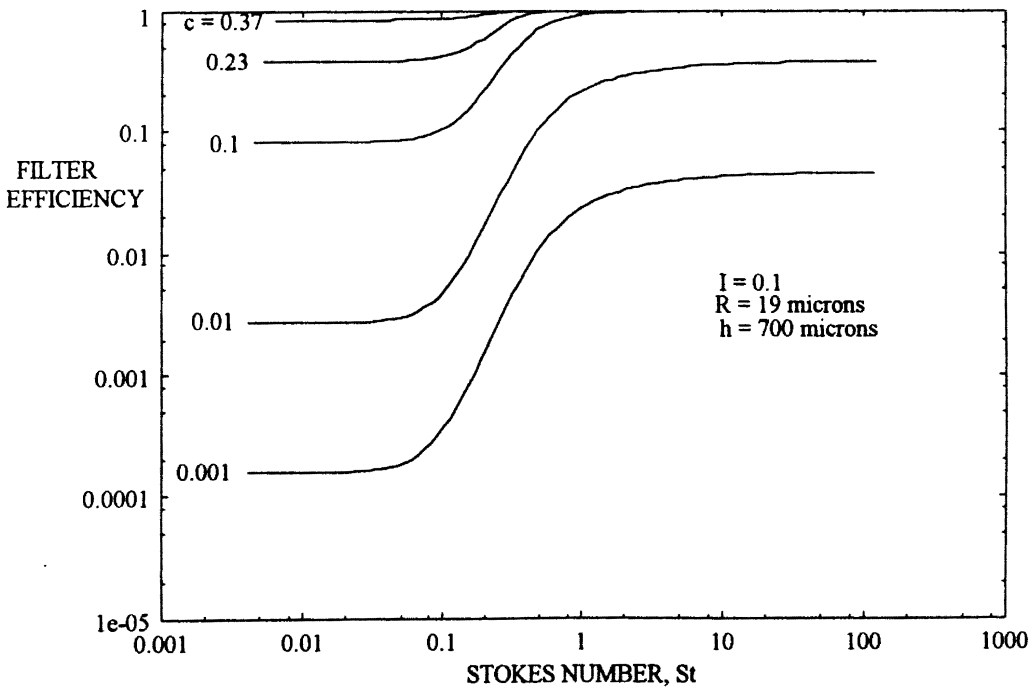

Figure 4.1 Plain Paper Filter Efficiencies Due to Inertial Interception

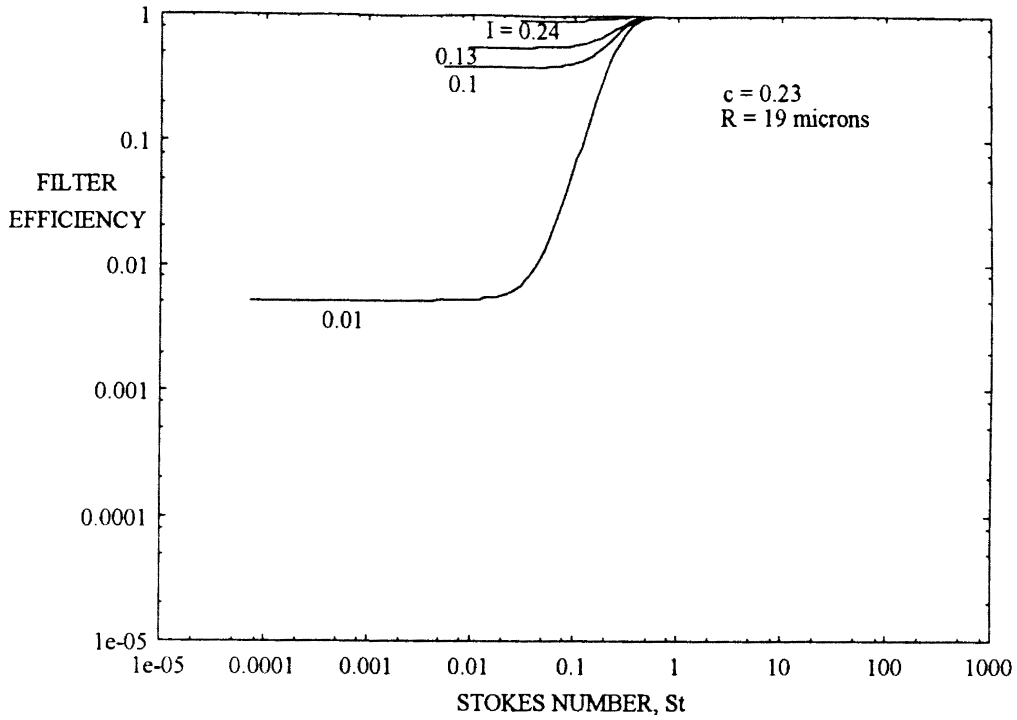

Figure 4.2 Plain Paper Filter Efficiencies Due to Inertial Interception

4.2 Methodology for Calculation of Pleated Filter Efficiencies

With the available models of filtration, it is possible to determine the filtration efficiencies as a function of the aerosol velocities. There are other parameters that would affect the filtration, like the aerosol particle size and its size distribution, properties of the filter media, etc. The effect of velocity can be studied by holding all but one parameter constant.

To calculate the overall filter efficiency for a filter with the velocity distribution described in Chapter IV, the filter is first divided into small elements. The elements are such that each velocity measurement location coincides with one element on the filter. For the purpose of calculating efficiencies, it is assumed that the measured velocity is uniform over each of the corresponding elements. The velocities measured and indicated in

Chapter III are the velocities of the fluid before entering the pleat, denoted by say, V_{op}. If it is assumed that the flow is uniformly distributed within the pleat, then, the velocity of the fluid entering the media (inside the pleat), V_{ip}, can be obtained by equating the flow entering the element and the flow passing through the total surface area of the media contained in the element. Consider an element of width Δx and length Δy. Then for a filter having pleats of slant height, H_f, and pleats with pitch, P_f, the total area of the media contained within an element, a_e, will be given by

$$a_e = \frac{\Delta x \Delta y}{P_f} 2H_f. \tag{4.1}$$

The slant height, H_f, of the pleat can be approximated by the height of the pleat with a maximum error of about 0.3%, which acceptable for these calculations. Therefore V_{ip} can be given by

$$V_{ip} = \frac{V_{op}\Delta x \Delta y}{\frac{\Delta x \Delta y}{P_f} 2H_f} = \frac{V_{op} P_f}{2H_f} \tag{4.2}$$

Thus the analysis that follows reflects the effects of large scale non-uniformities only. The effects of small scale non-uniformities are totally absent because of the assumption of uniform flow distribution within the pleat.

The combination of the models proposed by Lee (1982) and Jaroszczyk (1991), which is described earlier in Section 1.6.4, is used in a computer program to calculate the efficiencies for each element. The efficiencies of each of such elements is hereafter referred to as *elemental efficiency* and is denoted by η_e. The elemental penetration, P_e, can then be given by

$$P_e = 1 - \eta_e. \tag{4.3}$$

Let the particle number density or the dust concentration towards the inlet side of the filter be C, then the particle number density at the exit of the filter will be (CP_e). The

unit of C in SI units is m^{-3}. If Q_F is the air volume flow rate through the filter, the number rate of particles entering the flow will be CQ_F. If N_e represents the number rate of particles penetrating an element having an area, a_e, and velocity, V_{ip}, then N_e can be given by

$$N_e = (CP_e)a_e V_{ip}. \tag{4.4}$$

Where the product, $a_e V_{ip}$, represents the local air volume flow rate entering an element. The total number rate of particles penetrating the filter, N, can be given by

$$N = \sum_{i=1}^{n} \{(CP_e)a_e V_{ip}\}_i. \tag{4.5}$$

where, n is the number of elements in a filter and the subscript i refers to the ith element.

Then the overall efficiency of the filter can be given by

$$\eta_F = \frac{\sum_{i=1}^{n} \{(CP_e)a_e V_{ip}\}_i}{CQ_F}. \tag{4.6}$$

For the sake of simplicity of calculations, it is assumed that only monodisperse dust exists in the flow. Separate calculations can be performed for different sized particles to study the effect of particle size on filtration efficiency. This assumption of monodisperse particles in conjunction with the efficiency equation (4.6), means that although the efficiency is based on particle number count, the same efficiencies would result if the approach were based on volume or weight of the aerosol particles.

4.3 Assumptions Regarding Particle Distribution

4.3.1 Assumption I : Uniform Particle Number Density Distribution

In practice it is really hard to say how valid the assumption of uniform particle number density is. There are other possible approaches to account for the particle concentration distribution over the filter, which are conveniently represented with the help

of Figures 4.3 and 4.4. In these two figures the typical velocity, V_{op}, distribution is represented by the thin lined curve. In Figure 4.3 assumption I represents the case of uniform particle number density distribution. Another way to represent the particle distribution over a pleated filter would be in terms of number of particles, N_p, passing a unit area per unit time. The number of particles passing per unit area per unit time, N_p, and the local particle concentration are related by

$$N_p = CV_{op} \tag{4.7}$$

where, V_{op} is the velocity of fluid before entering the pleat. Since for assumption I, the particle density, C, is constant throughout the filter, the particle distribution obtained by using equation (4.5) will be similar to the velocity profile as shown in Figure 4.4.

4.3.2 Assumption II : Particle Concentration Proportional to Local Velocity

Research work on particle number density distribution over pleated air filters is being simultaneously performed in this lab at Oklahoma State University. The preliminary results (Haldhani, 1993) indicate that the particle number density, C, could peak at the center of the filter with a profile similar to the bell shaped velocity profile over the pleated air filter as discussed in Figures 3.9 and 3.15. This kind of distribution is represented in Figure 4.3 by the curve "assumption II". Mathematically this distribution can be represented by

$$C = kV_{op} \tag{4.8}$$

where, k is a constant characteristic of the flow. From equation (4.6), the number of particles passing per unit area per unit time, N_p, for this case will be given by

$$N_p = CV_{op} = (kV_{op})V_{op} = kV_{op}^{\,2}. \tag{4.9}$$

The particle distribution in this case will be proportional to the square of the local velocity and is shown in Figure 4.4.

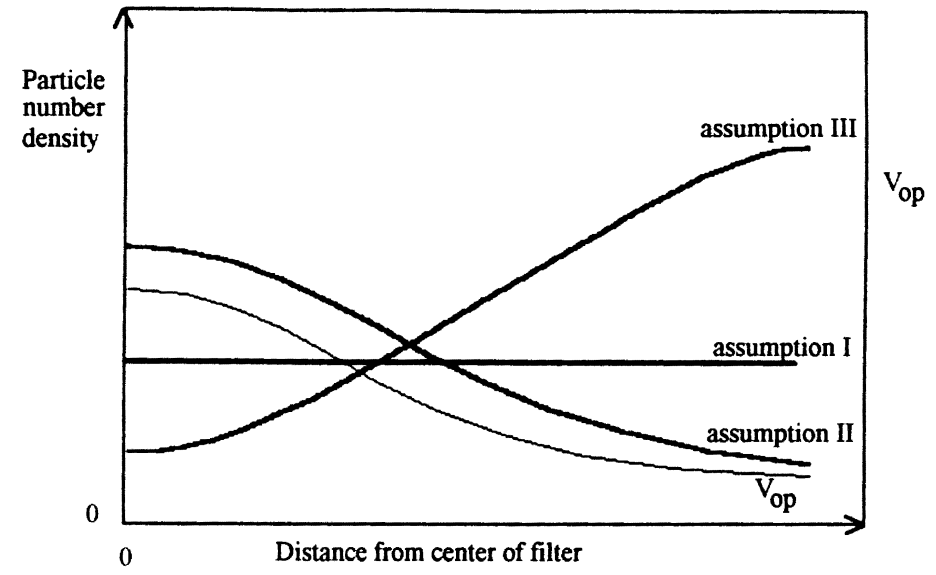

Figure 4.3 Various Assumptions for Particle Density Distribution Over a Pleated Filter

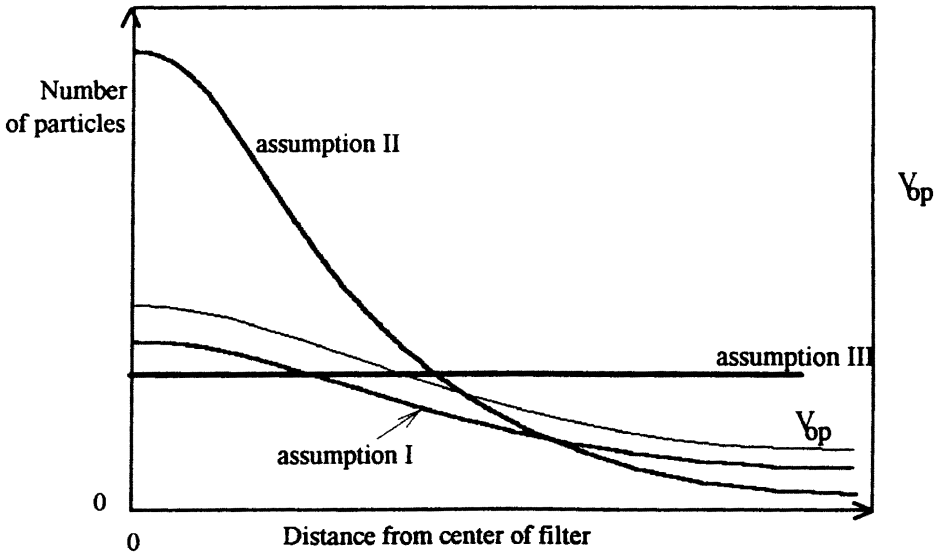

Figure 4.4 Various Assumptions for Particle Number Distribution Over a Pleated Filter

4.3.3 Assumption III : Uniform Particle Number Distribution

The other possible assumption could be that of uniform particle number distribution. This will be represented by a horizontal straight line on a plot of N_P verses location on filter as shown in Figure 4.4. In this case

$$N_p = CV_{op} = \text{const.}$$
$$\therefore\ C = \frac{\text{const.}}{V_{op}} \tag{4.10}$$

Hence the plot of particle number density would have a valley at the center of the filter as is shown in Figure 4.3. But this possibility of particle distribution seems more unrealistic than the two distributions described in assumptions I and II. In the absence of the knowledge of the parameter, k, in equation (4.6), assumption I, i.e. the assumption of uniform particle number density distribution is thought to be the most practical one. Assumption I is applied for all the calculations except when a study of the effect of changing assumptions is made and is mentioned at the appropriate places.

A computer program listed in Appendix D, which is based on the above theory was developed and used in the ensuing calculations. The data generated from the velocity measurements is stored in a file and used as an input file to the computer program. A small point to be brought to the notice of the reader is that one of the velocity readings over the filter AF3592 corner was -0.256 m/s. Since the efficiency for this element cannot be calculated, the velocity for this element was assumed to be zero throughout the calculations. However, this will not result in any unacceptable errors in the results as the area of this corner element constitutes up to only 0.053% of the total area of the filter.

4.4 Frazier Air Permeability of Filter Media

The relation between air permeability and the three main characteristics of a media; R, h, and c, are given by equation (1.48). Using this relation, the Frazier air permeability for a range of the media used for the pleated air filters studied in this report and specified in Appendix C are calculated and the results are presented graphically in Figure 4.5 and Figure 4.6. In Figure 4.5, for a filter of given uniform diameter, the air permeability decreases as the packing density, c, increases. The increase in packing density can be considered as adding in more fibers in a filter of given thickness which will increase the resistance to air flow. For the same packing density, the effect of reducing the fiber diameter is to decrease the air permeability. Physically this can be thought of as splitting of the thick fibers into many smaller fibers so that the volume of fibers in the given volume of filter still remains the same. Since the number of obstructions has increased in this case, the result is a decrease in air permeability. For the same fiber diameter and packing density, the effect of reducing the filter thickness is to increase air permeability which is evident from the two figures.

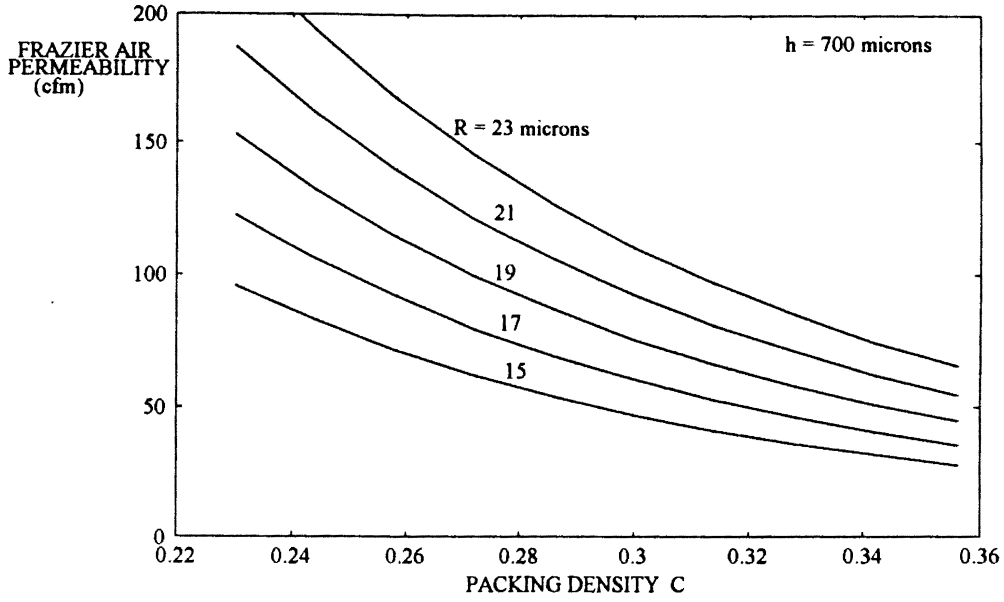

Figure 4.5 Frazier Air Permeability for a Filter Media Thickness of 700 μm

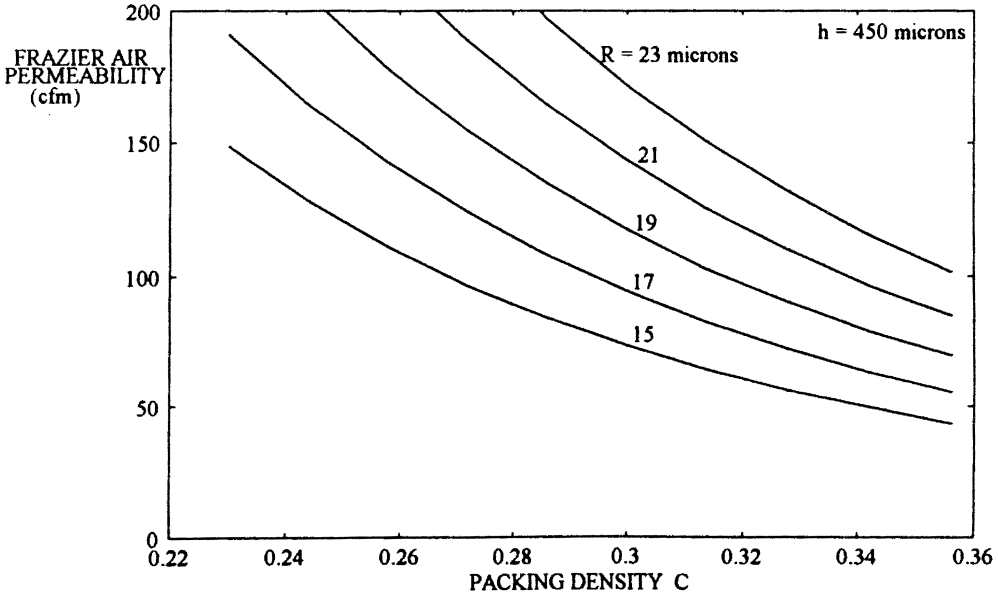

Figure 4.6 Frazier Air Permeability for a Filter Media Thickness of 450 μm

4.5 Efficiencies of Pleated Air Filters

The large scale variations in the flow distribution over the pleated air filter were discussed earlier in Chapter III. The flow is further distributed within an individual pleat which would result in small scale non-uniformities of flow distribution. As mentioned earlier in Section 4.3, these small scale non-uniformities will be neglected and the analysis will be performed assuming that once the flow enters a pleat, the flow is uniformly distributed over the area of the pleat. Thus the analysis to follow will indicate the effects of large scale non-uniformities in velocity distribution. There are also other assumptions in the present calculations which were discussed earlier in detail and are listed below together.

4.5.1 List of Assumptions

The following calculations to follow are based on the following assumptions:

a) perfect adhesion, i. e. E_a=1.0,

b) no re-entrainment of particles,

c) no filtration takes place due to diffusive mechanism and gravitational settling,

d) the concentration of the aerosol particles, C, at the inlet to the filter is constant,

e) the aerosol particles are monodisperse

f) the filter media has a uniform fiber radius, R, throughout the filter, and the value R is determined by taking the weighted mean of the distribution of the fiber radii in actual filter media,

g) the filter packing density, c, of the filter media is uniform throughout the filter,

h) the velocity distribution within the pleats, V_{ip}, is uniform, and

i) clogging of filters is not considered or the calculated efficiencies indicate the initial efficiencies of the filter.

4.5.2 Single Fiber Efficiencies in Pleated Air Filters

The Stokes number for different elements of the pleated air filter are not uniform as a result of the variation in the velocities. Since the single fiber efficiencies are a function of Stokes number, the single fiber efficiencies are also non-uniform. The variations in single fiber efficiencies given by equation (1.33) for the two filters AF3192 and AF3592 are indicated in Figure 4.7 and Figure 4.8 respectively. The reason for the specific choice of the value of fiber radius, R=19μm, is explained in Appendix C. A value of particle radius, a=2.5μm, was chosen because nearly 39% of the fine grade dust by weight or by volume is sized below this particle radius (see Appendix B). The central part of the filter which is exposed to higher velocities has high efficiency values in both the filters. Very low single fiber efficiencies are observed towards the edges.

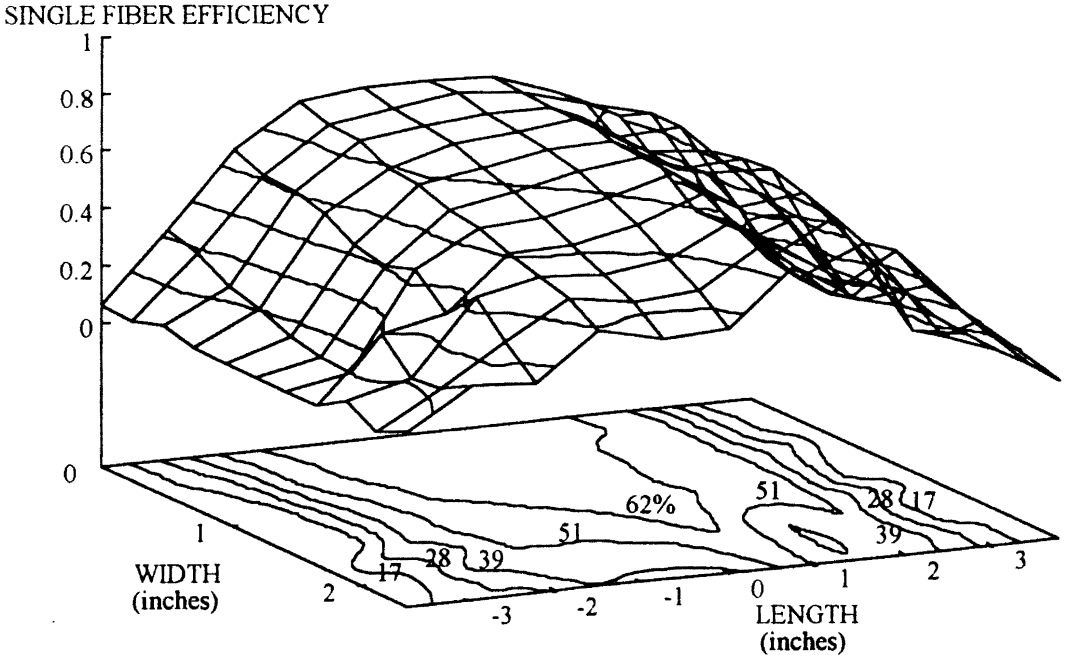

Figure 4.7 Single Fiber Efficiencies for Filter AF3192. R = 19μm, a = 2.5 μm

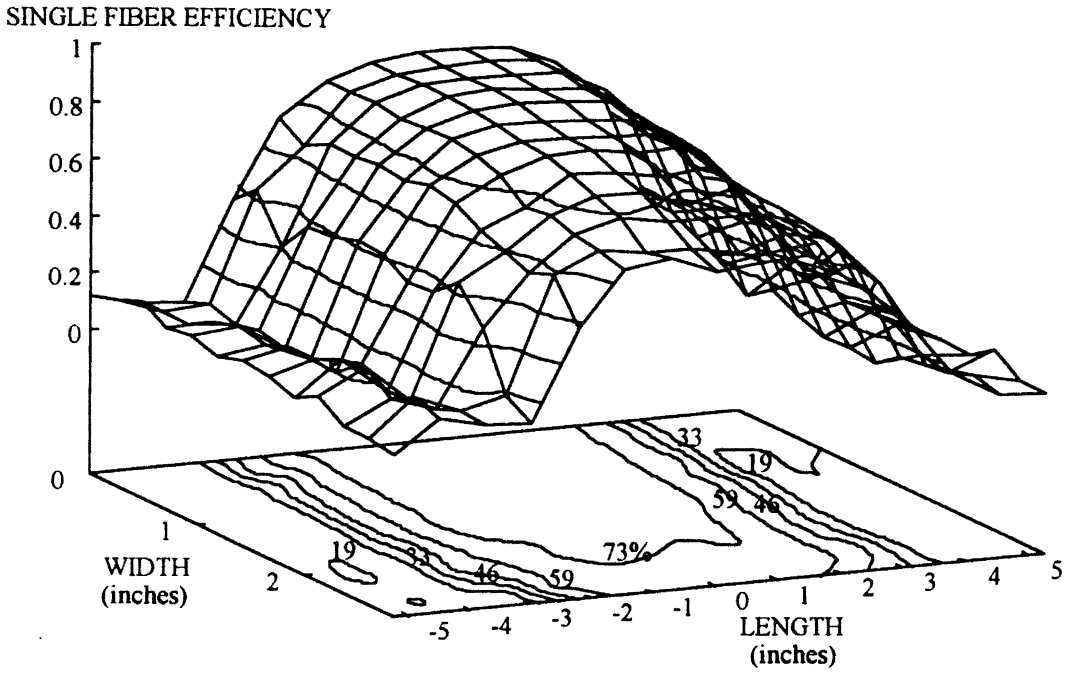

Figure 4.8 Single Fiber Efficiencies for Filter AF3592. R = 19μm, a = 2.5 μm

4.5.3 Filtration Efficiencies of Pleated Air Filters

Elemental efficiencies in the filter can be obtained from the velocity distribution by using equations (1.7) and (1.33). Various plots of such efficiencies for different sized dust particles are presented in the Figures 4.9 to 4.16. The overall filter efficiencies for those particular cases can be obtained by using the method described in Section 4.3. The ideal case of flow distribution would be that in which the velocities are uniform throughout the filter. Hence the ideal efficiency of a pleated air filter with uniform velocity distribution, denoted by η_U, can be calculated from the flow rate and area of the filter. The ratio, η_F/η_U indicates the deviation of the efficiency of the filter from the design or the ideal condition.

In Figure 4.9, it is seen that most of the filter operates at efficiencies above 88%. In fact, the flat portion of the efficiency surface indicates efficiencies above 99%. As the velocities drop, so does the Stokes number and the single fiber efficiencies as seen in previous figures. Due to the exponential nature of the filter efficiency equation (1.7), the element efficiencies drop sharply towards the edge as seen in Figure 4.9. The overall efficiency of the filter calculated with the assumption I, mentioned earlier, comes out to be 95.14% in this case. Had the flow been distributed uniformly, the efficiency of the filter would be 96.88%. Hence it is seen that the filter is operating at 98.2% of its designed efficiency.

The effect of smaller sized particles on filtration efficiencies of filter AF3192 is shown in Figures 4.10 and 4.11. In the case with a = 0.5 μm, the element efficiencies all over the filter drop to values below 4%. For the two cases in Figures 4.10 and 4.11, the ratio, η_F/η_U, is larger than one indicating that the filters are indeed operating at higher efficiencies with non-uniform flow than with uniform flow. This could be because of the varying slope of the filter efficiency curve in Figure 4.2. In fact, Figures 4.10 and 4.11 suggest that the entire filter should be operated at higher velocities so that the filter operates in the regime where the inertial filtration is dominant for smaller particles also.

Figure 4.12 is a case with smallest value of a such that all the elemental efficiencies are above 99%. A similar figure for any larger sized particle will have a similar efficiency surface and the filter would operate at nearly 100% efficiency. The figure also shows that there is no scope for improvement in the efficiencies by making the velocities uniform for this and larger sized particles.

Figures 4.13 to 4.16 are similar figures for filter AF3592. All the efficiency surfaces are similar to the ones observed in filter AF3192.

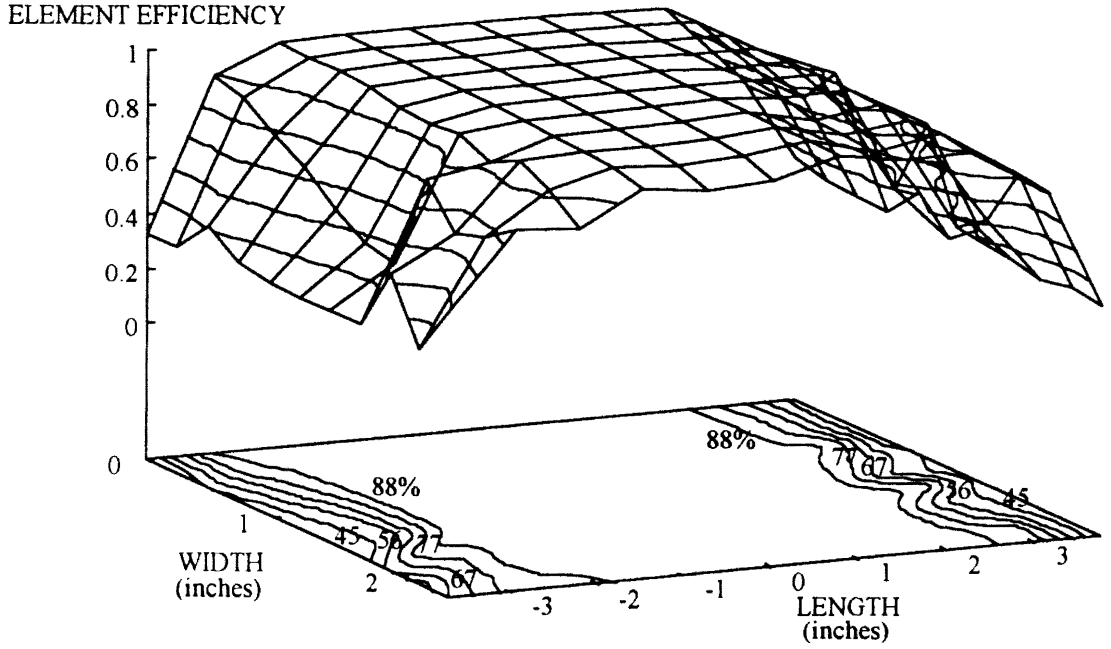

Figure 4.9 Elemental Efficiencies for Filter AF3192. a = 2.5 μm, h = 700 μm,
η_F = 95.14%, η_U = 96.88 %, η_F/η_U = 98.20

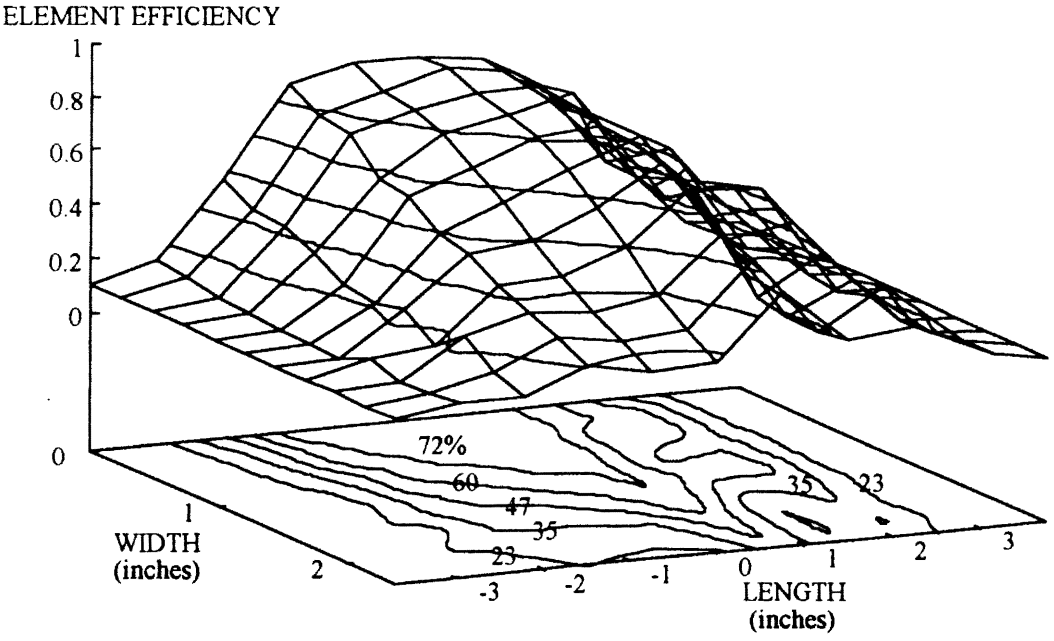

Figure 4.10 Elemental Efficiencies for Filter AF3192. a = 1.25 μm, h = 700 μm,
η_F = 51.71%, η_U = 34.55%, η_F/η_U = 149.67

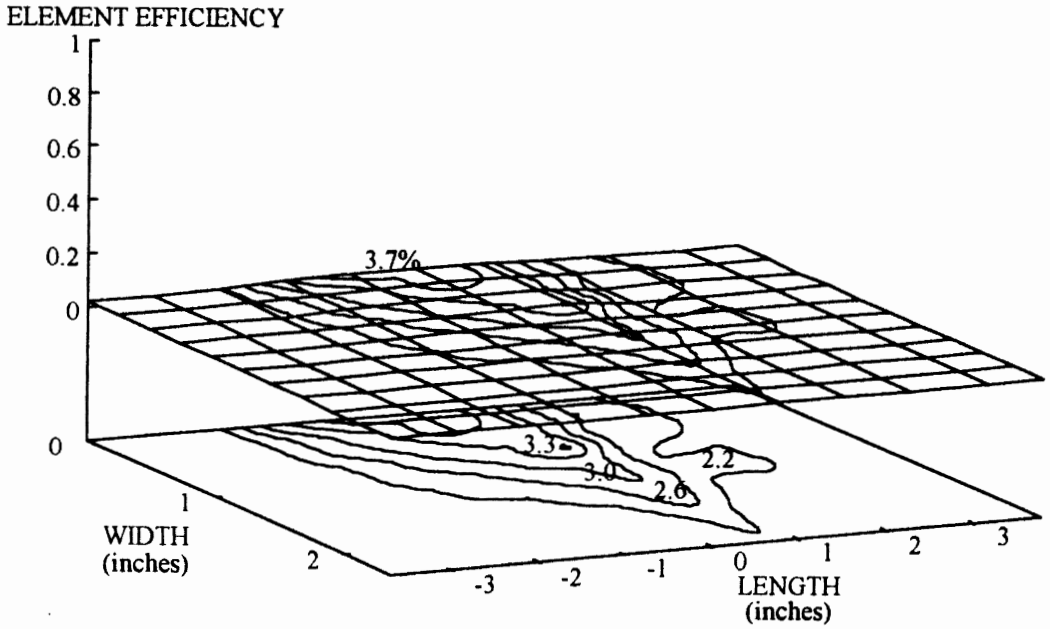

Figure 4.11 Elemental Efficiencies for Filter AF3192. a = 0.5 μm, h = 700 μm, η_F = 2.52%, η_U = 2.00%, η_F/η_U = 126.00

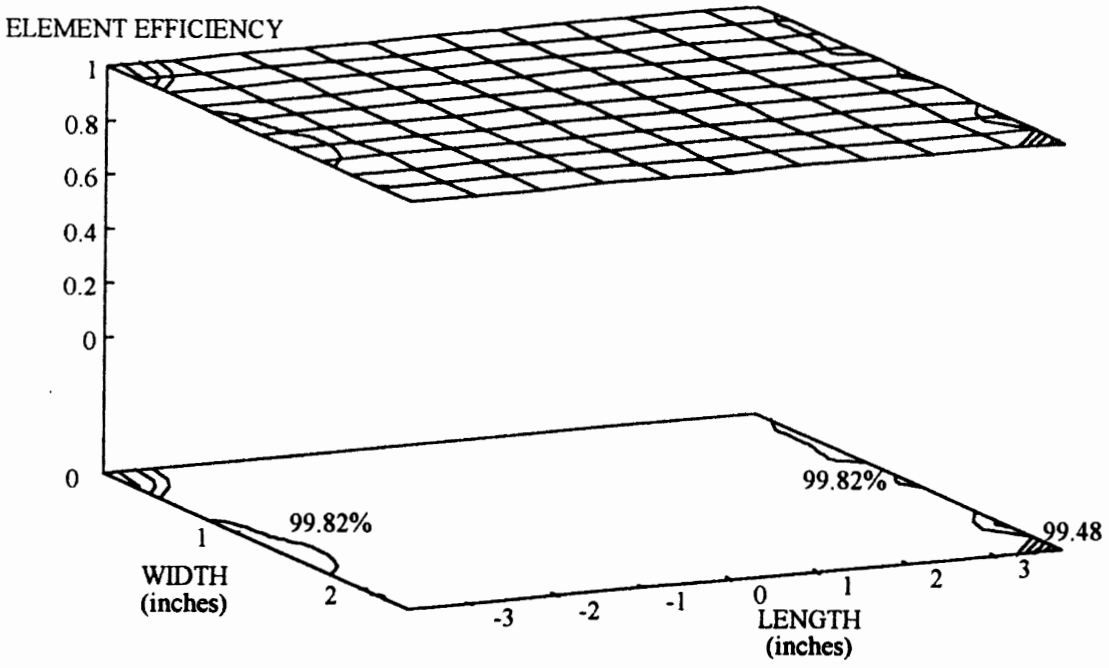

Figure 4.12 Elemental Efficiencies for Filter AF3192. a = 10.0 μm, h = 700 μm, η_F = 99.90%, η_U = 99.90%, η_F/η_U = 100.00

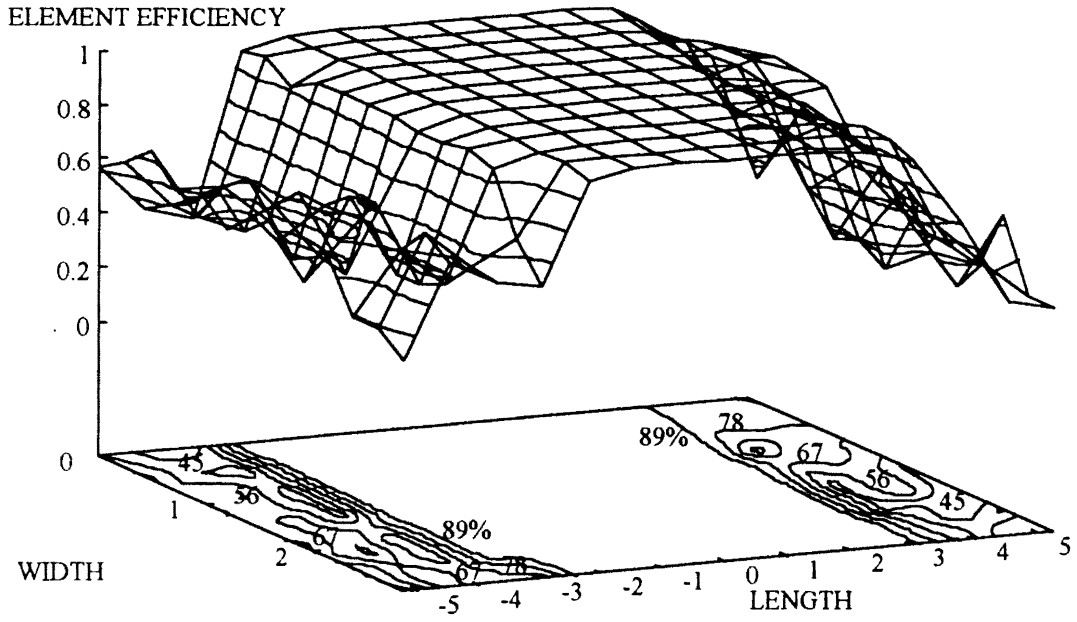

Figure 4.13 Elemental Efficiencies for Filter AF3592. a = 2.5 μm, h = 700 μm, η_F = 96.86%, η_U = 98.99 %, η_F/η_U = 97.85

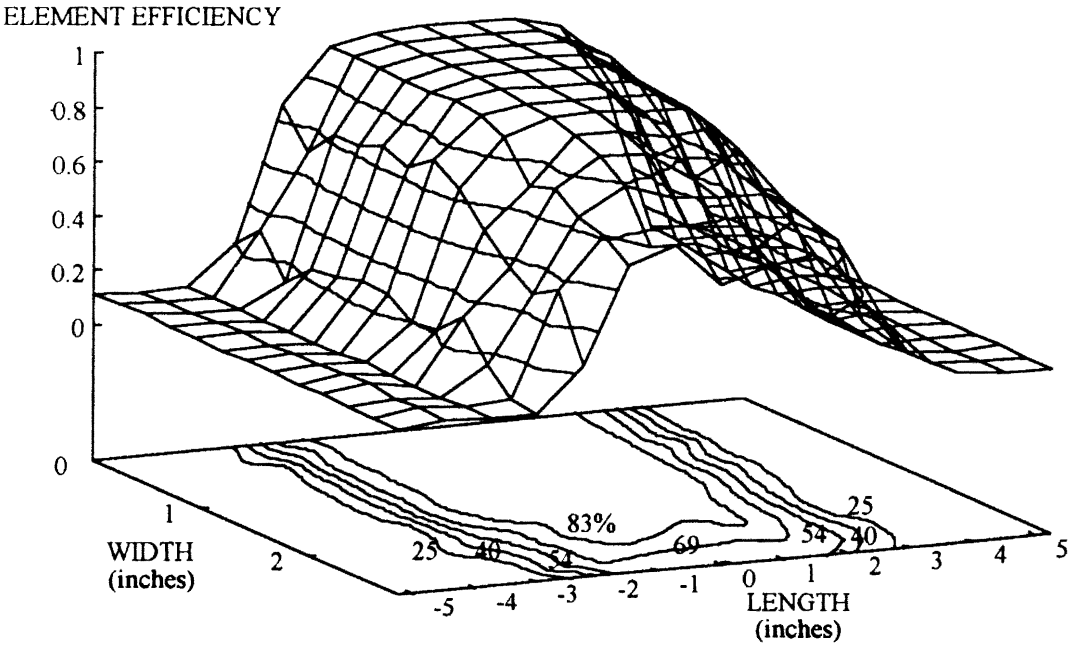

Figure 4.14 Elemental Efficiencies for Filter AF3592. a = 1.25 μm, h = 700 μm, η_F = 79.64 %, η_U = 67.85 %, η_F/η_U = 117.38

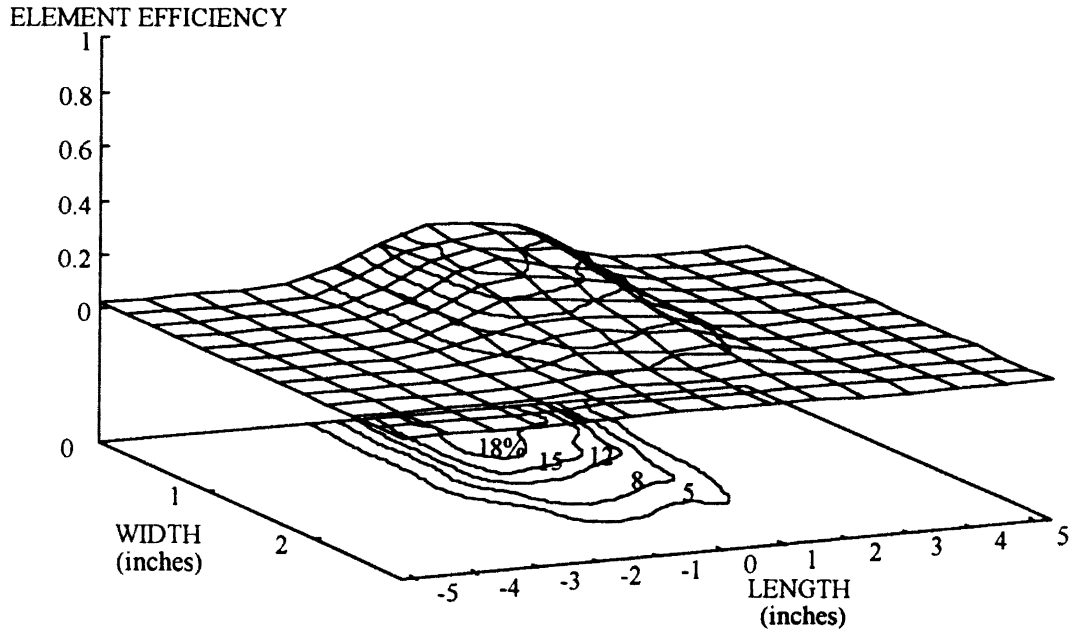

Figure 4.15 Elemental Efficiencies for Filter AF3592. a = 0.5 μm, h = 700 μm,
η_F = 9.08 %, η_U = 2.75 %, η_F/η_U = 330.18

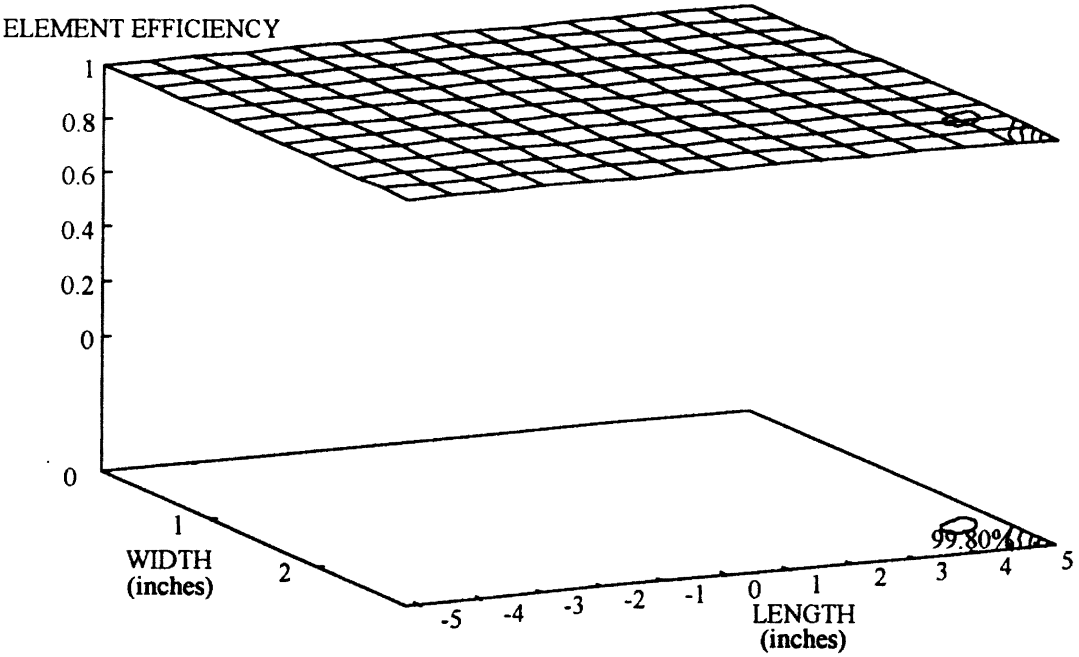

Figure 4.16 Elemental Efficiencies for Filter AF3592. a = 10.0 μm, h = 700 μm,
η_F = 99.90%, η_U = 99.90%, η_F/η_U = 100.00

TABLE II

EFFICIENCIES OF FILTERS FOR VARIOUS PARTICLE SIZES

	FILTER AF3192			FILTER AF3592		
PARTICLE RADIUS	η_F %	η_U%	η_F/η_U%	η_F %	η_U%	η_F/η_U%
0.5 μm	2.52	2.00	126.0	9.08	2.75	330.18
1.25 μm	51.71	34.55	149.67	79.64	67.85	117.38
2.5 μm	95.14	96.88	98.20	96.86	98.99	97.85
10.0 μm	99.90	99.90	100.00	99.90	99.90	100.00

It is seen from the above table that, for both the filters, efficiency drops to very low values if the particles are of very small size. The efficiencies for both the filters are below 10% when the particles are smaller than 1 μm (a = 0.5 μm). Also for both the filters, the efficiencies are nearly 100% for particles sized 20 μm (a = 10 μm). It can be seen from the particle distribution for the standard dust presented in Appendix B, that 90% by weight of the fine dust is sized below 20 μm. The efficiency of both the filters for particles larger than 20 μm will be practically 100%. Particle size affects the efficiency of a filter with uniform velocity in a similar manner as it affects a filter with non-uniform velocity distribution. The calculations indicate some scope of improvement in the filtration efficiencies for particles sized in the range 5 μm to 20 μm by making the flow distribution uniform. However, for particles smaller than 5 μm, there is actually a drop in the performance of the filter by making the flow distribution uniform. In fact it should be noted that the entire filter is operating at very low values of Stokes number and hence at very low element efficiencies. In the case of these small particles, the filter performs better

with non-uniform velocities because the portions of the filter that are exposed to velocities higher than the value of uniform velocities, filter much more efficiently as compared to any element of the filter with uniform velocity. For low values of interception parameters, it can be seen from Figure 4.2 that once the Stokes number exceeds a certain value in the range of 0.025 to 0.05 the efficiencies increase substantially. In fact by looking at Figures 4.11 and 4.15 it is observed that most of filter operates in the range where the efficiencies flatten out to nearly zero. Substantial improvements in the filter performance with particles smaller than 1 μm can be made by increasing the flow rates through the filter. Hence, the calculations, under the given assumptions, do not indicate for sure whether the improvements in the test housing to provide a uniform flow will result in a overall improved performance for a polydisperse dust, such as used in filter performance tests.

A direct comparison between the two filters for which the results in Table II are presented is very difficult because the two filters have different geometric dimensions, operate at different flow rates and face velocities and have different velocity distributions. However, it is seen that the filter AF3592, which is operated at higher flow rates has higher efficiencies with marked difference as the particle size decreases. Hence this analysis would indicate that the efficiencies are higher when the filters are operated at higher flow rates.

It must be noted that these calculations and discussions are based on the assumption of perfect adhesion, *i.*e. E_a = 1.0. As mentioned earlier, it is a very well known fact that perfect adhesion is not possible for the reasons mentioned. The effect of incomplete adhesion and re-entertainment is to decrease the efficiencies of the filter at higher velocities or higher Stokes number. This could possibly result in reduced values of η_F for the cases presented in Table II for particles in the range 5 μm and above, but this would also mean that the ratio η_F/η_U would also reduce. Lower values of the ratio η_F/η_U means, there is a larger scope for filter performance improvement by making the velocity distribution uniform. Another implication of imperfect adhesion is that not as

much of improvement in efficiencies will be observed, as was discussed in the previous paragraph, by increasing the fluid velocities. However, the exact extent to which these efficiencies will be affected by imperfect adhesion needs to be studied in detail.

As the filter accumulates dust, more obstacles are created for the incoming dust particles which is equivalent to increasing the packing density of the filter which eventually results in an increase in efficiencies. Hence the initial efficiencies, which only are considered in this study are always the lowest, and as the filter accumulates dust, its efficiency increases. As the dust accumulates, a point may be reached when the dust already adhering to the filter can no longer adhere to the filter and gets re-entrained into the flow resulting is drastic drops in efficiencies (Jaroszczyk and Wake, 1991). This again forms a very involved and separate subject of study which is not at all addressed here.

The effect of filter packing density and fiber radius on the overall filter efficiency of filter AF3192 for various sizes of dust is shown in Figures 4.17 to 4.19. In Figure 4.17, it is seen that the efficiency increases with increase in the fiber diameter for the same packing density. This can be explained on the same lines as the variation in air permeability was explained. By reducing the fiber diameter while holding the same packing density means the splitting of the fibers in a give volume of filter. This will increase the flow obstacles and will result in increased efficiency. It is also seen that the efficiency increases with increasing packing density for the same fiber diameter. This is because as the packing density is increased the number of fibers in a given volume increases, increasing the obstacles which increases the efficiency. As the particle size being filtered drops, the efficiencies also drop drastically. Figure 4.20 is for the same parameters as Figure 4.17 but for h = 450 μm instead of h = 700 μm. The penetration can be seen to have increased in the case with the smaller thickness filter. Similar curves for filter AF3592 are drawn in Figures 4.21 to 4.24.

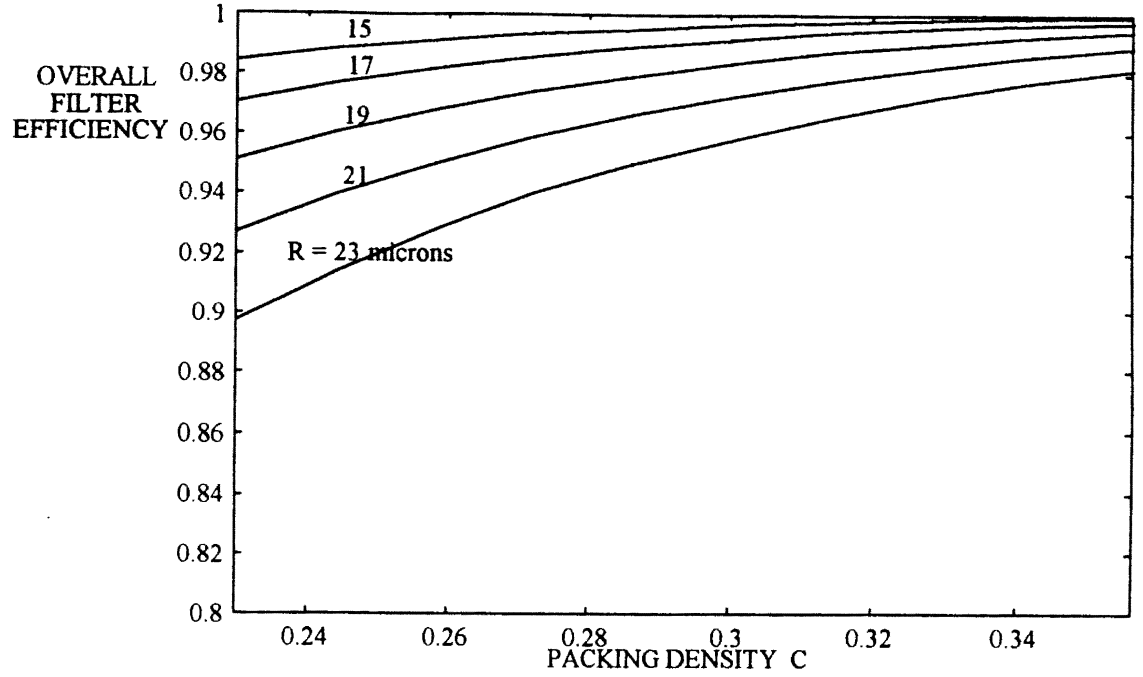

Figure 4.17 Overall Filter Efficiencies for Filter AF3192. h = 700 μm, a = 2.5 μm

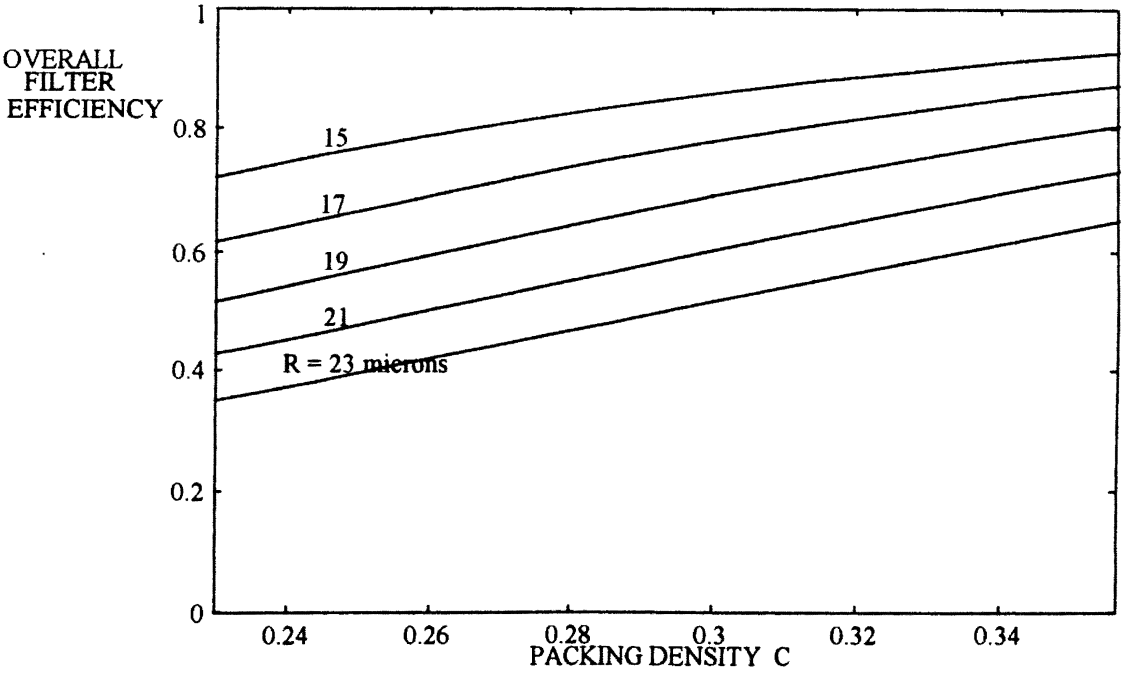

Figure 4.18 Overall Filter Efficiencies for Filter AF3192. h = 700 μm, a = 1.25 μm

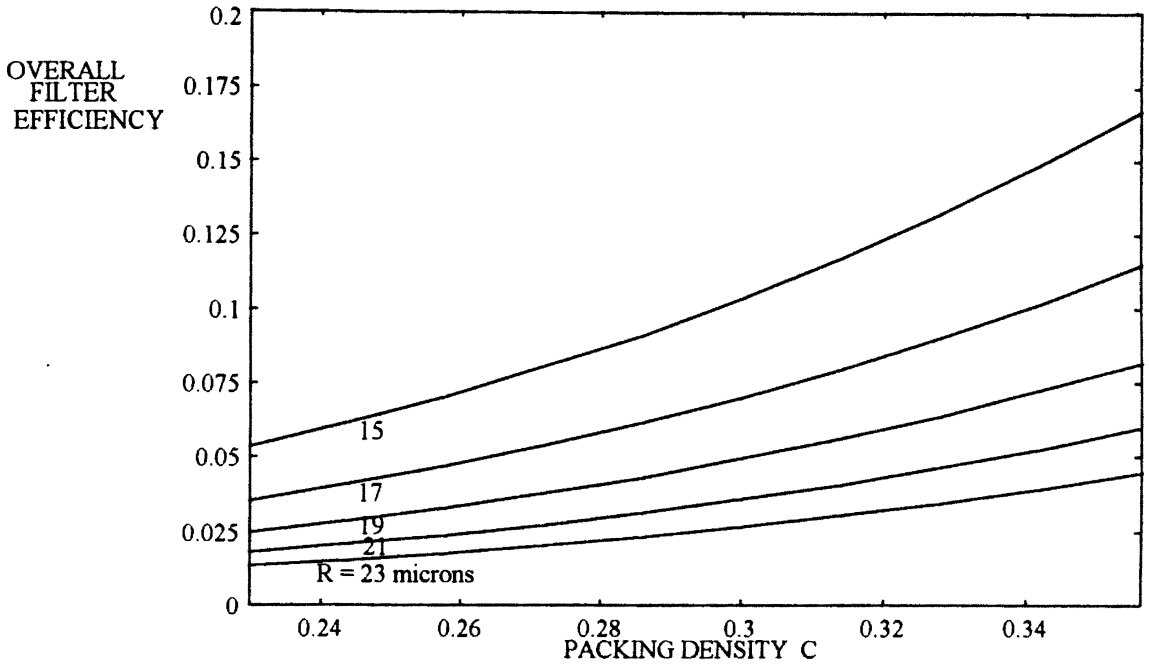

Figure 4.19 Overall Filter Efficiencies for Filter AF3192. h = 700 μm, a = 0.5 μm

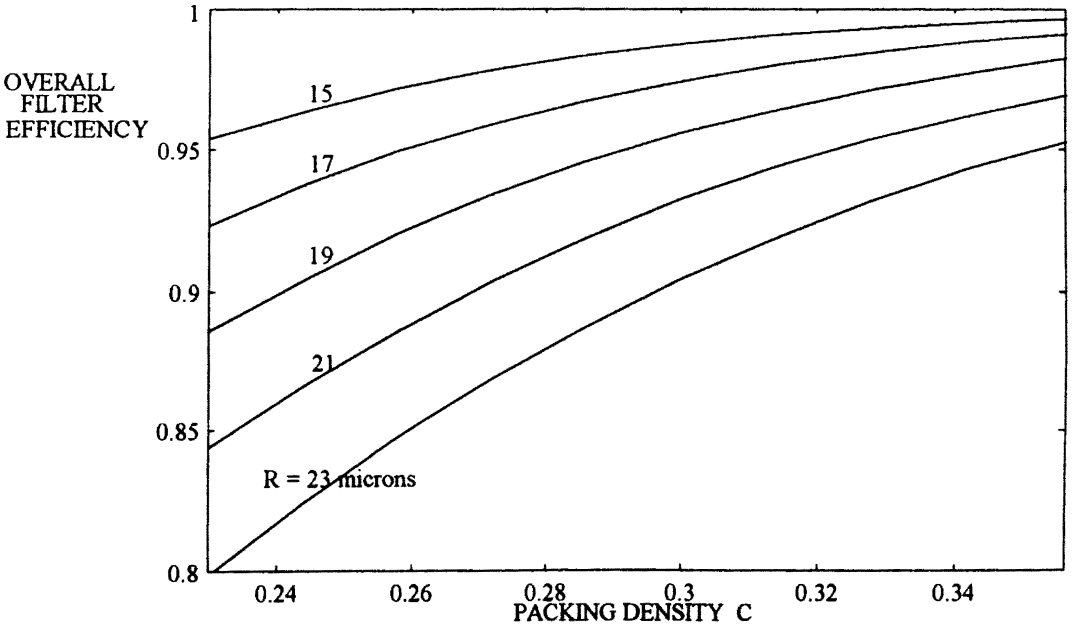

Figure 4.20 Overall Filter Efficiencies for Filter AF3192. h = 450 μm, a = 2.5 μm

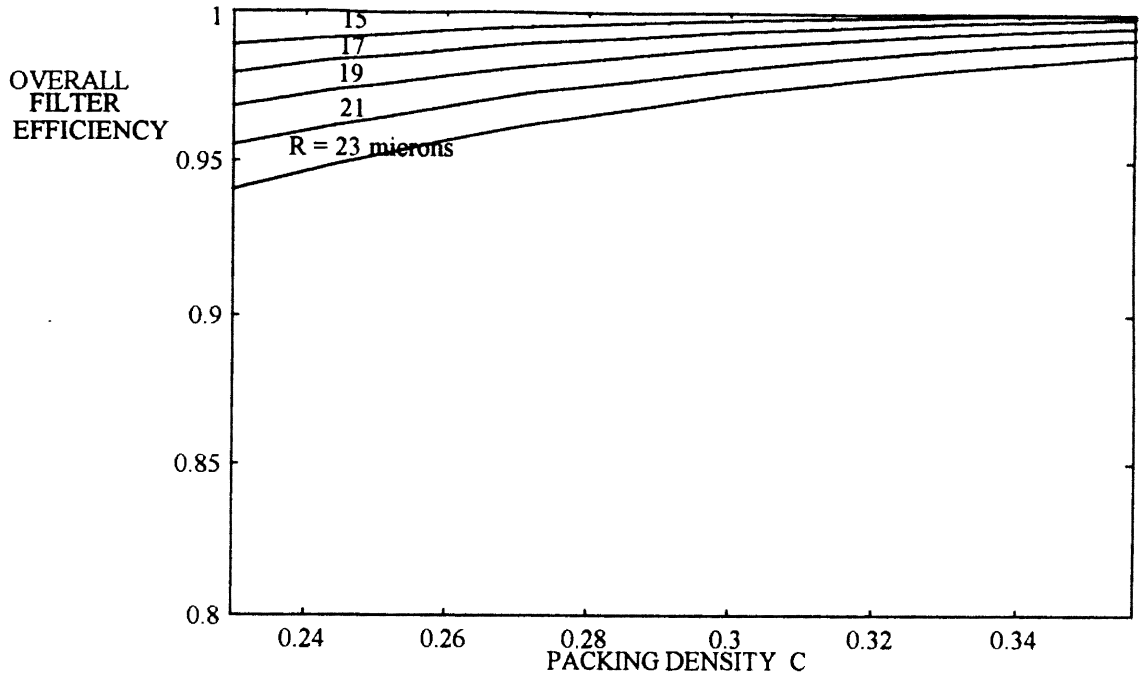

Figure 4.21 Overall Filter Efficiencies for Filter AF3592. h = 700 μm, a = 2.5 μm

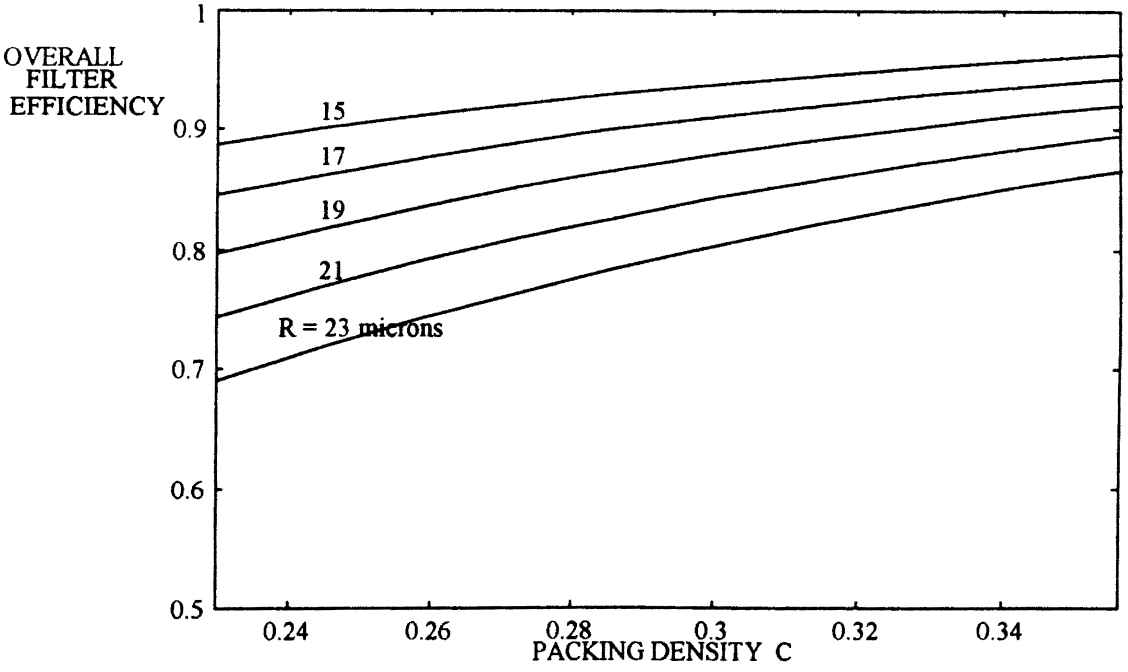

Figure 4.22 Overall Filter Efficiencies for Filter AF3592. h = 700 μm, a = 1.25 μm

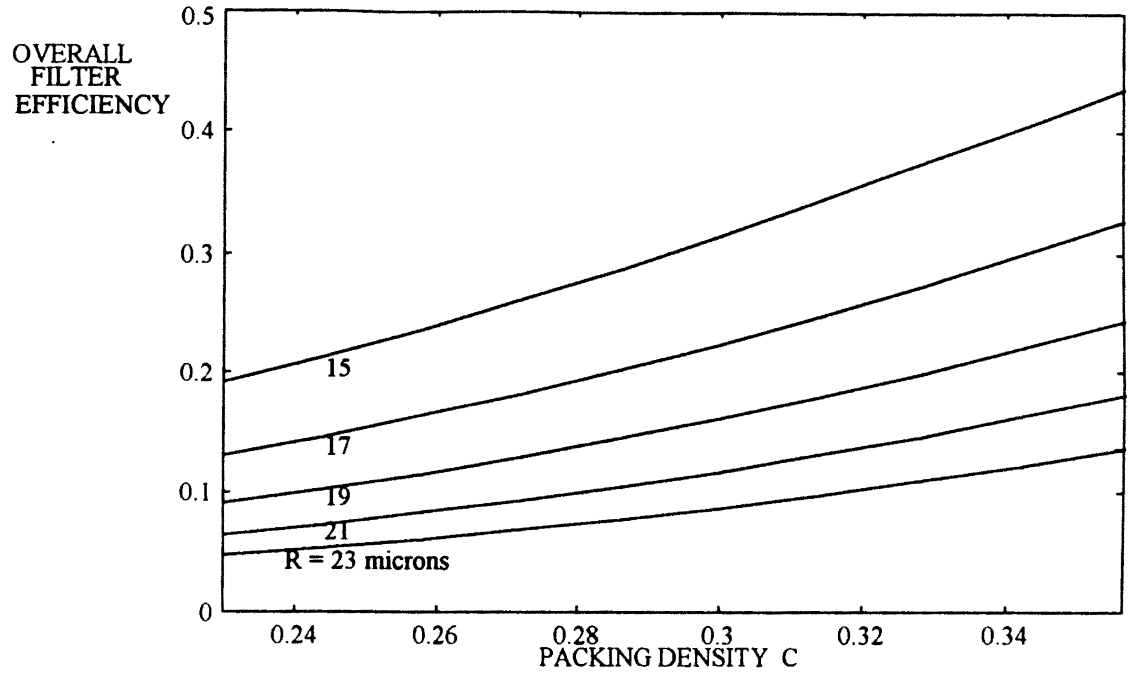

Figure 4.23 Overall Filter Efficiencies for Filter AF3592. h = 700 μm, a = 0.5 μm

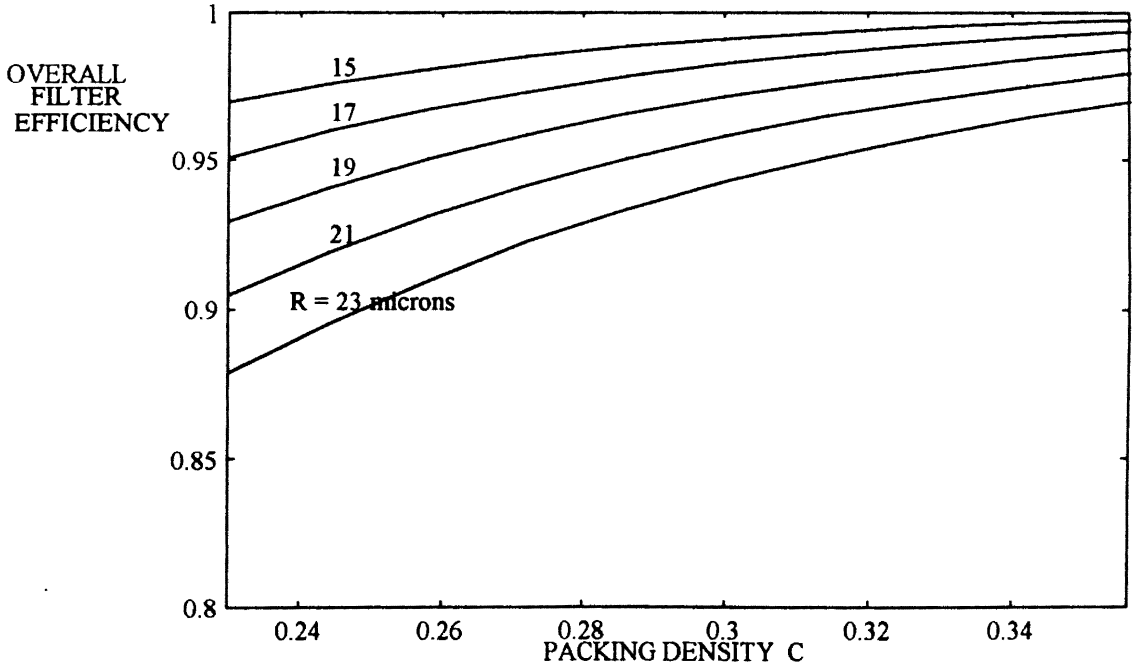

Figure 4.24 Overall Filter Efficiencies for Filter AF3592. h = 450 μm, a = 2.5 μm

Figure 4.25 is drawn for the same parameters as Figure 4.17 is drawn, but the assumption here is assumption III, uniform particle number distribution, described in Section 4.3. The overall filter efficiencies in this case are arrived at by simply taking the area weighted averages of the elemental efficiencies. Lower efficiencies are obtained by using assumption III. This can be explained as follows. In assumption I, a maximum number of the particles strikes the central portion of the filter as is shown in Figure 4.3. Also the efficiencies are high in these central regions. Hence very few particles pass through the filter. In assumption III, the particles are uniformly distributed as shown in Figure 4.3. So more particles pass the filter from the regions near the edge of the filter where the element efficiencies are low. Hence we observe that the overall efficiencies given by assumption III are lower than those given by assumption I.

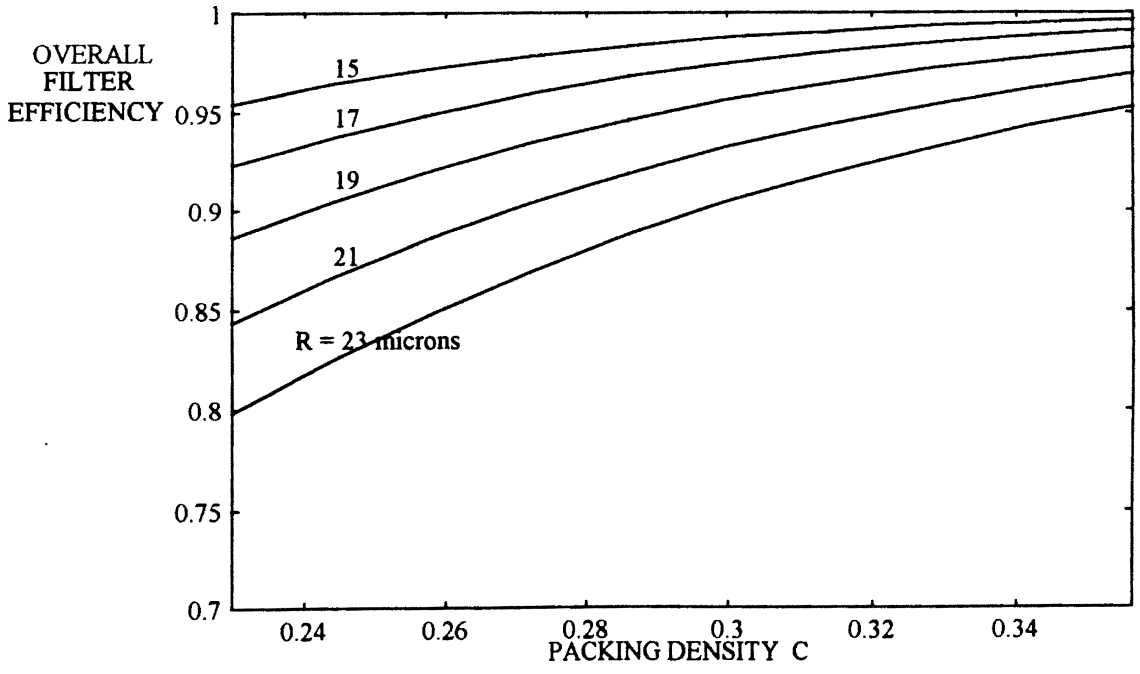

Figure 4.25 Overall Filter Efficiencies With the Assumption of Uniform Particle Number Distribution for Filter AF3192. h = 700 μm, a = 2.5 μm

It is seen from the above results and discussion that the air resistance offered by the filter is dependent on the properties of the filter and these filter properties in turn determine the efficiency of filters. In a given pleated filter, the overall filter efficiency varies substantially. For larger particles, overall filter efficiency nearly reaches 100% whereas, for small particles, it drops down below 10%. The calculations, under the given assumptions, suggest that filter efficiency can be improved for particles above a certain size by making the velocity distribution uniform. For smaller particles, the non-uniformities in the velocity distribution tend to enhance the overall filtration efficiency. Hence, the calculations, under the given assumptions, do not indicate for sure, if improvements in the test housing to provide uniform flow will result in a overall improved performance for a polydisperse dust. Filtration efficiencies of polydisperse dust may be approximated by weighting the efficiencies of various sized particles according to the distribution of the size in the given dust. This will account for the fact that different sized particles have a differing effect on filtration efficiencies.

CHAPTER V

CONCLUSIONS AND RECOMMENDATIONS

5.1 Conclusions

The following conclusions can be drawn from the present study:

1) The flow field inside the universal panel filter test housing is very turbulent and separated from the housing walls.

2) The impinging jet like flow provides the filter with a bell shaped non-uniform velocity distribution for both the filters studied.

3) There is a strong dependence of the filtration efficiencies on the fluid velocities and characteristics of the aerosol particles being filtered.

4) Due to the low values of Stokes number for particles smaller than 1 μm, the calculated initial efficiencies in case of both the filters were observed to be below 10% for these 1 μm sized particles. For such particles, assumption of perfect adhesion and no re-entrainment holds good.

5) As the particle size increases, the initial efficiencies also increase and for particles larger than 20 μm size, the initial efficiencies for these (larger than 20 μm) particles are nearly 100%, where the assumptions of perfect adhesion and no re-entrainment are applied.

6) Under the assumptions of perfect adhesion and no re-entrainment, the calculations indicate a possible improvement in the filter performance in terms of initial efficiency for particles of certain size, like the 5 μm particles, by making the flow

distribution over the filter uniform. However, for particles smaller than 2.5 μm, initial filtration efficiencies reduce by making the flow distribution uniform.

7) Under the assumptions of perfect adhesion and no re-entrainment, the calculations indicate that the initial efficiency for particles smaller than 2.5 μm can be increased by operating the filter at higher flow rates.

5.2 Recommendations for Future Work

Further study of filtration efficiencies must be done on the following guidelines.

1) Models must consider adhesion and re-entrainment to give more realistic results.

2) Experimental values of filtration efficiencies for plain filter media subjected to uniform velocity and monodisperse dust must be obtained and compared with the efficiencies predicted by the present models. If necessary the models must be altered to accurately represent the experimental data by including some empirical constants.

3) Experimental values of filtration efficiencies for pleated filters subjected to uniform and non-uniform velocities and monodisperse dust must be obtained and compared with the efficiencies predicted in the present study.

4) Models must account for the variation of filtration efficiency with the accumulation of dust. This will indicate the performance of the filter over its life span.

5) The small scale variations in the velocity must be included in the analysis of the pleated filter.

REFERENCES

Apfeld, P. B., Ahlstrom Filtration. (1993). Personal communication, April, 1993. Ahlstrom Filtration, Chattanooga, Tennessee.

ASHRAE Handbook - Heating, ventilating, and air-conditioning systems and equipment. (1992). ASHRAE. Atlanta, GA.

Bahaners, T., & Schollmeyer, E. (1986). "Computer simulation of the filtration process in a fibrous filter collecting polydisperse dust," Journal of Aerosol Sciences, Vol. 17, No. 2, pp. 191-200.

Cai, C. (1993). "Study of air filter flow by computational fluid dynamics," M. S. Thesis, Oklahoma State University, Department of Mechanical and Aerospace Engineering, Stillwater, Oklahoma.

Cai, J., & Peterson, F. (1989). "Efficiency for monodisperse particles in instationary filtration," Journal of Aerosol Sciences, Vol. 20, No. 8, pp. 955-958.

Cheikhrouhou, M., & Sigli, D. (1988). "Influence of the structure of the fabric filter on the velocity and stress fields of filtration flows in their vicinity," Textile Research Journal, Vol. 58, pp. 371-379.

Davies, C. N. (1973). Air filtration, Academic Press Inc., New York.

Flagan, R. C., & Seinfeld, J. H. (1988). Fundamentals of air pollution engineering, Prentice Hall, New Jersey.

Grant, D. C., Liu, B. Y. H., & Fisher, W. G. (1989). "Particle capture mechanisms in gases and liquids: An analysis of operative mechanisms in membrane/fibrous filters," The Journal of Environmental Sciences, Vol. 31-32, pp. 43-51.

Gurumoorthy, V., Bawabe, A. J., Brown, G. A., & Lessmann, R. C. (1990). "Prediction of pressure drop in automotive air induction systems," Third Annual Meeting of the American Filtration Society, March 1990, Washington D. C.

Haldhani, M. K. (1993). "Particle number density distribution and its time history for an automotive air filter," M. S. Thesis, Oklahoma State University, Department of Mechanical and Aerospace Engineering, Oklahoma.

Harrop, J. A., & Stenhouse, J. I. T. (1969). "The theoretical prediction of inertial impaction efficiency on fibrous filters," Chemical Engineering Science, Vol. 24, Part 2, pp. 1475-1481.

Huang, J. Y. C. & Garcia-Maura F. (1986). "Effect of influent property on filter performance," Journal of Environmental Engineering, Vol. 112, No. 4, pp. 701-717.

Igwe, G. J. I. (1988). "Design of a simple gas and solid filtration apparatus," Textile Research Journal, Vol. 58, pp. 280-286.

Ingham, D. B., & Hildyard, M. L. (1989). "The particle collection efficiency of a cascade of cylinders," The Canadian Journal of Chemical Engineering, Vol. 67, pp. 545-553.

Jaroszczyk, T., & Wake, J. (1991). "Critical aerosol velocity in nonwoven filtration," TAPPI Proceedings, Nonwoven Conference, pp. 125-135.

Jaroszczyk, T., Ptak, T. J., Fallon, S. L., & Wake, J. (1993). "Particulate and odor control in car ventilation systems," SAE Technical Paper Series, March 1993, Paper No. 930014.

Kinsley,Jr. H. B. (1989). "The relationship between fiber diameter and filtration efficiency," TAPPI Journal, Vol. 72, Part 4, Nov. 1989, pp. 153-156.

Kuwabara, S. (1959). "The forces experienced by randomly distributed parallel circular cylinders or spheres in a viscous flow at small Reynolds number," Journal of Physical Society of Japan, Vol. 14, No. 4, pp. 527-532.

Landahl, H. D., & Herrmann, R. G. (1949). "Sampling of liquid aerosols by wires, cylinders, and slides, and the efficiency of impaction of the droplets," Journal of Colloid Science, Vol. 4, pp. 103-136.

Lee, K. W., & Liu, B. Y. H. (1982a). "Experimental study of aerosol filtration by fibrous filters," Aerosol Science and Technology, Vol. 1, pp. 35-46.

Lee, K. W., & Liu, B. Y. H. (1982b). "Theoretical study of aerosol filtration by fibrous filters," Aerosol Science and Technology, Vol. 1, pp. 147-161.

McLaughlin, C., McComber, P., & Gakwaya, A. (1986). "Numerical calculation of particle collection by a row of cylinders in a viscous fluid," The Canadian Journal of Chemical Engineering, Vol. 64, pp. 205-210.

Orr, C. (1977). Filtration - principles and practices, Part I, Marcel Dekker, Inc. New York and Basel.

Payatakes, A. C. (1979). "Advances in dendritic deposition of aerosols by inertial impaction and/or interception," Proceedings of The Second World Filtration Congress, pp. 507-519.

Ptak, T., & Jaroszczyk, T. (1990). "Theoretical-experimental aerosol filtration model for fibrous filters at intermediate Reynolds number," Proceedings of The Fifth World Filtration Congress, Nice, France, pp. 566-572.

Ramarao, B. V., & Tien C. (1988). "Stochastic simulation of aerosol deposition in model filters," AIChE Journal, Vol. 34, No. 2, pp. 253-262.

Riest C. Parker, (1984) Introduction to aerosol sciences, New York, Macmillan Publishing Company.

Rodman, C. A. (1979). "Filter media performance and fiber morphology," Proceedings of The Second World Filtration Congress, pp. 257-267.

Rodman, C. A., & Lessmann R. C. (1988). "Automotive nonwoven filter media: their construction and filter mechanisms," TAPPI Journal, Vol. 71, Part 4, pp. 161-168.

Rollin, A. L., Denis, R., Estaque, L., & Masounave, J. (1982). "Hydraulic behavior of synthetic non-woven filter fabrics," The Canadian Journal of Chemical Engineering, Vol. 60, pp. 226-234.

Seo, Y., & Kim, K. U. (1992). "Finite element modeling of ultra fine particle filtration by a membrane filter," Polymer Engineering and Science, Vol. 32, pp. 98-106.

Shapiro, M., & Brenner, H. (1989). "Dispersion and deposition of aerosol particles in filters," Journal of Aerosol Sciences, Vol. 20, No. 8, pp. 951-954.

Shapiro, M., Kettner, I. J., & Brenner, H. (1991). "Transport mechanics and collection of submicrometer particles in fibrous filters," Journal of Aerosol Sciences, Vol. 22, No. 6, pp. 707-722.

Spielman, L. A. (1977). "Particle capture from low-speed laminar flows," Annual Review of Fluid Mechanics, Vol. 9, pp. 297-319.

Spuruny, K. R. (1986) Physical and chemical characterization of individual air borne particles, Ellis Harwood Limited, Chichester.

Stechkina, I. B., & Fuchs, N. A. (1966). "Studies on fibrous aerosol filters - I. Calculation of diffusional deposition of aerosols in fibrous filters," The Annals of Occupational Hygiene, Vol. 9, pp. 59-64.

Stechkina, I. B., Kirsch, A. A., & Fuchs, N. A. (1969). "Studies on fibrous aerosol filters - IV. Calculation of aerosol deposition in model filters in the range of maximum penetration," The Annals of Occupational Hygiene, Vol. 12, pp. 1-8.

Stenhouse, J. I. T. (1975). "Filtration of air by fibrous filters," Filtration and Separation, Vol. 12, pp. 268-274.

Suneja, S. K., & Lee, C. H. (1974). "Aerosol filtration by fibrous filters at intermediate Reynolds number," Atmospheric Environment, Vol. 8, pp. 1081-1094.

Wake, D., & Brown, R. C. (1991). "Filtration of monodisperse aerosols and polydisperse dusts by porous foam filters," Journal of Aerosol Sciences, Vol. 22, No. 6, pp. 693-706.

White, F. M. (1991). Viscous fluid dynamics, McGraw-Hill, Inc., U.S.A., 2nd ed.

White, P. A. F., & Smith, S. E. (1964). High-efficiency air filtration, Butterworths, London.

Wilkinson, E. T., & Davis, G. A. (1985). "A stochastic model for the filtration of dilute suspensions using non-woven cloths," The Canadian Journal of Chemical Engineering, Vol. 63, pp. 891-902.

Zia M., Faghri, M., & Lessmann, R. C. (1990). "The effect of different flow field models on aerosol particle capture in nonwoven fibrous filters," The Third Annual Meeting of the American Filtration Society, Washington D. C.

APPENDIX A

FILTER SPECIFICATIONS

TABLE III

FILTER SPECIFICATIONS

Sr. No.	DESCRIPTION	(units)	FILTER AF3192	FILTER AF3592
1.	Length of filter	(m)	0.193	0.268
2.	Width of filter	(m)	0.121	0.143
3.	Height of pleat	(m)	0.030	0.020
4.	Pitch of pleat	(m)	0.003125	0.003125
5.	Design flow rate	(cfm)	125.0	150.0
6.	Design uniform velocity outside pleat	(m/s)	2.5269	1.8476
7.	Design uniform velocity inside pleat	(m/s)	0.1316	0.1443
8.	Actual* flow rate	(cfm)	115.72	212.34
9.	Uniform velocity outside pleats (corresponding to Sr. No. 8)	(m/s)	2.3393	2.6155
10.	Uniform velocity inside pleats (corresponding to Sr. No. 8)	(m/s)	0.1218	0.2043

*Actual flow rate is calculated by numerical integration of the available velocity readings over the area of the filter.

Filter Manufacturer : Purolator Products, Inc.

APPENDIX B

DUST SIZE DISTRIBUTION

The SAE J726 Air Cleaner Test Code recommends the use of two grades of dust, labeled *fine* and *coarse*, as standard test dust for filter performance tests. The particles size distribution by volume shall be as follows:

TABLE IV

PARTICLE SIZE DISTRIBUTION BY VOLUME, %

Size, μm	Fine Grade (% less than)	Coarse Grade (% less than)
5.5	38±3	13±3
11	54±3	24±3
22	71±3	37±3
44	89±3	56±3
88	97±3	84±3
125	100	100

TABLE V

PARTICLE SIZE DISTRIBUTION BY WEIGHT, %

Size, μm	Fine Grade (% less than)	Coarse Grade (% less than)
0 - 5	39±2	12±2
5 - 10	18±3	12±3
10 - 20	16±3	14±3
20 - 40	18±3	23±3
40 - 80	9±3	30±3
80 - 200	----	9±3

APPENDIX C

TYPICAL PROPERTIES OF AUTOMOBILE AIR FILTRATION PAPER

The cellulose wood pulp fibers typically used in automobile air filtration media fall into three basic categories, viz. southern softwood kraft (SSK), mercerized SSK, northern and southern or eucalyptus hardwood kraft wood pulps. The average fiber diameters are given in the following table.

TABLE VI

AVERAGE FIBER DIAMETERS OF SEVERAL TYPICAL FIBERS USED IN AUTOMOBILE AIR FILTRATION PAPER.

Fiber Type	Average Fiber Diameter
SSK	45 μm
Mercerized SSK	40 - 45 μm
Northern US, Southern US, Eucalyptus Hardwood Kraft Pulp	18 - 30 μm

The typical mixtures in auto air filter papers range from a formulation of 80 % mercerized SSK, 15% SSK, 5% hardwood (for a very high permeability grade) to 50% mercerized SSK, 25% SSK, 25% hardwood (for a higher efficiency grade).

A range of typical properties, for auto air filtration, include:

Frazier air permeability* (cfm)	60 - 120
Basis weight (gm/m^2)	110 - 165
Media thickness (μm)	450 - 750
Unsaturated paper density (gm/cc)	0.18 - 0.22

*number of ft^3/minute of air to pass through one ft^2 of given thickness media at a Δp of 0.5 inches of water.

The above technical information was obtained from Ahlstrom Filtration.

For the purpose of calculation of filtration efficiencies, it is necessary to assume that all the fibers in the filter are of uniform diameter because the models used are based on such an assumption. The above technical data was used as an input to decide what diameter fibers should be assumed for the filtration models for calculating the filtration efficiencies. No standard methods or suitability of any method have been described anywhere. One possible way to arrive at a uniform equivalent diameter is to take the mean by weighting each of the fibers by its percentage composition. For example, in the case of high permeability grade,

uniform equivalent diameter = $(45\mu m \times 80 + 42.5\mu m \times 15 + 24\mu m \times 5)/100 = 44\mu m$

where the diameters of Mercerized SSK and Northern US, Southern US, Eucalyptus Hardwood Kraft Pulp fiber are taken to be the mean of the range presented in Table V. Similarly, in the case of high efficiency grade,

uniform equivalent diameter = $(45\mu m \times 50 + 42.5\mu m \times 25 + 24\mu m \times 25)/100 = 39\mu m$.

Assuming the paper to be of a very high efficiency grade, the fiber radius was taken to be 19 μm and the packing density to be 0.23 which corresponds to a Frazier air permeability of 150 cfm. Most of the results presented in Chapter 4 are presented for this particular case of high efficiency grade paper.

APPENDIX D

COMPUTER PROGRAM FOR FOR CALCULATION OF
FILTER EFFICIENCIES

```
c**************************************************************************
c    THIS PROGRAM FINDS EFFICIENCY OF PLEATED AIR FILTERS AS A
c    FUNCTION  OF VELOCITY AS PER THE METHOD DESCRIBED IN SECTION
c    4.2 OF THE THESIS.  THE INPUT DATA FILE IS THE VELOCITY DATA FILE
c    FOR FILTER AF3192  IN THE PLANE CLOSEST TO THE FILTER i.e. PLANE 4
c    AS PER THE  CONVENTION IN THESIS.
c**************************************************************************
c    ace          area of corner element (in sq. ft)
c    alee         area of element on the edges of the length (in sq. ft)
c    ane          area of normal element (in sq. ft)
c    awee         area of element on the edges of the width (in sq. ft)
c    efri         efficiency of element due to inertial interception
c    eri          single fiber efficiency due to inertial interception
c    i            counter for do loop
c    lf           length of filter (inches)
c    ntr          ntr th traverse
c    numsr        serial number of reading in ntr th traverse
c    pentot       total penetration
c    qcfm         total flow rate (cfm)
c    qtot         total flow rate (-)
c    st           Stokes number
c    u(2)         X coordinate of filter where measurement is done (inches)
c    u(3)         Y coordinate of filter where measurement is done (inches)
c    u(6)         axial velocity at location (u(2),u(3)) (m/s)
c    wf           width of filter (inches)

      implicit real (a-z)
      integer ntr,numsr,i
      dimension u(12)
      qtot=0.
      pentot=0.
      open(6,file="effin.dat")
      open(7,file="effout.dat")
```

```
      ane=0.2375*0.75/144.
      ace=0.12564*0.4242/144.
      awee=0.2375*0.4242/144.
      alee=0.12564*0.75/144.
      wf=4.76378
      lf=7.5984

c*****This loop represents the traverses performed
      do 100 ntr=1,11
c********This loop represents the 11 readings taken in each traverse do 200
          numsr = 1,11
              read(6,*,end=30)( u(i),i=1,12 )
c************The following series of if statements check if the location
c                 of measurement is at the edge of the filter, in which
c                 case the area of the element is different.
              if (ntr .eq. 1 .or. ntr .eq. 11) then
                 if (numsr .eq. 1) then
                    qtot=qtot+u(6)*awee
                    call filteff(u(6),efri,st,eri)
                    write(7,20)numsr,u(2),u(3),u(6),efri,st,eri
                    pentot=pentot+(1.-efri)*awee*u(6)
                    goto 200
                 endif
                 if (numsr .eq. 11) then qtot=qtot+u(6)*ace*2.
                    call filteff(u(6),efri,st,eri)
                    write(7,20)numsr,u(2),u(3),u(6),efri,st,eri
                    pentot=pentot+(1.-efri)*ace*2.*u(6)
                    goto 200
                 endif
                 qtot=qtot+u(6)*awee*2.
                call filteff(u(6),efri,st,eri)
                 write(7,20)numsr,u(2),u(3),u(6),efri,st,eri
                 pentot=pentot+(1.-efri)*awee*2.*u(6)
                 goto 200
              endif
              if (numsr .eq. 1) then
                 qtot=qtot+u(6)*ane
                 call filteff(u(6),efri,st,eri)
                 write(7,20)numsr,u(2),u(3),u(6),efri,st,eri
                 pentot=pentot+(1.-efri)*ane*u(6)
                 goto 200
              endif
              if (numsr .eq. 11) then qtot=qtot+u(6)*alee*2.
                 call filteff(u(6),efri,st,eri)
                 write(7,20)numsr,u(2),u(3),u(6),efri,st,eri
                 pentot=pentot+(1.-efri)*alee*2.*u(6)
```

```
                goto 200
              endif
              qtot=qtot+u(6)*ane*2.
               call filteff(u(6),efri,st,eri)
              write(7,20)numsr,u(2),u(3),u(6),efri,st,eri
              pentot=pentot+(1.-efri)*ane*2.*u(6)
200     continue
          write(7,21)
100  continue


       close(6)
       qcfm=qtot*196.8
       print*," avrg_u = m/s", qtot/(wf*lf/144.)
       print*, " flow rate Q = ", qcfm ," CFM"
       print*, " "
       print*, "overall filter efficiency = ",
      &              1.-(pentot/qtot)

       goto 40
        20  format(1x,i3,3x,f6.3,3x,f6.3,3x,f6.3,3x,f6.4,3x,f6.3,3x,f6.4)
21     format()
30     print*, "ERROR: END OF FILE WAS REACHED"
40     stop
       end


c**********************************************************************
subroutine filteff(vop,efri,st,eri)
c
c       Subroutine to find the elemental efficiency as per the theory
c       described in section 4.2 of thesis.
c**********************************************************************

c   a           aerosol particle radius (m)
c   c           filter packing density
c   cc          Slip correction factor
c   efri        efficiency of element due to inertial interception
c   er          single fiber efficiency due to interception
c   ei          single fiber efficiency due to inertial impaction
c   eri         single fiber efficiency due to inertial interception
c   h           thickness of filter (m)
c   hf          height of pleat of filter (m)
c   ip          interception parameter
c   K           Hydrodynamic factor of Kuwabara flow
c   Kn          Knudsen number
c   lmda        mean free path of air (m)
```

```
c   neta        air dynamic viscosity (Pa.s)
c   pf          pitch of pleats in filter (m)
c   r           radius of fiber (m)
c   ro          aerosol particle density  (Kg/m3)
c   st          Stokes number
c   vop         velocity of air outside pleats (m/s)
c   vip         velocity of air inside pleats (m/s)
c   wf          width of filter (m)

      implicit real (a-z)
      c=0.23
      ro=2723.0
      neta=1.806*10.**(-5.)
      r=19.*10.**(-6.)
      h=.0007
      pi=3.1416
      a=10.*10.**(-6.)
      ip=a/r
      wf=0.121
      hf=.03
      pf=.003125
      lmda=0.065*10.**(-6.)
      kn=lmda/a
      cc=1.+1.257*kn k=-0.5*log(c)-0.75+c-0.25*c**2.

      vip=vop*pf/(2.*hf)
      st=(a**2.*ro*(vip/(1.-c)))*cc/(9.0*neta*r)
      er=(1.-c)/k*ip**2./(1.+ip)
      ei=st**3./(st**3.+0.77*st**2.+0.22)
      eri=1.-((1.-er)*(1.-ei))
      efri=1.-exp(-2.*c*eri*h/(pi*(1.-c)*r))
      return
      end
```

VITA

Sabnis Rajendra
Candidate for the Degree of
Master of Science

Thesis: EFFECTS OF NON-UNIFORM AIR FLOW THROUGH FILTERS ON FILTRATION EFFICIENCY

Major Field: Mechanical Engineering

Biographical:

Personal Data: Born in Islampur, India, June 8, 1968, son of Shailaja Sabnis and late Digambar Sabnis.

Education: Graduated from Yashwant Rao Chavan College of Science, Karad, India, in June 1985; received Bachelor of Science Degree in Mechanical Engineering from Shivaji University, Kolhapur, India in July 1989; completed requirements for the Master of Science degree at Oklahoma State University in July, 1993.

Professional Experience: Research Assistant, Department of Mechanical and Aerospace Engineering, Oklahoma State University, March, 1992, to June 1993.
Teaching Assistant, Department of Mechanical and Aerospace Engineering, Oklahoma State University, August, 1992, to December, 1993.
Engineer, Research and Development, Thermax Ltd., India, July, 1989, to July, 1991. Designed, developed and tested multiple effect thermal desalination plant, and fluidized bed boilers. Developed and tested two stage vapor absorption chiller, ceramic tube hot air generator, fluidized bed incinerator, "Exergy" drier, and steam jet refrigerator.